HISTORY MATCHING AND PREDICTION OF A POLYMER FLOOD PILOT IN HEAVY OIL RESERVOIR ON ALASKA NORTH SLOPE

By

Xindan Wang

A Thesis Submitted in Partial Fulfillment of the Requirements

for the Degree of

Master of Science

in

Petroleum Engineering

University of Alaska Fairbanks

December 2021

APPROVED:

Dr. Yin Zhang, Committee Chair
Dr. Abhijit Dandekar, Committee Co-Chair
Dr. Santanu Khataniar, Committee Member
Dr. Abhijit Dandekar, Department Chair
Department of Petroleum Engineering
Dr. William Schnabel, Dean
College of Engineering and Mines
Dr. Richard Collins
Director of the Graduate School

Abstract

The first-ever polymer flood pilot to enhance heavy oil recovery on Alaska North Slope is ongoing. After more than 3 years of polymer injection, significant benefit has been observed from the decrease in water cut from 65% to less than 15% in the project producers. The primary objective of this study is to develop a robust history-matched reservoir simulation model capable of predicting future polymer flood performance. In this work, the reservoir simulation model has been developed based on the geological model and available reservoir and fluid data. In particular, four high transmissibility strips were introduced to connect the injector-producer well pairs, simulating short-circuiting flow behavior that can be explained by viscous fingering and reproducing the water cut history. The strip transmissibilities were manually tuned to improve the history matching results during the waterflooding and polymer flooding periods, respectively. It has been found that higher strip transmissibilities match the sharp water cut increase very well in the waterflooding period. Then the strip transmissibilities need to be reduced with time to match the significant water cut reduction. The viscous fingering effect in the reservoir during waterflooding and the restoration of injection conformance during polymer flooding have been effectively represented. Based on the validated simulation model, numerical simulation tests have been conducted to investigate the oil recovery performance under different development strategies, with consideration for sensitivity to polymer parameter uncertainties. The oil recovery factor with polymer flooding can reach about 39% in 30 years, twice as much as forecasted with continued waterflooding. Besides, the updated reservoir model has been successfully employed to forecast polymer utilization, a valuable parameter to evaluate the pilot test's economic efficiency. All the investigated development strategies indicate polymer utilization lower than 3.5 lbs/bbl in 30 years, which is less than that of the same polymer used in a polymer pilot in Argentina.

Table of Contents

Nomenclature

Variables:

A	Cross-section area	[cm^2]
B	Formation volume factor	[bbl/STB]
C_{ads}	Adsorbed polymer concentration	[μg/g]
C_{ads}^{max}	Maximum adsorbed polymer concentration	[μg/g]
C_p	Polymer concentration	[mg/L]
C_{sep}	Effective salinity	[meq/mL]
D	Depth	[m]
J	Leverett J-function	[-]
K	Permeability	[Darcy]
K_o	Effective permeability of oil phase	[Darcy]
K_w	Effective permeability of water phase	[Darcy]
k_{ro}	Relative permeability of oil phase	[-]
k_{rw}	Relative permeability of water phase	[-]
L	Length	[cm]
M	Mobility ratio	[-]
P	Pressure	[atm]
P_c	Capillary pressure	[Pa]
Q	Well rate	[STB/day]
q	Flow rate	[cm^3/s]
R_k	Permeability reduction factor	[-]
RRF	Residual resistance factor	[-]

S_{or}	Residual oil saturation	[-]
S_p	Salinity exponent	[-]
S_w	Water saturation	[-]
S_{wc}	Critical water saturation	[-]
T	Fluid transmissibility	[mD-ft/cP]
T_{mult}	Transmissibility multiplier	[-]
t	Time	[hr]
V	Reservoir volume	[m^3]
ΔP_w	Pressure drop of water phase	[Pa]
γ	Specific gravity	[-]
$\dot{\gamma}_{eff}$	Effective shear rate	[1/s]
μ_p^0	Polymer viscosity at the absent of shear rate	[mPa·s]
μ	Fluid viscosity	[mPa·s]
μ_{app}	Apparent polymer viscosity	[mPa·s]
μ_o	Oil viscosity	[mPa·s]
μ_w	Water viscosity	[mPa·s]
λ_w	Mobility of water phase	[m^2/Pa·s]
ν	Shear velocity	[1/s]
σ	IFT	[mN/m]
φ	Porosity	[-]

Abbreviations:

2D	Two Dimensional
3D	Three Dimensional
ANS	Alaska North Slope
API	American Petroleum Institute
ASP	Alkali-Surfactant-Polymer
bbl	Barrel
BHP	Bottom Hole Pressure
bopd	Barrels Oil per Day
CF	Centrifuge
cP	Centipoise
CVFE	Control Volume Finite Element
DOE	Department of Energy
EIA	Energy Information Administration
EOR	Enhanced Oil Recovery
FP	Flopaam
ft	Feet
HM	History Matching
HPAM	Hydrolyzed Polyacrylamide
hr	Hour
IFT	Interfacial Tension
IAPV	Inaccessible Pore Volume
KRU	Kuparuk River Unit

lb	Pound
LPG	Liquefiable Petroleum Gas
mD	MilliDarcy
MICP	Mercury Injection Capillary Pressure
MMbbls/day	Million Barrels per Day
MMP	Minimum Miscibility Pressure
MMSTB	Million Stock Tank Barrels
MPU	Milne Point Unit
OOIP	Original Oil in Place
PBU	Prudhoe Bay Unit
PIU	Polymer Injection Unit
PP	Porous Plate
ppm	Parts Per Million
psi	Pound per Square Inch
PV	Pore Volume
PVT	Pressure Volume Temperature
RF	Recovery Factor
SAGD	Steam-Assisted Gravity Drainage
STB	Stock Tank Barrels
STB/day	Stock Tank Barrels per Day
TVDSS	True Vertical Depth Subsea
VR-WAG	Viscosity Reducing Water-Alternating-Gas
WF	Water Flood

°C	Degree Celsius
°F	Degree Fahrenheit

List of Figures

List of Tables

Acknowledgments

First of all, I wish to express my sincere gratitude and appreciation to my supervisor, Professor Yin Zhang, for the full support and guidance through my studying time. I also wish to express my thanks to my committee members, Professor Abhijit Dandekar and Professor Santanu Khataniar, for giving suggestions to my research work.

Further, I would like to thank the funding support from the U.S. Department of Energy (DOE) project under Award Number DE-FE0031606 and Hilcorp Alaska, LLC for co-sponsoring this project. Also, I am very thankful and grateful to Dr. Samson Ning, Dr. Dongmei Wang, Dr. Randy Seright, Dr. Baojun Bai, and all other members of the DOE project for their continuous and endless assistance. Special thanks go to Dr. Samson Ning for his guidance in my simulation work.

Also, I would like to thank the Department of Petroleum Engineering for providing me with this opportunity to complete my master's study at the University of Alaska Fairbanks. I am very grateful to all my fellow students, especially Yaoze Cheng, Hongli Chang, Anshul Dhaliwal, and Cody Keith, for making my stay at UAF fun and enjoyable.

Finally, I would like to thank my family and my friends for their endless motivations and encouragement. Thank you for being with me and keeping my spirit up at all times.

Fairbanks, October 2021

Xindan Wang

1. Introduction

Fossil resources, such as crude oil and natural gas, are essential for developing the energy industry around the world, which can improve our quality of life, create employment opportunities and expand a vibrant global economy. The main uses of fossil resources include generating heat for the manufacturing industry, supplying energy for the transportation industry, and fueling the generation of electricity. With the energy mix moving forward, the utility and development of clean energy is paid more attention, but oil and natural gas still account for 58% of the global energy consumption, as shown in Figure 1.1.

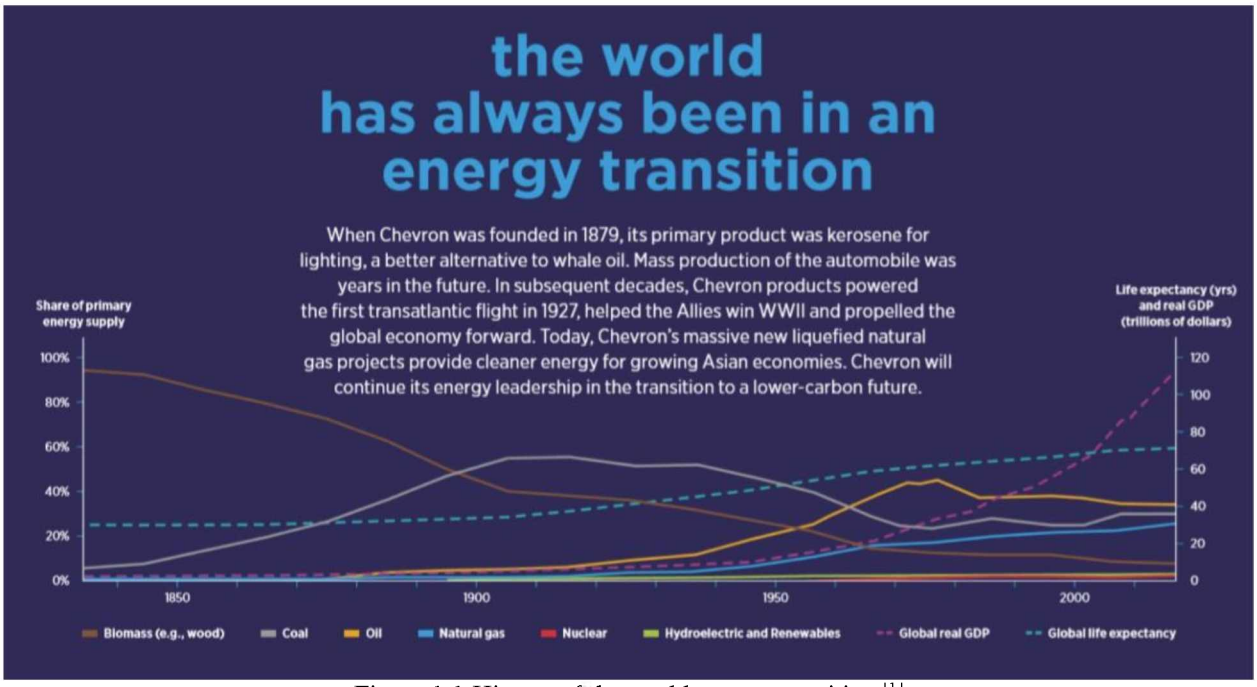

Figure 1.1-History of the world energy transition [1]

According to U.S. Energy Information Administration (EIA), the consumption of petroleum and natural gas is expected to continuously increase over the next 30 years, as shown in Figure 1.2. In addition, the forecasted world liquid fuels consumption averages about 101 MMbbls/day in 2022, as shown in Figure 1.3. Considering the growing consumption of fossil resources over the next 2

or 3 decades, advanced technologies like horizontal well and enhanced oil recovery (EOR) methods to increase recovery from heavy oil reservoirs are required to achieve higher production levels.

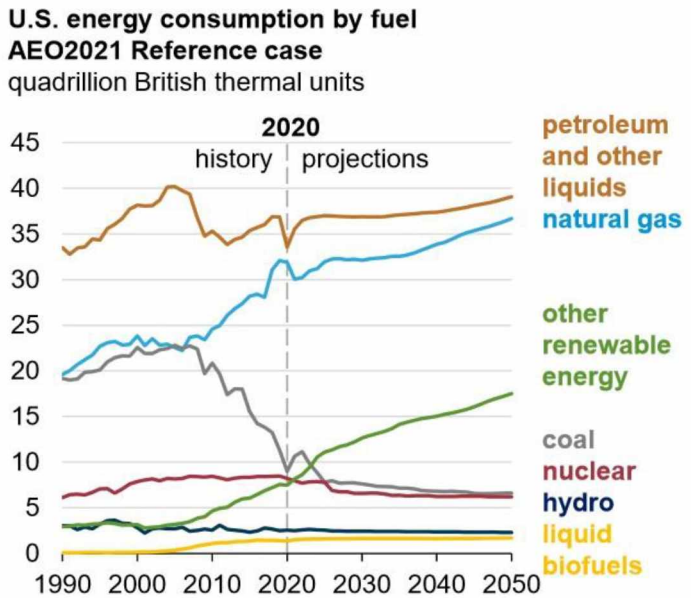

Figure 1.2-U.S. energy consumption by fuel [2]

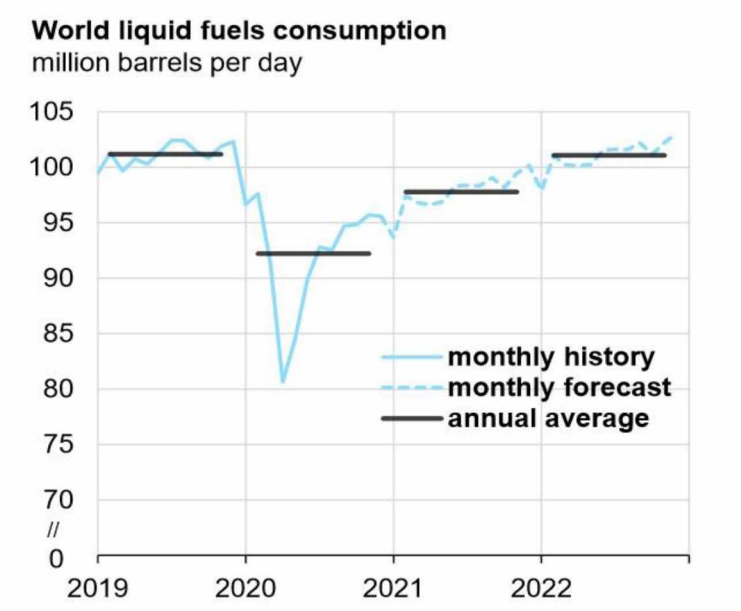

Figure 1.3-World liquid fuels consumption [2]

1.1. Applications of EOR methods

Previously, EOR referred to the oil recovery by injecting any material that does not normally exist in the reservoir at the tertiary recovery stage. However, one of the EOR methods, thermal practices are mostly implemented at the secondary recovery stage [3-5] or even from the beginning of exploitation [6]. Thus, a more specific description of EOR has been proposed, and it is defined as "injecting a fluid, with or without additives, to the reservoir to displace oil while changing the oil and/or interfacial properties and providing extra pressure at the secondary, tertiary, or even primary stage" [7]. Figure 1.4 illustrates all EOR methods which are applied to change rock or fluids properties to enhance oil recovery by viscous or gravity forces.

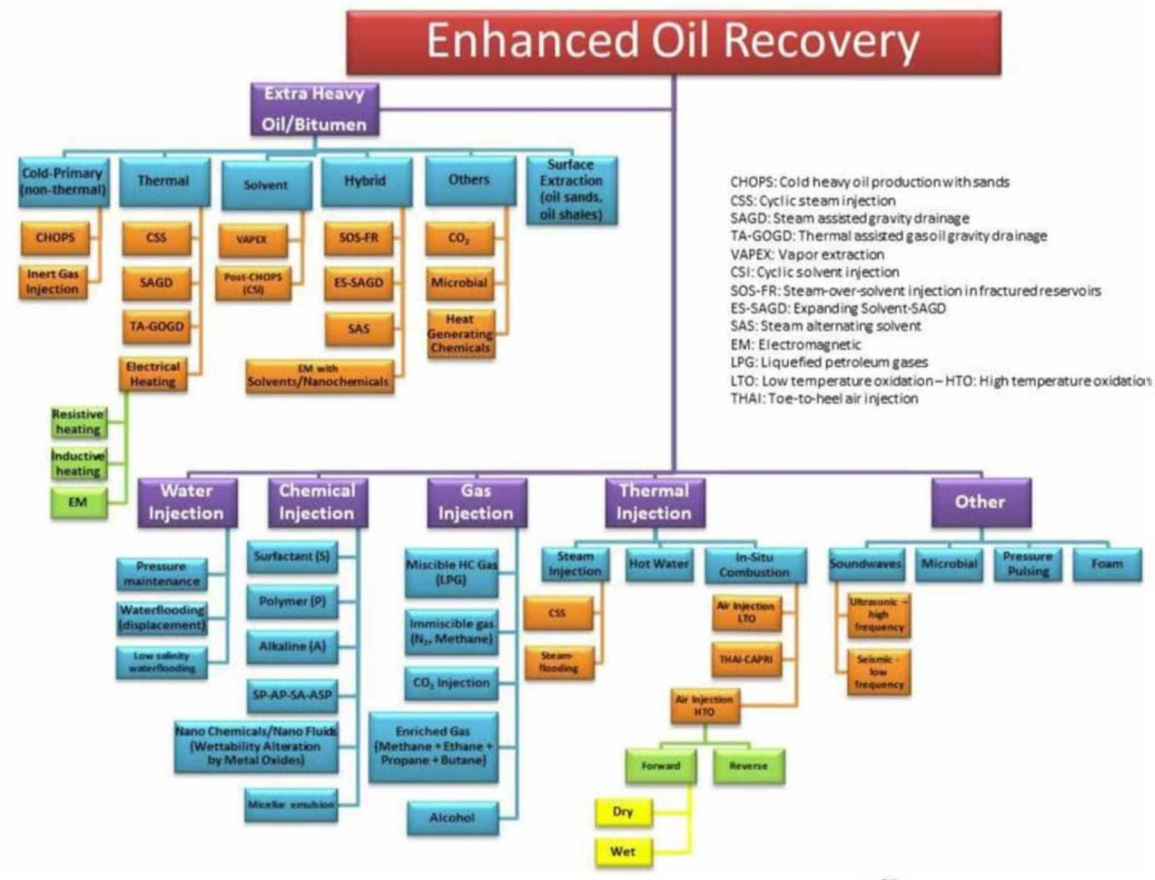

Figure 1.4-Extended classification of EOR methods [7]

EOR methods are grouped into four main categories: chemical injection, gas injection, thermal injection, and other methods. The oil displacement mechanisms of EOR methods have been investigated extensively in the last few decades, and different and sustainable EOR projects have been successfully applied worldwide. Figure 1.5 illustrates the number of EOR projects and total EOR production worldwide at different periods.

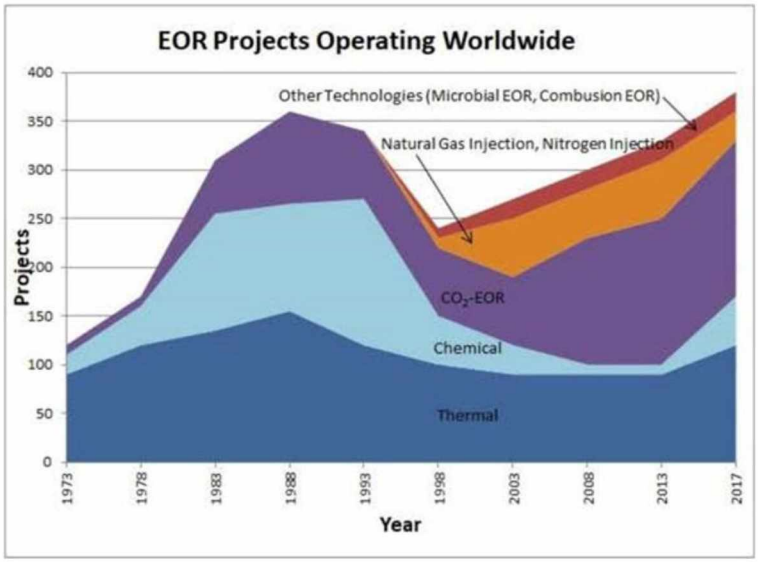

(a)

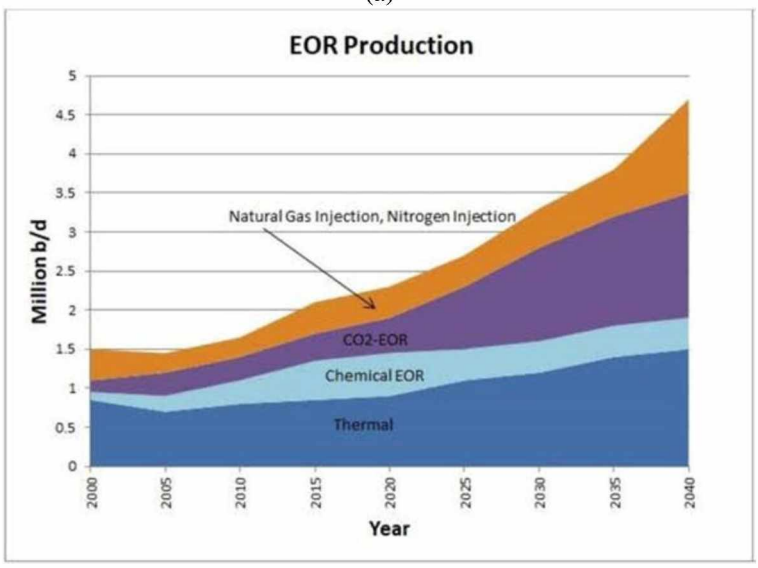

(b)

Figure 1.5-(a) the number of current EOR operations worldwide, and (b) total EOR production worldwide and future prospect [7]

Among the various EOR techniques, the chemical injection can effectively enhance oil recovery compared to conventional waterflooding by adding chemical additives to injected fluids. Generally, the polymer is added to increase the viscosity of the displacing fluid, thereby improving the mobility ratio [8-10]. In addition, surfactant and alkali can be added to reduce the interfacial tension (IFT) between oil and displacing fluids [11-13]. Moreover, the injected alkali is able to change the wettability of the rock matrix [14]. The combined alkali-surfactant-polymer (ASP) EOR method can increase sweep efficiency through mobility control and improve displacement efficiency by decreasing IFT, resulting in a more significant ultimate oil recovery. Some of the sustainable chemical flooding applications are listed in Table 1.1. Note that the "at least" in end date is put based on the publication date of literature.

Table 1.1-Selected field cases of chemical injection

Case #	Field name (country)	Application	Start-end date	Reference
C1	Pelican Lake (Canada)	Polymer	2005-at least 2014	Delamaide et al. [15]
C2	Mooney (Canada)	ASP, Polymer	2008-at least 2014	Delamaide et al. [15]
C3	Seal (Canada)	Polymer	2010-at least 2013	Delamaide et al. [15]
C4	Taber South (Canada)	ASP	2006-at least 2013	Delamaide et al. [15]
C5	Suffield Upper Mannville (Canada)	ASP	2007-at least 2013	Delamaide et al. [15]
C6	Daqing (China)	ASP	1994-today	Wyatt et al. [16]

The gas injection, including miscible and immiscible flooding, can increase displacement efficiency for many different types of reservoirs. The injected gas composition is typically hydrocarbon gas, carbon dioxide, nitrogen, or acid gas (CO2 and H2S) [17-20]. For miscible flooding,

the fundamental principle is to achieve the miscibility between the oil phase and injected gas, reducing the IFT between oil and displacing fluids to improve displacement efficiency [21]. The miscibility of oil and injected gas is significantly affected by the pressure, temperature, and composition of fluids. So minimum miscibility pressure (MMP), the lowest pressure at which the miscibility of residual oil and injected gas is achieved after multiple contacts at the reservoir temperature, is proposed to evaluate the miscibility. In general, liquefiable petroleum gas (LPG) or enriched gas can be used to improve the miscibility and reduce the MMP [22]. However, applications of miscible displacement to heavy oil reservoirs are hampered by the complex phase behavior. Immiscible flooding, especially CO2 immiscible flood, plays a significant role in enhancing heavy oil recovery, which can reduce oil viscosity and improve the mobility ratio [23, 24]. A number of gas injection applications are summarized in Table 1.2.

Table 1.2-Selected field cases of gas injection

Case #	Field name (country)	Application	Start-end date	Reference
G1	Midale-Weyburn (Canada)	CO2 miscible	2000-today	Barnhart and Coulthard [25]
G2	Zama (Canada)	Acid gas - miscible	1998-2000 2004-today	Davison et al. [26] Trivedi et al. [27]
G3	Prudhoe Bay (USA)	Enriched gas (65%) and CO2 (35%)	1997-1998 1999-at least 2000	McGuire and Holt [28]
G4	Ula (Norway)	Miscible gas	1997-at least 2013	Zhang et al. [29]
G5	Handil (Indonesia)	Lean gas	1995-at least 1998	Gunawan and Cale [30]
G6	Wasson Denver Unit (USA)	CO2 miscible	1983-at least 2000	Thai et al. [31]

The thermal injection is mainly applied to enhance heavy oil recovery, achieving a higher oil recovery factor by raising the reservoir temperature and reducing the oil viscosity. The well-known thermal recovery methods are steam injection, cyclic steam injection, in-situ combustion, and steam-assisted gravity drainage (SAGD) [32-34]. In the last few years, unconventional thermal approaches that heat the reservoir using electrical energy have been investigated to improve oil recovery, which can be applied to cases that conventional thermal methods are not commercially economical [35]. A few long-term ongoing thermal injection applications are listed in Table 1.3.

Table 1.3-Selected field cases of thermal injection

Case #	Field name (country)	Application	Start-end date	Reference
T1	Duri (Indonesia)	Steam	1985-today	Fuaadi et al. [3] Nath et al. [36]
T2	Cold Lake (Canada)	Steam	1985-today	Stark [37]
T3	Kern River (USA)	Steam	1964-today	Williams et al. [38]

Other methods include microbial injection, foam injection, sonic method, etc. So far, they are limited to small-scale field applications [39-42].

1.2. Heavy oil recovery on Alaska North Slope

Prudhoe Bay Unit (PBU) and Kuparuk River Unit (KRU) on Alaska North Slope (ANS), as shown in Figure 1.6, are two of the largest oil fields in North America [43, 44]. The Schrader Bluff reservoirs in Orion and Polaris fields within the PBU, the West Sak and Ugnu heavy oil formations within the KRU, and the Schrader Bluff reservoir within the Milne Point Unit (MPU) form a heavy oil belt, as shown in Figure 1.7, which holds 20 to 25 billion barrels of heavy oil in place [45]. The

various oil bearing formations are illustrated in Figure 1.8. The sands of interest in the Schrader Bluff reservoir consist of the N-sands and O-sands, which are poorly consolidated. The porosities range from 25% to 35%, and the permeabilities vary from 100 mD to 2 Darcy. The initial reservoir pressure is approximately 1600 psi at 3500 ft true vertical depth subsea (TVDSS), and the reservoir temperature is about 80 °F. The oil gravity ranges from 14 to 22 °API with in-situ viscosity greater than 300 cP, as shown in Figure 1.9.

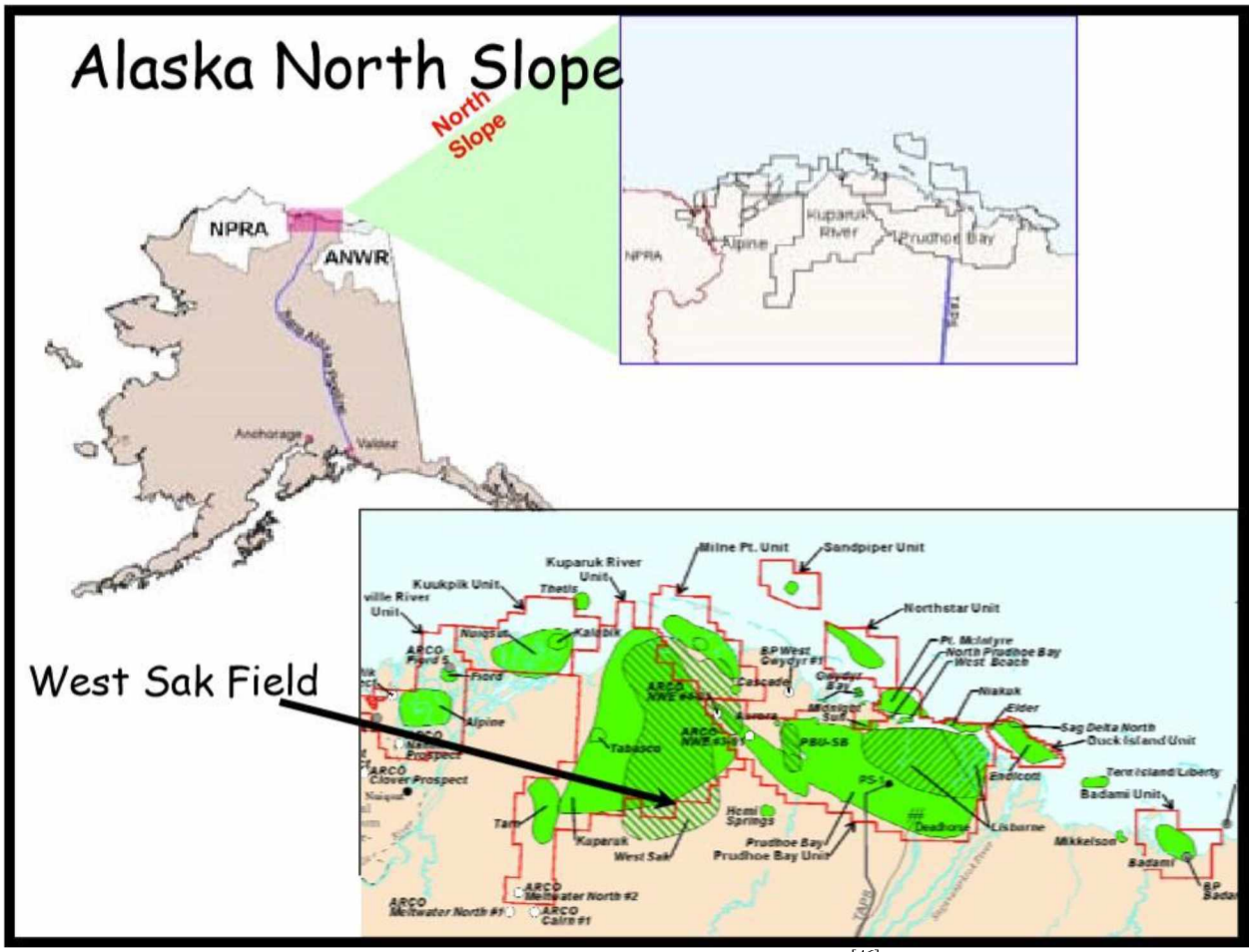

Figure 1.6-PBU and KRU location indicator [46]

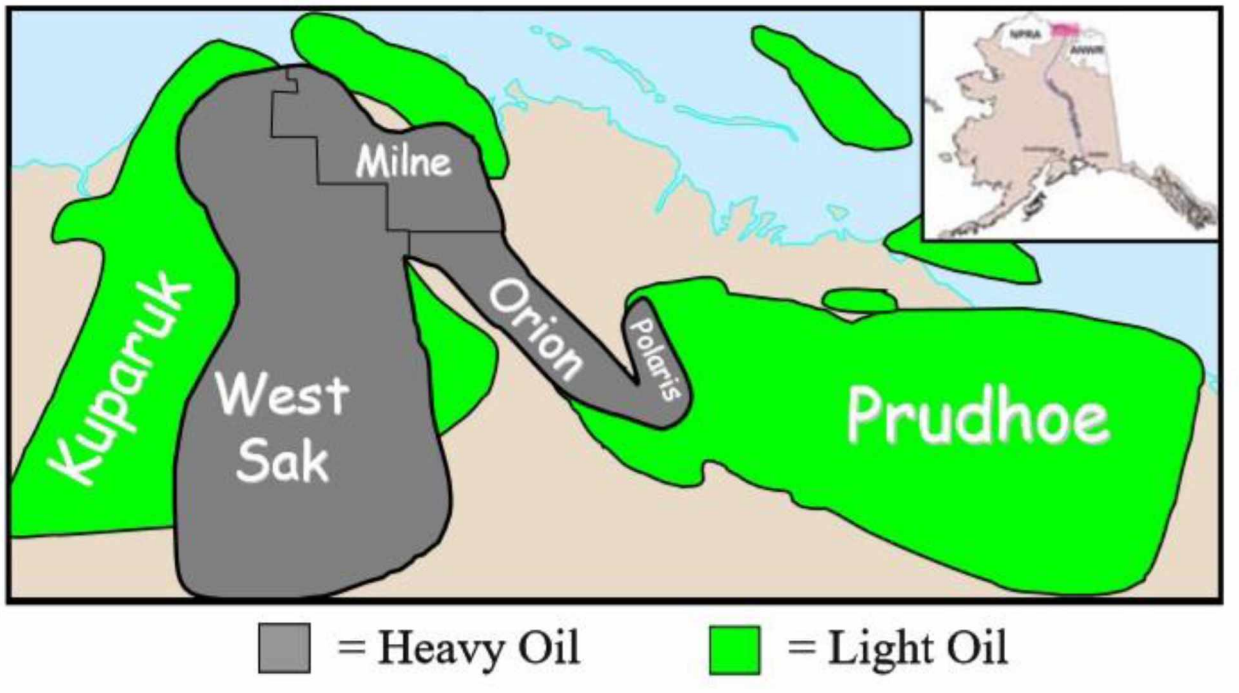

Figure 1.7-The heavy oil belt within PBU, KRU, and MPU [45]

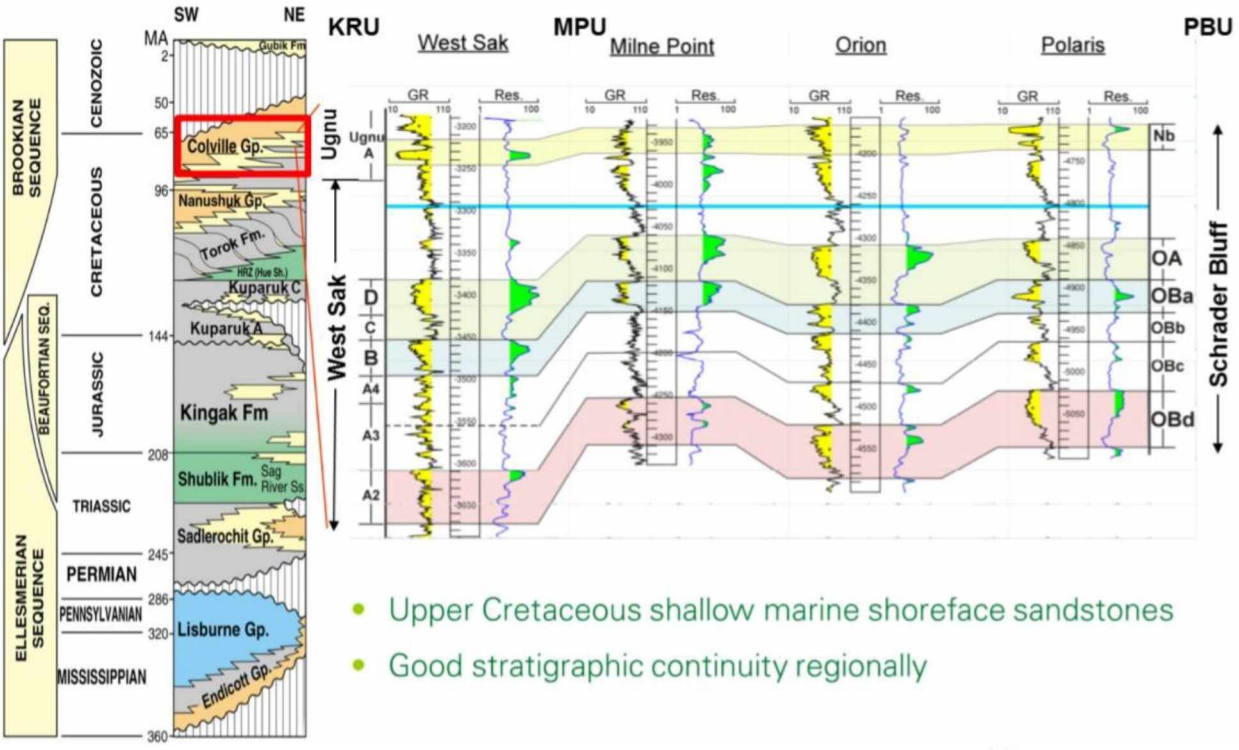

Figure 1.8-Schrader Bluff reservoir with multiple commercial horizons [47]

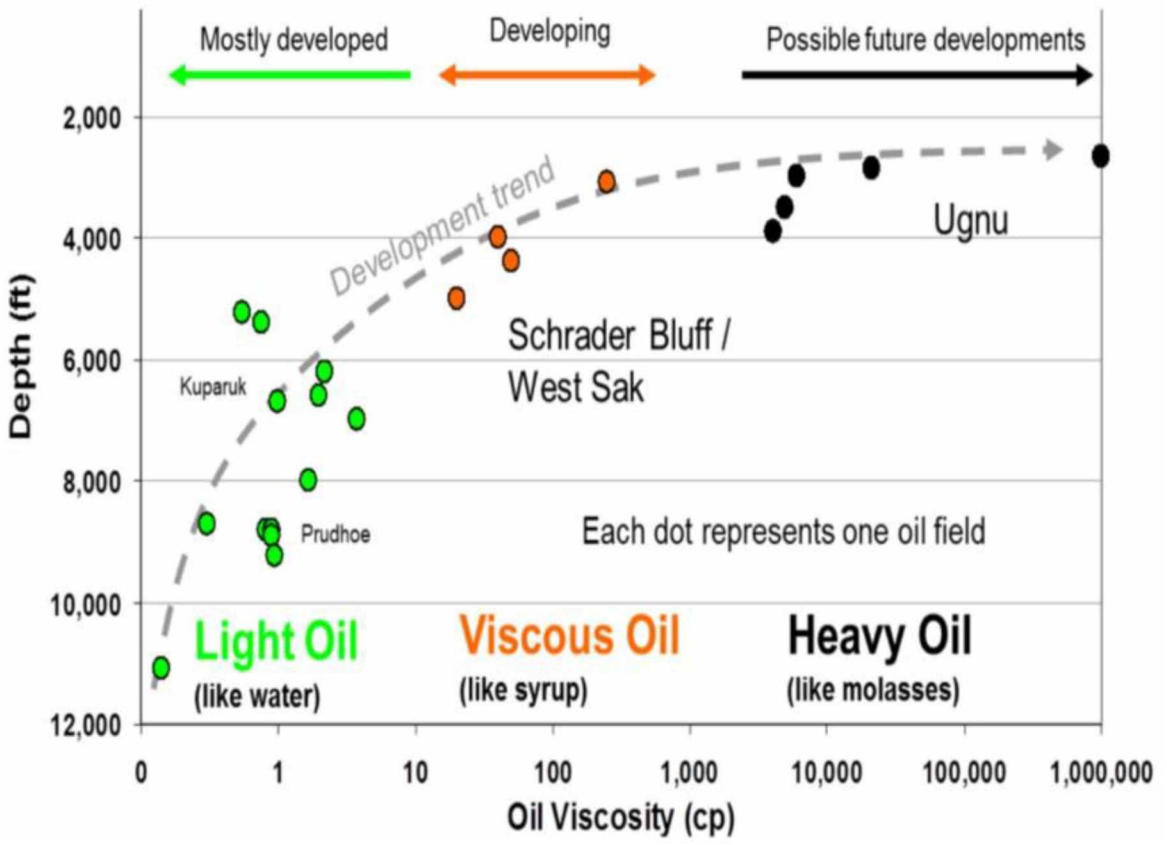

Figure 1.9-Viscosity of various ANS oils vs. depth [47]

West Sak heavy oil was first developed using vertical wells with waterflooding; these wells produced only up to 400 bopd. Starting from 1998, horizontal single or multi-lateral wells were drilled, significantly increasing the oil rate to between 1000 and 3000 bopd per well [45, 47]. As a result, the total well count increased remarkably to improve heavy oil recovery through 2010, as shown in Figure 1.10. Despite that, cumulative Schrader Bluff/West Sak heavy oil production to date only represents about 1% of the heavy oil in place from the North Slope. Due to the low oil recovery factor, high operation costs, and arctic conditions, new approaches to unlock the heavy oil resources on ANS are warranted.

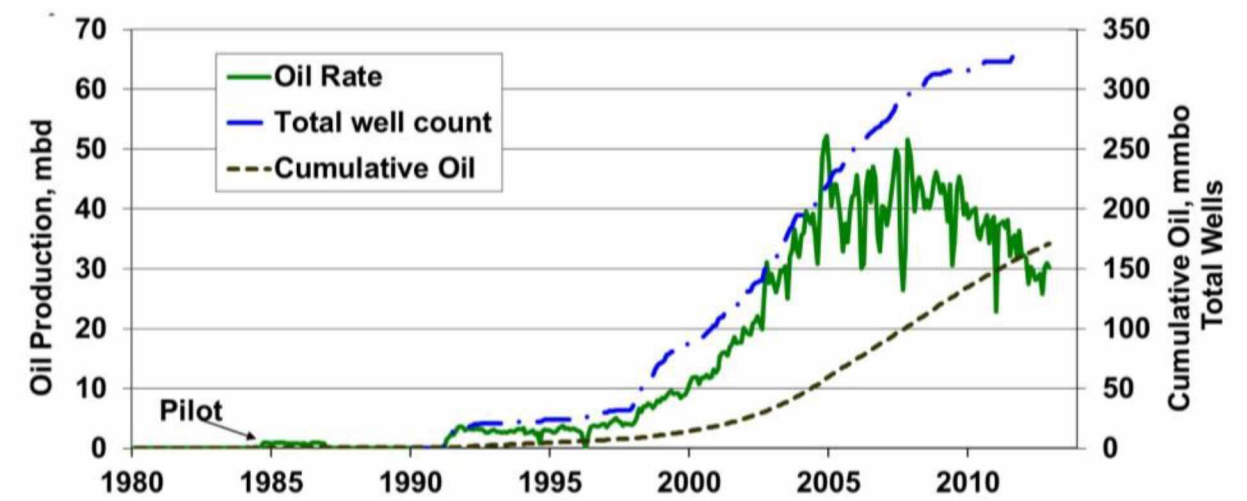

Figure 1.10-Heavy oil production history in Schrader Bluff reservoir [47]

Thermal recovery methods and gas injection have been widely applied globally as effective heavy oil recovery techniques. However, these methods are impractical on ANS. The close vertical proximity of ANS heavy oil reservoirs to the nearly 2000 ft continuous permafrost makes thermal methods, such as steam injection, impractical. This is because the thermal methods could melt this permafrost body, leading to subsidence and irreversible damage to development infrastructure and the environment. Miscible flooding is not adopted because the MMP between the heavy oil and the solvent (hydrocarbon-based or CO2) is much higher than the reservoir pressure. Although the immiscible enriched gas injection has been applied in the West Sak heavy oil reservoirs via the viscosity reducing water-alternating-gas (VR-WAG) process [48], the expected incremental oil recovery is relatively small compared with the miscible process. Given the poor volumetric sweep efficiency of water flooding, polymer flooding can increase sweep efficiency by improving the mobility ratio, which has been considered to be the most promising technique to enhance oil recovery from heavy oil reservoirs on ANS [49]. Thus the ongoing first-ever polymer flood pilot, shown on the map in Figure 1.11, has been conducted to validate the polymer EOR benefit in the Schrader Bluff heavy oil reservoir at the MPU [50-53]. Positive effects have been proven, observable

from the decrease in water cut from 65% to less than 15% after more than 2.5 years of polymer injection [54].

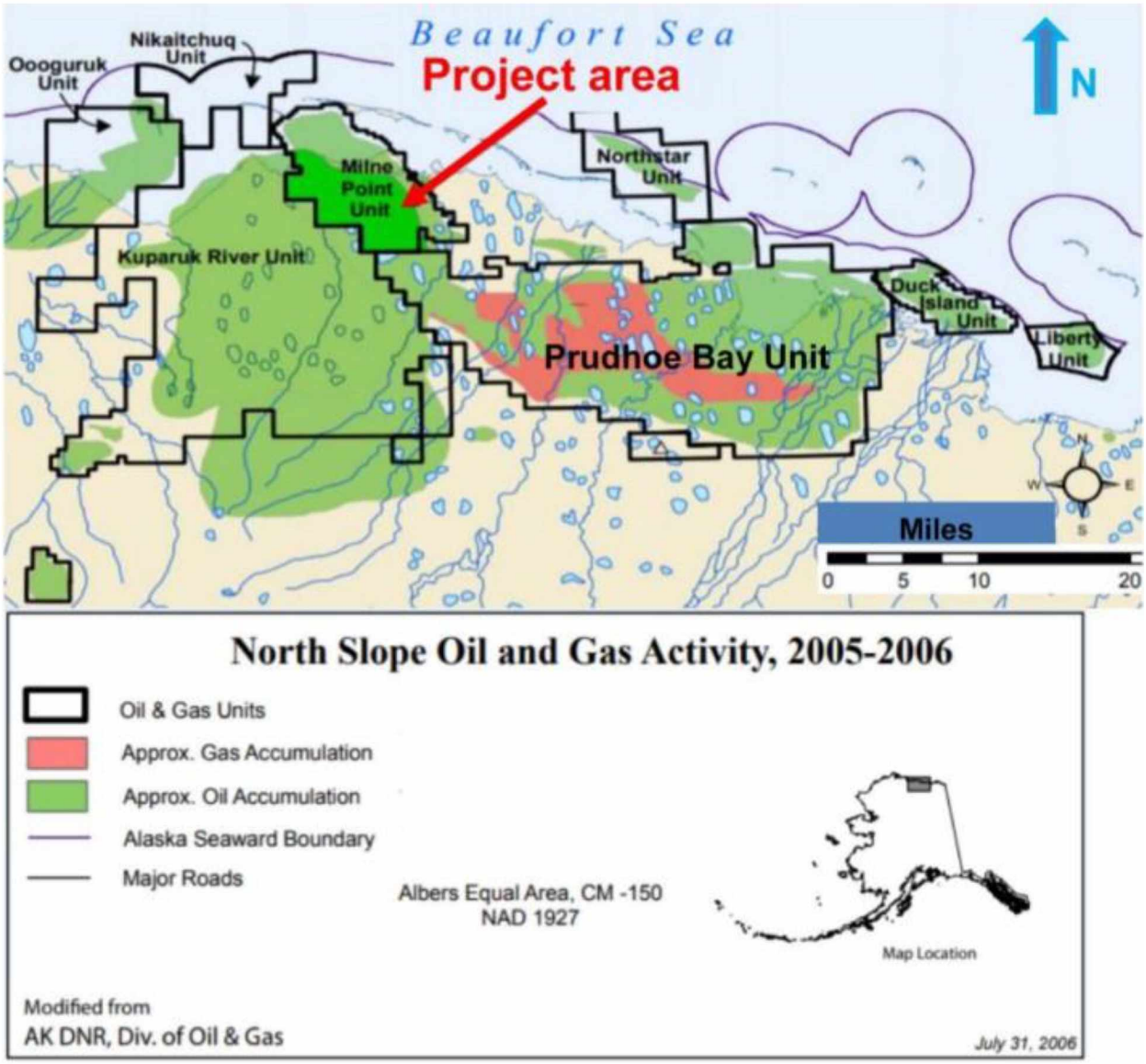

Figure 1.11-Map of the project area for the first-ever polymer flood pilot [50]

1.3. Field-scale polymer flooding simulation

A reliable reservoir simulation model plays an important role in predicting the oil recovery performance of the EOR pilot and evaluating the success of the proposed technique. Calibrating the reservoir simulation model through history matching (HM) has always been a great challenge

for polymer flooding in heavy oil reservoirs. In particular, viscous fingering effects are difficult to capture in the simulation since the grid block size is larger than the viscous finger wavelength. A number of approaches to this problem have been proposed. Mostaghimi et al.[55] used an adaptive mesh control volume finite element (CVFE) method to represent this physical phenomenon by optimizing the mesh resolution based on fingering structures, as shown in Figure 1.12, incurring a high computational cost. Luo et al.[56] applied an effective-fingering model, as shown in Figure 1.13, to a synthetic polymer flooding case in a heavy oil field; this was able to capture the improvement of local displacement efficiency and model the field-scale unstable flows. However, model parameters of the effective-fingering model need to be adjusted and fitted by history matching displacement experiments with different oil viscosities, injection rates, and core diameters. Considering the unstable floods in the heavy oil reservoirs, the oil/water relative permeabilities determined by the analytical method from displacement experiments cannot be directly applied to the field-scale models, which require modification to history match the lab-scale and field-scale production data [57, 58]. Besides, history matching the polymer flooding pilot data should be conducted by verifying the laboratory properties of the polymer solution with consideration of its behavior under reservoir conditions [59]. Once an accurate, history-matched simulation model has been calibrated, it can be used to optimize the development strategy.

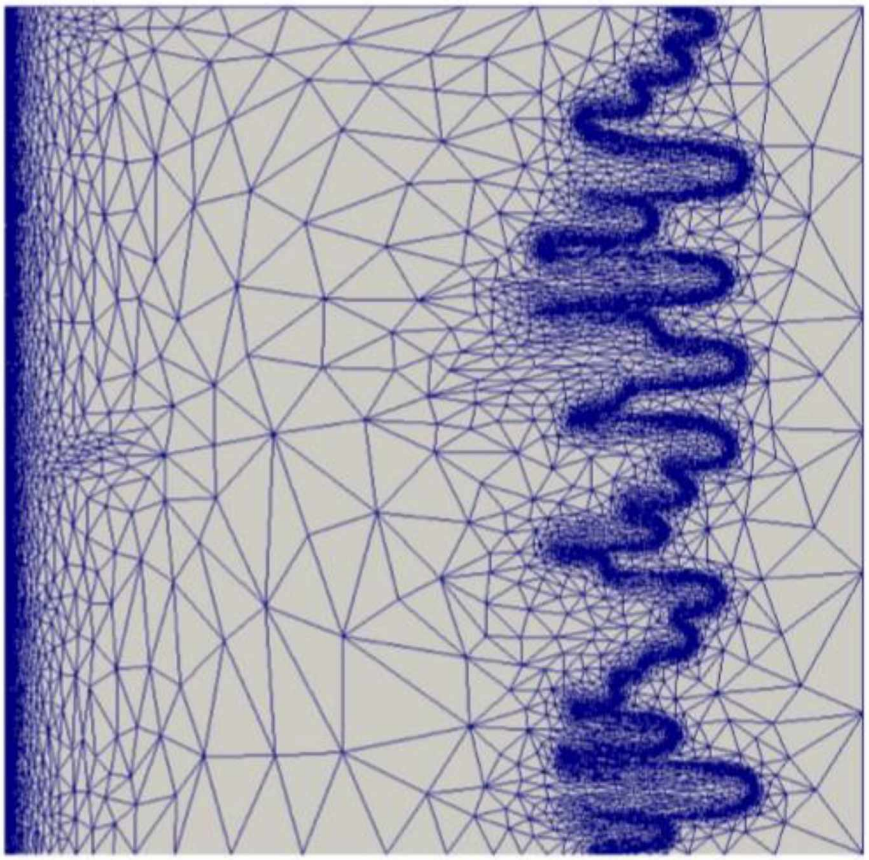

Figure 1.12-Anisotropic meshes generated by CVFE method [55]

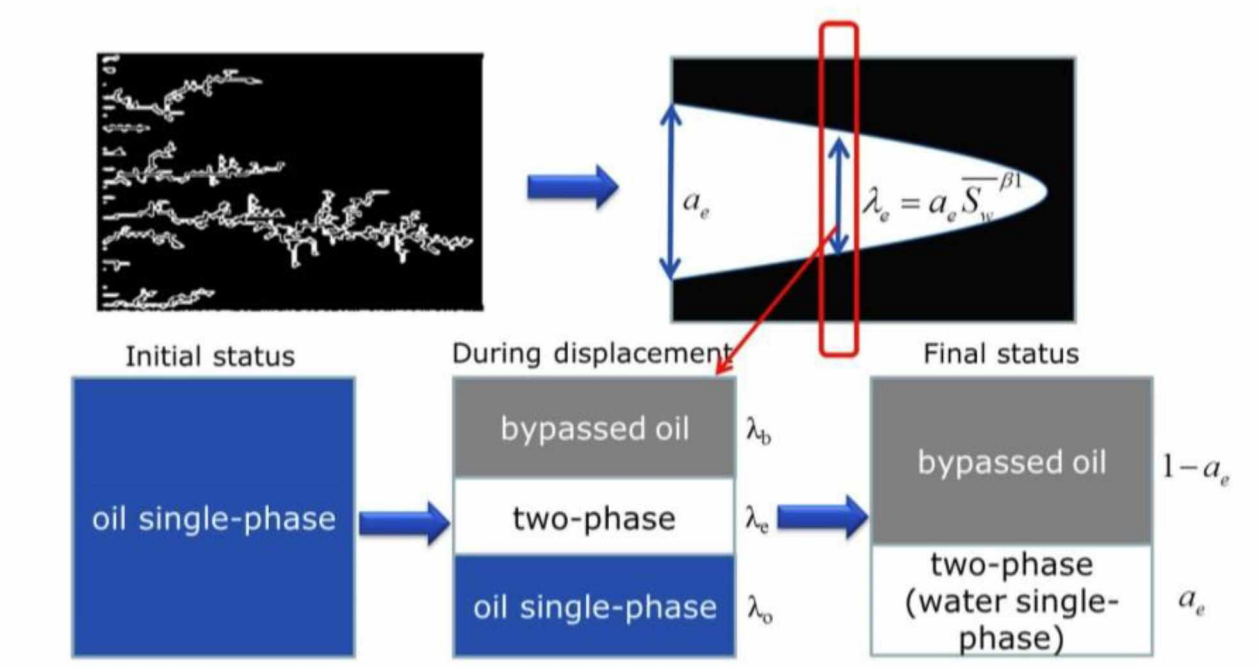

Figure 1.13-Schematic of the effective-fingering model [56]

In this study, a reservoir simulation model for the polymer flooding pilot in the Schrader Bluff heavy oil reservoir at the MPU has been developed and calibrated so that it is capable of predicting future polymer flooding performance and evaluating the economic success of the proposed EOR technique. The reservoir simulation model was developed based on the geological model and available reservoir and fluid data (i.e., PVT data, relative permeability, and polymer properties). Instead of directly simulating viscous fingers using fine grids, high transmissibility strips were introduced to connect the injectors and producers, simulating the short-circuiting flow behavior explainable by viscous fingering and reproducing the water cut history more efficiently. The validated simulation model has then been employed to investigate the oil recovery performance under different development strategies, with consideration for sensitivity to polymer parameter uncertainties. A polymer utilization parameter was used to evaluate the pilot's economic efficiency.

2. Polymer flooding

2.1. Relative permeability and capillary pressure curves

Petro-physical parameters such as porosity and permeability are important to understand the fluids saturation distribution and fluids flow behavior in the hydrocarbon reservoirs. More precisely, for reservoir simulation, relative permeability and capillary pressure curves are indispensable parameters to determine the multi-phase flow behavior in the reservoir model.

Porosity is defined as the fraction of the rock void space over the total volume. Permeability is defined by Darcy's Law (as shown in Equation 2.1) to measure the rock ability to transmit fluids when the porous media is completely saturated by a single fluid phase.

$$q = -\frac{KA}{\mu} \cdot \frac{dP}{dL} \qquad \text{Equation 2.1}$$

where q is the flow rate; K is permeability; A is the cross-section area; μ is the fluid viscosity; P is pressure; and L is length.

The porous media are generally saturated with two or more fluids in the hydrocarbon reservoirs, while each fluid phase will present a different effective permeability associated with a given saturation distribution. Relative permeability is defined as the ratio of the effective permeability to a base permeability (i.e., the absolute air permeability or the permeability of the oil phase at connate water saturation) for each fluid phase. When displacing a fluid phase by another, the saturation distribution changes, and the effective permeability of each fluid phase will correspondingly change, resulting in a relative permeability versus saturation curve. The relative permeability curve is usually measured from the core flooding experiments and then mapped into

the field-scale simulation model. Figure 2.1 presents the typical oil/water relative permeability curves for oil-wet and water-wet cores.

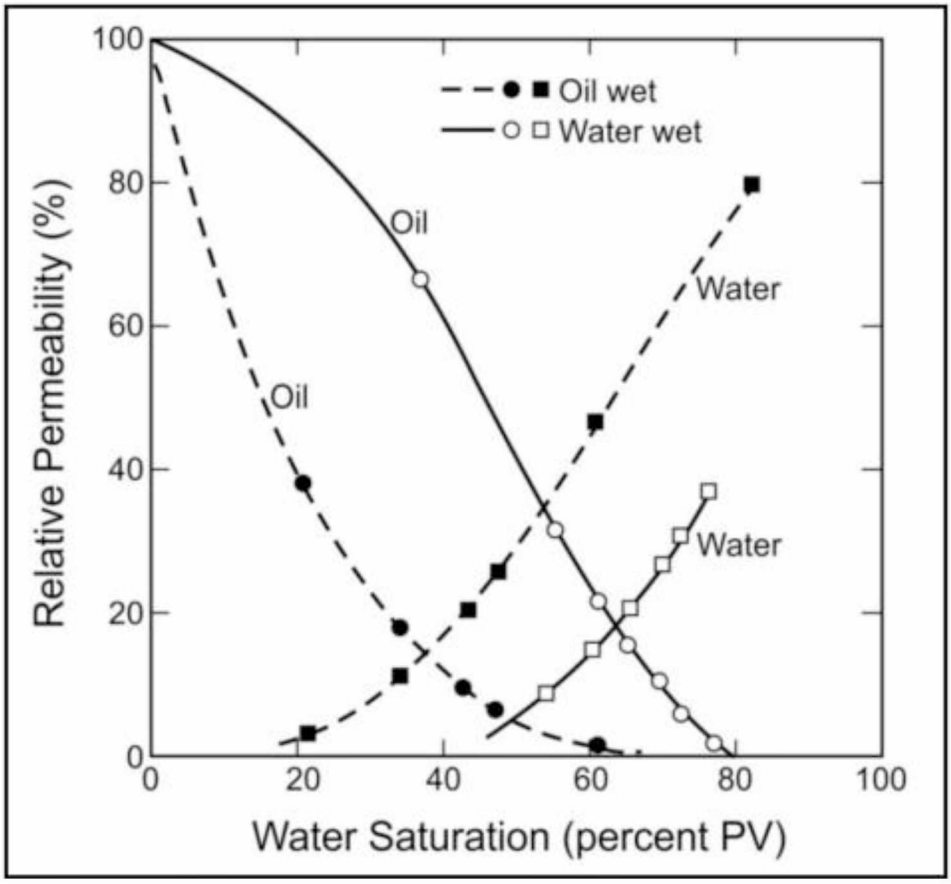

Figure 2.1-Typical oil/water relative permeability curves [60]

Capillary pressure is defined as the pressure difference across the interface of two immiscible fluids in the porous media, resulting from the interactions of forces between the fluids and rock. It can serve as a driving force when the rock is water-wet or an opposing force when the rock is oil-wet for waterflooding in the reservoir. The capillary pressure curve is measured on core samples by deploying porous plate (PP), centrifuge (CF), or mercury injection capillary pressure (MICP) test [61], which can give insight into the pore structures such as degree of sorting and pore throat distributions. Figure 2.2 shows a typical capillary pressure curve. However, laboratory tests are

expensive and time consuming. Only a limited number of core samples are used for testing, resulting in an incomplete reservoir description. Thus, the mathematical capillary pressure models have been developed over the last decades; the well-known capillary pressure model is J-function [62], a semi-empirical relationship incorporating the porosity and absolute permeability, as shown in Equation 2.2.

$$J(S_w) = \frac{P_c(S_w)}{\sigma} \cdot \sqrt{\frac{K}{\varphi}} \qquad \text{Equation 2.2}$$

where J is Leverett J-function; P_c is capillary pressure; σ is IFT; K is permeability; and φ is porosity.

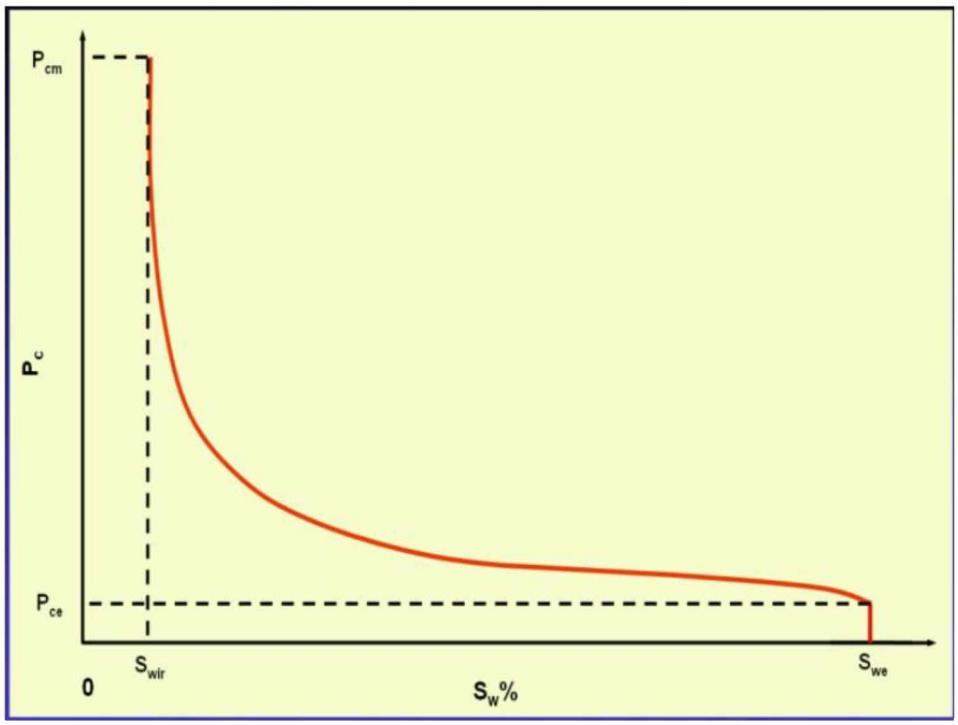

Figure 2.2-A typical capillary pressure curve [63]

2.2. Mobility and mobility ratio

The mobility ratio is widely used to measure the relative movement of fluids and describe the efficiency during a displacement process. It is defined as the ratio of the mobility of displacing

phase to the mobility of the displaced phase. Mobility of a fluid is defined as the effective permeability of the fluid divided by the fluid viscosity. The mobility ratio for waterflooding can be described as:

$$M = \frac{K_w/\mu_w}{K_o/\mu_o} = \frac{k_{rw}}{k_{ro}} \cdot \frac{\mu_o}{\mu_w} \qquad \text{Equation 2.3}$$

where M is mobility ratio; K_w is the effective permeability of water phase; K_o is the effective permeability of oil phase; μ_w is the water viscosity; μ_o is the oil viscosity; k_{rw} is the relative permeability of water phase; and k_{ro} is the relative permeability of oil phase.

The displacement process is considered stable if the mobility ratio is less than one, leading to an efficient recovery. Otherwise, it is considered unstable if the mobility ratio is greater than one, and viscous fingering is likely to take place during the unfavorable displacement process. Viscous fingering is a physical phenomenon that the arbitrary perturbation grows in the displacement front if the displacing phase is less viscous than the displaced phase. It can be visualized by monitoring the two-dimensional (2D) flood experiments in Bentheimer outcrop slabs through X-ray scanning [64]. Figure 2.3 illustrates the 2D X-ray images of viscous fingering for various oil-water viscosity ratios at different pore volume (PV) of injected water.

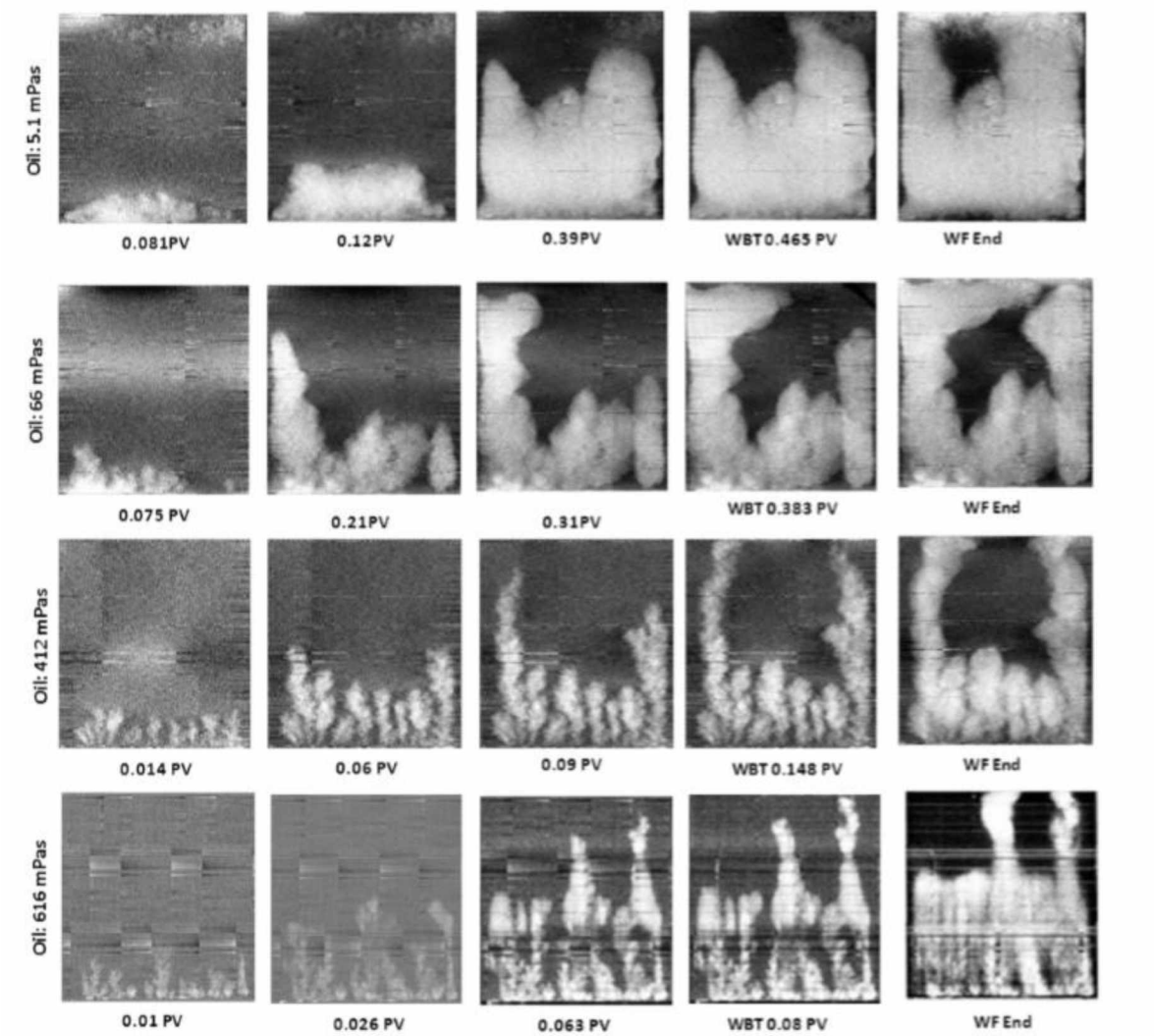

Figure 2.3-2D X-ray images of viscous fingering [64]

Numerical studies have also been conducted to understand the initiation and propagation of viscous fingers during the unstable displacement processes. Kumar et al.[65] employed fine-scale simulation models to investigate the effects of viscous fingers on field performance during waterflooding. The simulation results reveal that viscous fingers dominate oil recovery response at a higher mobility ratio, and the oil recovery reduces significantly at large adverse mobility contrast. The viscous fingers for different oil-water viscosity ratios using the fine-scale model are presented in Figure 2.4. As can be seen from this figure, multiple fingers have developed at the waterflood front

during the displacement processes, and the viscous fingers are likely to move faster at the higher viscosity ratio.

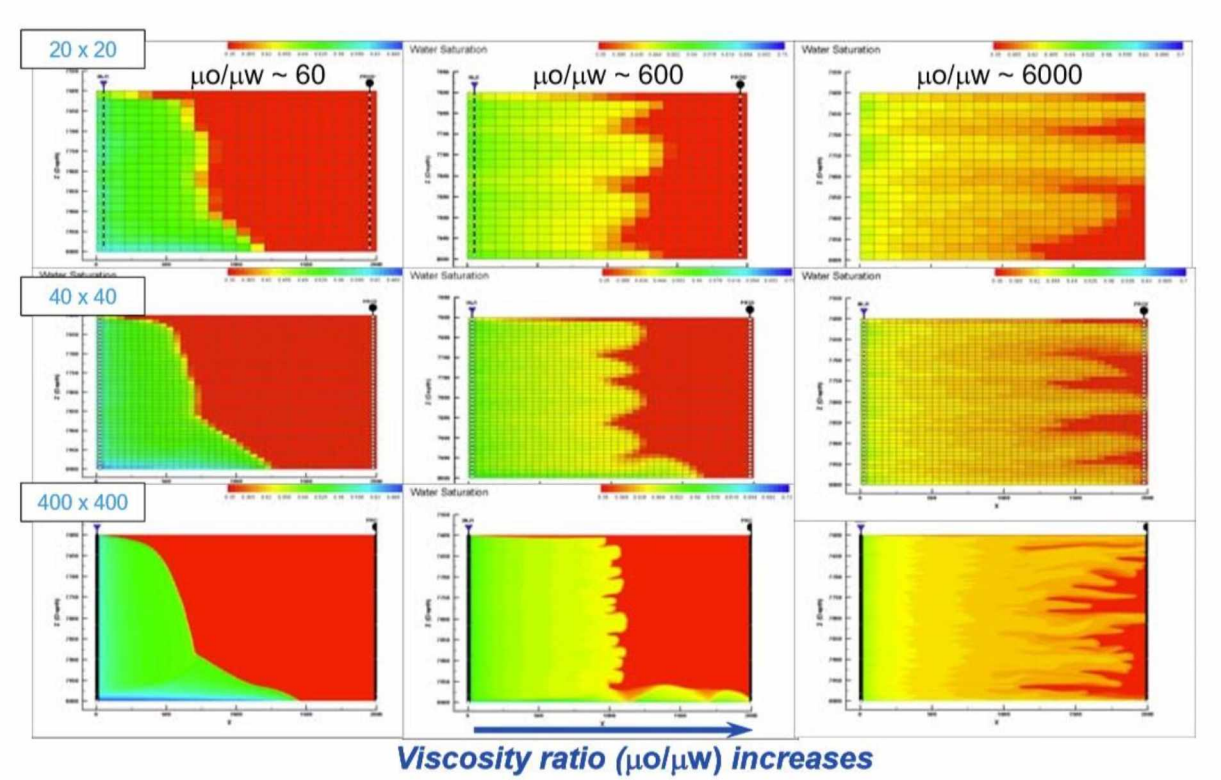

Figure 2.4-Simulation results of viscous fingering [65]

2.3. Polymer rheology

The sweep efficiency of waterflooding in heavy oil reservoirs is impaired by flow instability due to the unfavorable mobility contrast. Adding polymer can be used to increase water viscosity and improve mobility ratio, which reduces viscous fingering and enhances oil recovery.

In general, two types of polymer (i.e., synthetic polymers and biopolymers) have been applied to enhance oil recovery over decades. Partially hydrolyzed polyacrylamide (HPAM) is the most commonly used synthetic polymer, whereas xanthan gum is a typical biopolymer. Both HPAM and xanthan exhibit complex rheology when flowing in porous media, which is reported to show

almost stable viscosity at low shear rates, and shear-thinning behavior at moderate shear rates [66, 67]. Shear-thinning is that fluid viscosity decreases with increased shear rate, while shear-thickening is that fluid viscosity increases with increased shear rate. Xanthan is still shear-thinning at high shear rates. However, HPAM shows shear-thickening behavior at high shear rates, resulting from the viscoelastic response as polymer molecules flow through pore throats [68].

Many approaches have been developed to model polymer rheology in the past [69, 70]. The most common model to describe shear-thinning behavior is the Carreau model:

$$\mu_{app} = \mu_w + (\mu_p^0 - \mu_w)[1 + (\lambda\dot{\gamma}_{eff})^2]^{(n-1)/2} \quad \text{Equation 2.4}$$

where μ_{app} is the apparent polymer viscosity; μ_w is the water viscosity; $\dot{\gamma}_{eff}$ is the effective shear rate; λ and n are fitting parameters; μ_p^0 is the polymer viscosity at the absent of shear rate, which is modeled using the modified Flory-Huggins equation [71]:

$$\mu_p^0 = \mu_w[1 + (A_{p1}C_p + A_{p2}C_p^2 + A_{p3}C_p^3)C_{sep}^{S_p}] \quad \text{Equation 2.5}$$

where C_p is the polymer concentration; C_{sep} is the effective salinity; S_p is the salinity exponent; A_{p1}, A_{p2}, and A_{p3} are empirical constants obtained from laboratory data.

HPAM solution shows shear-thickening behavior at high shear rates in porous media, which cannot be characterized by the shear-thinning model. Delshad et al.[72] proposed a unified viscosity model for HPAM, covering a wide range of shear rate. The unified viscosity model consists of shear-thinning and shear-thickening:

$$\mu_{app} = \mu_w + (\mu_p^0 - \mu_w)[1 + (\lambda\dot{\gamma}_{eff})^2]^{(n-1)/2} + \mu_{max}\{1 - \exp[-(\lambda_2\tau_r\dot{\gamma}_{eff})^{n_2 - 1}]\} \quad \text{Equation 2.6}$$

where λ_2, τ_r, and n_2 are fitting parameters obtained by matching experimental data; μ_{max} is given as

$$\mu_{max} = \max[\mu_w(AP_{11} + AP_{22} \ln C_p)C_{sep}^{S_p}, 0] \quad \text{Equation 2.7}$$

where AP_{11} and AP_{22} are fitting parameters obtained from laboratory measurements.

Figure 2.5 represents the apparent viscosity of HPAM as a function of shear rate, which is calculated from Equation 2.6.

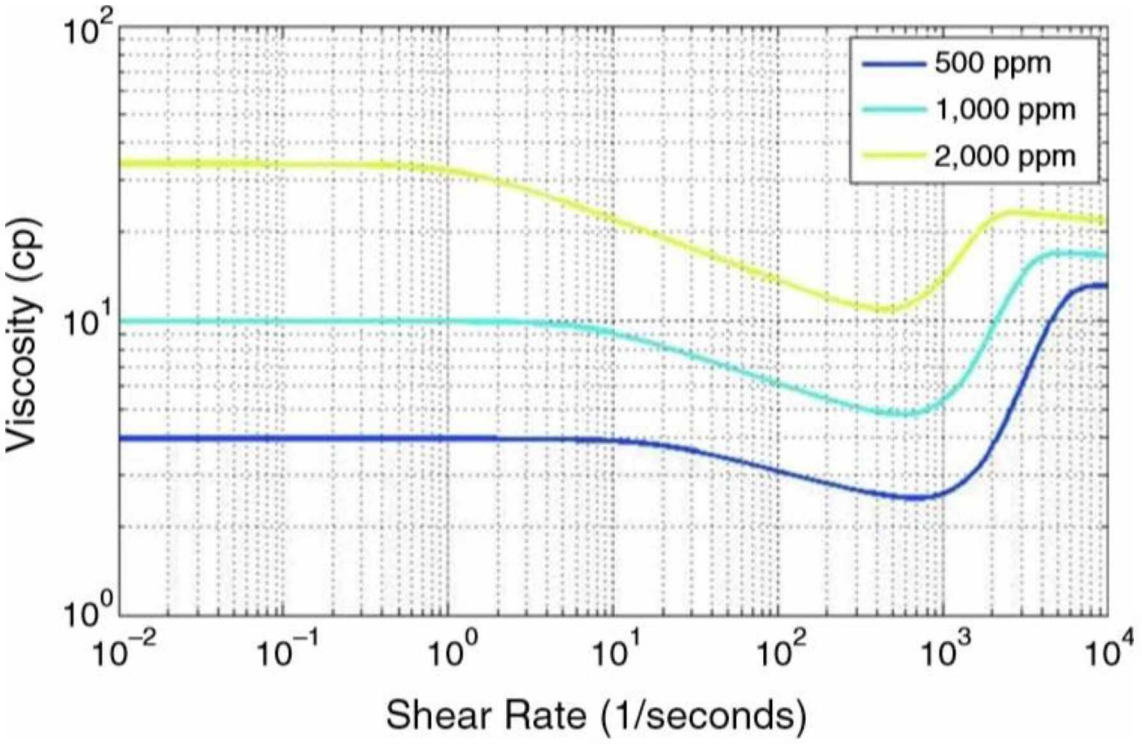

Figure 2.5-Schematic of rheology functions for HPAM solution at different polymer concentrations [73]

2.4. Polymer retention

Polymer retention is the effect of irreversible polymer adsorption, mechanical entrapment, and hydrodynamic retention in porous media [74], which can cause the reduction of polymer

concentration and affect the efficiency of polymer flooding. The schematic of polymer retention mechanisms in porous media is shown in Figure 2.6.

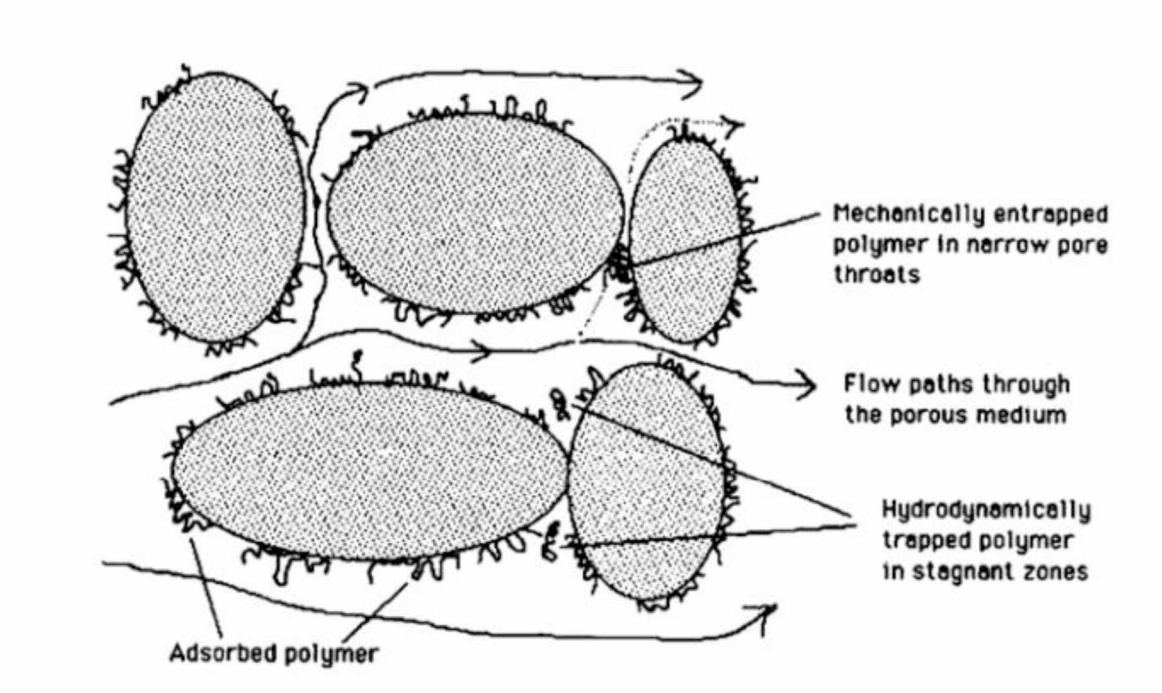

Figure 2.6-Schematic of polymer retention mechanisms in porous media [74]

Polymer adsorption is a physical phenomenon that polymer molecules bind and attach to the rock surfaces driven by van der Waal's and hydrogen bonding [75]. It occurs instantaneously when polymers flow into porous media and then diminish dramatically as maximum adsorption is satisfied. The Langmuir isotherm is commonly used to model polymer adsorption, which is a function of polymer concentration and water salinity:

$$C_{ads} = \frac{a_p C_p}{1 + b_p C_p} \qquad \text{Equation 2.8}$$

$$a_p = a_1 + a_2 C_{sep} \qquad \text{Equation 2.9}$$

where C_{ads} is the adsorbed polymer concentration; C_p is polymer concentration; C_{sep} is the effective salinity; a_1, a_2, a_p and b_p are empirical constants.

Mechanical entrapment refers to the larger polymer molecules that are lodged in the narrow pore throats. Hydrodynamic retention occurs at the stagnant zones, which is related to flow rate and tortuosity. The contribution of mechanical entrapment and hydrodynamic retention to total polymer retention is significantly affected by the pore structure.

2.5. Permeability reduction

Permeability reduction, mainly caused by polymer adsorption, has been observed in porous media during polymer flooding, which directly affects the flowability of the water phase [76]. The effective permeability of the water phase is expressed through the permeability reduction factor [77, 78]:

$$K_w^{eff} = \frac{K_w}{R_k} \quad \text{Equation 2.10}$$

$$R_k = 1 + (RRF - 1)\frac{C_{ads}}{C_{ads}^{max}} \quad \text{Equation 2.11}$$

where K_w^{eff} is the effective permeability of water phase; K_w is water permeability; R_k is the permeability reduction factor; C_{ads} is the adsorbed polymer concentration; C_{ads}^{max} is the maximum adsorbed polymer concentration; RRF is the residual resistance factor, which is a measure of the decrease in mobility of water phase after polymer injection [79],

$$RRF = \frac{\lambda_w}{\hat{\lambda}_w} = \frac{K_w}{\hat{K}_w} = \frac{\Delta\hat{P}_w}{\Delta P_w} \quad \text{Equation 2.12}$$

where λ_w, K_w, and ΔP_w are the mobility, permeability, and pressure drop of water phase before polymer injection, respectively; $\hat{\lambda}_w$, $\hat{K}_w$, and $\Delta\hat{P}_w$ are the mobility, permeability, and pressure drop of chase water after polymer injection, respectively.

2.6. Inaccessible pore volume

It has been reported that polymer molecules transport faster in porous media than the inert tracer species when there is no polymer retention [80, 81]. This phenomenon, referred to as inaccessible pore volume (IAPV), happens because large polymer molecules are not able to get in small pores during polymer flooding processes. IAPV is defined as the fraction of pore volume that polymer molecules cannot access. It depends on porosity, permeability, polymer molecular weight, and pore throat distribution. In terms of IAPV, large polymer molecules have negative effects on the sweep efficiency, which leave some oils unswept in the inaccessible pores. However, Seright et al.[82, 83] reported that polymer can access all the aqueous pore space in high permeability (>1 Darcy) sands, and IAPV is assumed to be zero in designing the polymer flood.

3. Reservoir modeling and validation

3.1. Pilot description

The polymer flooding pilot is located at the J-pad of the Milne Point field on ANS, as shown in Figure 3.1. The pilot program targets an isolated fault block in the Schrader Bluff NB-sands with two horizontal injectors (J-23A and J-24A) and two horizontal producers (J-27 and J-28), shown in Figure 3.2. The producing lengths of the horizontal wells range from 4200 to 5500 ft, and the average inter-well distance is 1100-1500 ft. The project wells were first put on waterflooding starting in June 2016, recovering about 7.6% of the original oil in place (OOIP) with a cumulative water injection of 0.09 PV. In August 2018, polymer solution injection commenced. Polymer solution, with a target viscosity of 45 cP, was introduced to both injectors by means of a polymer injection unit (PIU). By the end of December 2020, a total of 1.7 MMSTB of polymer solution has been injected, representing 0.08 PV in the flood pattern.

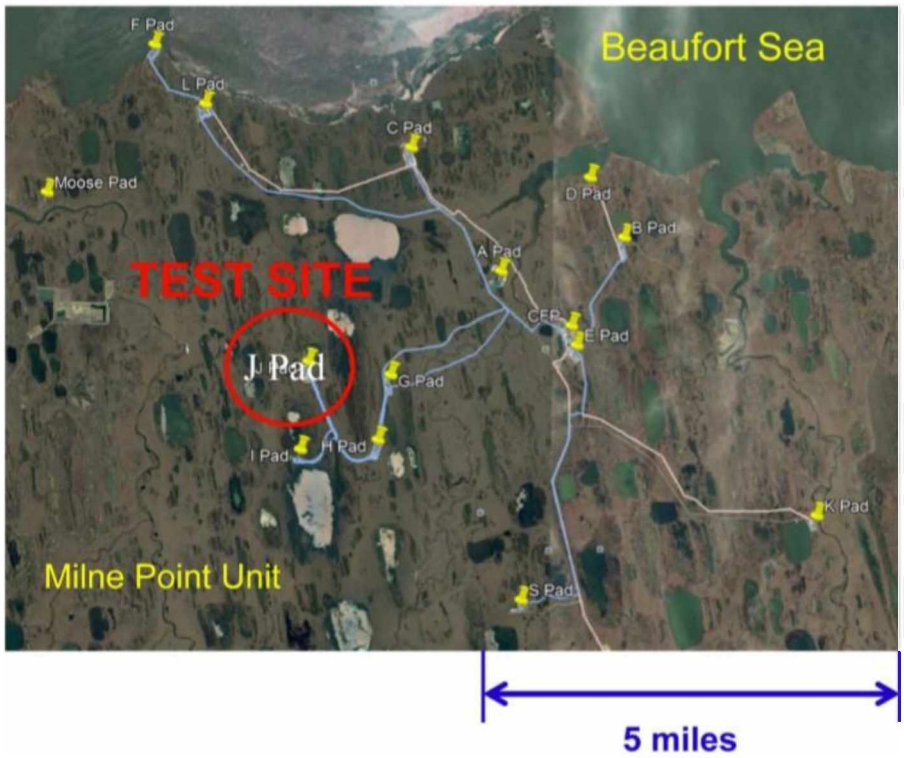

Figure 3.1-Location of the pilot area J-pad in MPU [50]

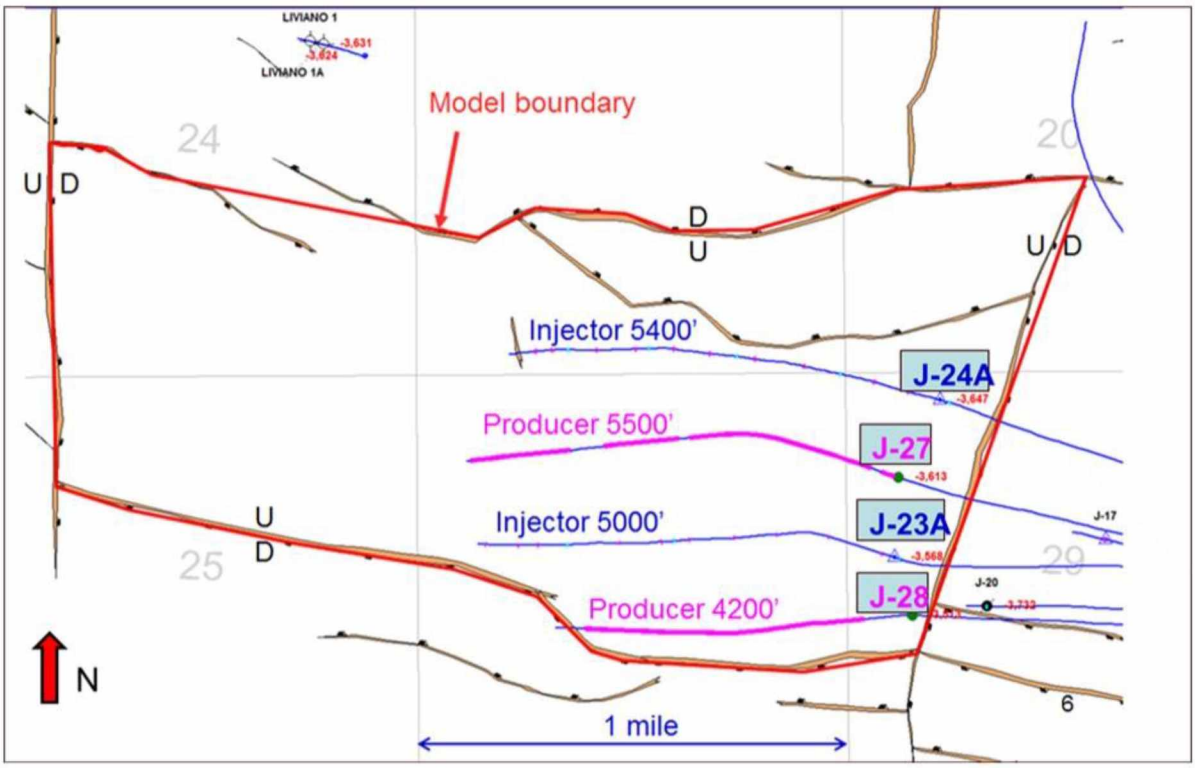

Figure 3.2-Polymer field pilot area boundary and injector-producer well patterns [50]

The water cuts and oil production rates of the two producers are depicted in Figures 3.3 and 3.4, respectively. A significant benefit of polymer flooding has been observed from the decrease in water cut from 65% to less than 15% in both producers. The oil production rate of producer J-27 (supported by both injectors) has increased continuously from 500 to 800 bopd in April 2019. The oil production rate of producer J-28 (supported only by J-23A to the north) also increased to about 700 bopd in late 2019, and stabilized at approximately 500 bopd in 2020.

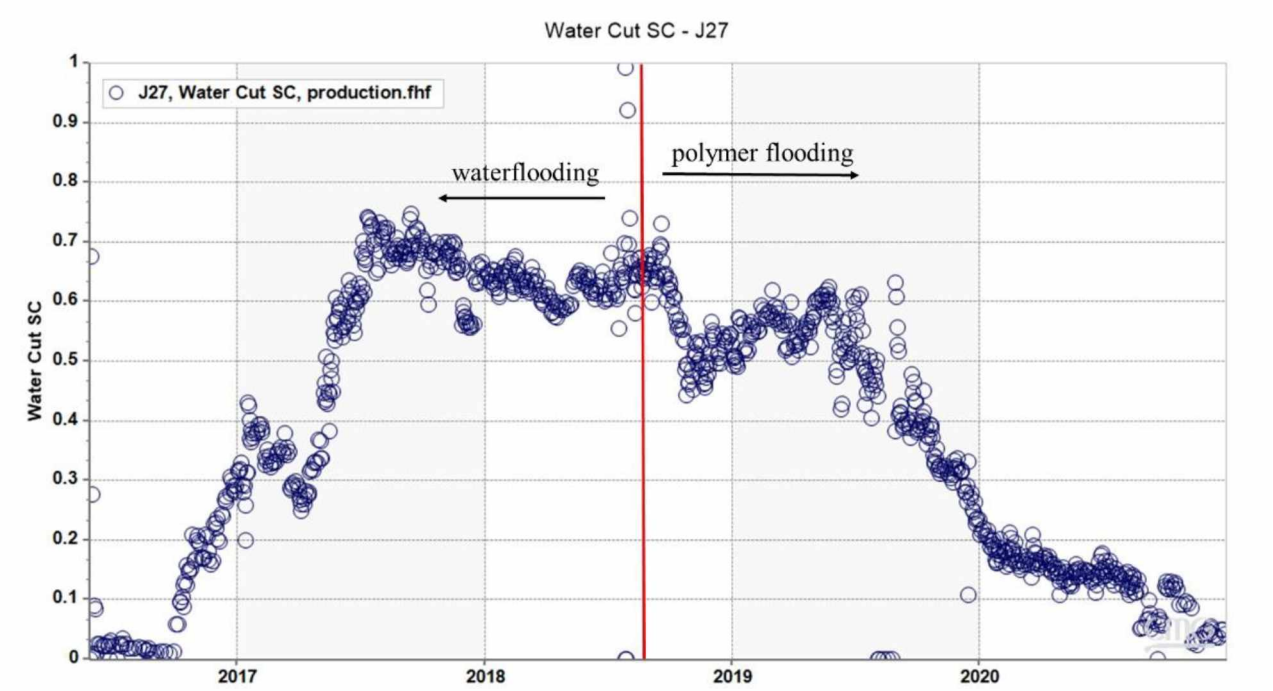

(a)

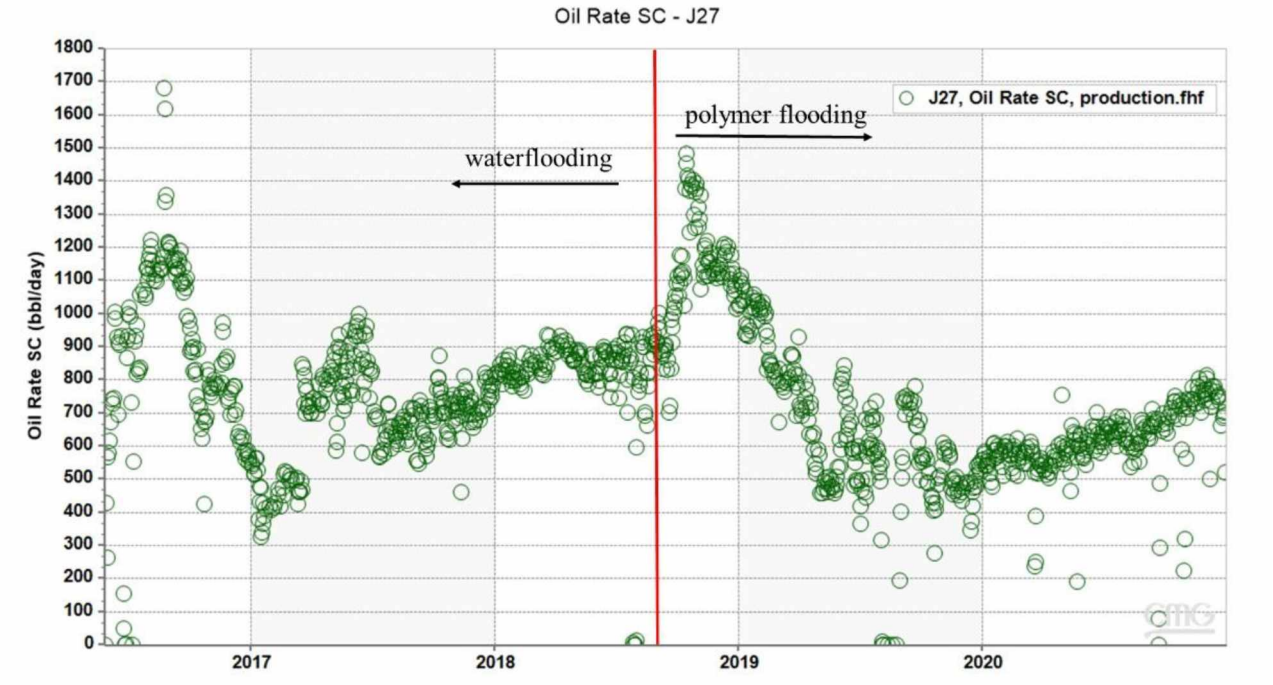

(b)

Figure 3.3-(a) water cut and (b) oil production rate for producer J-27

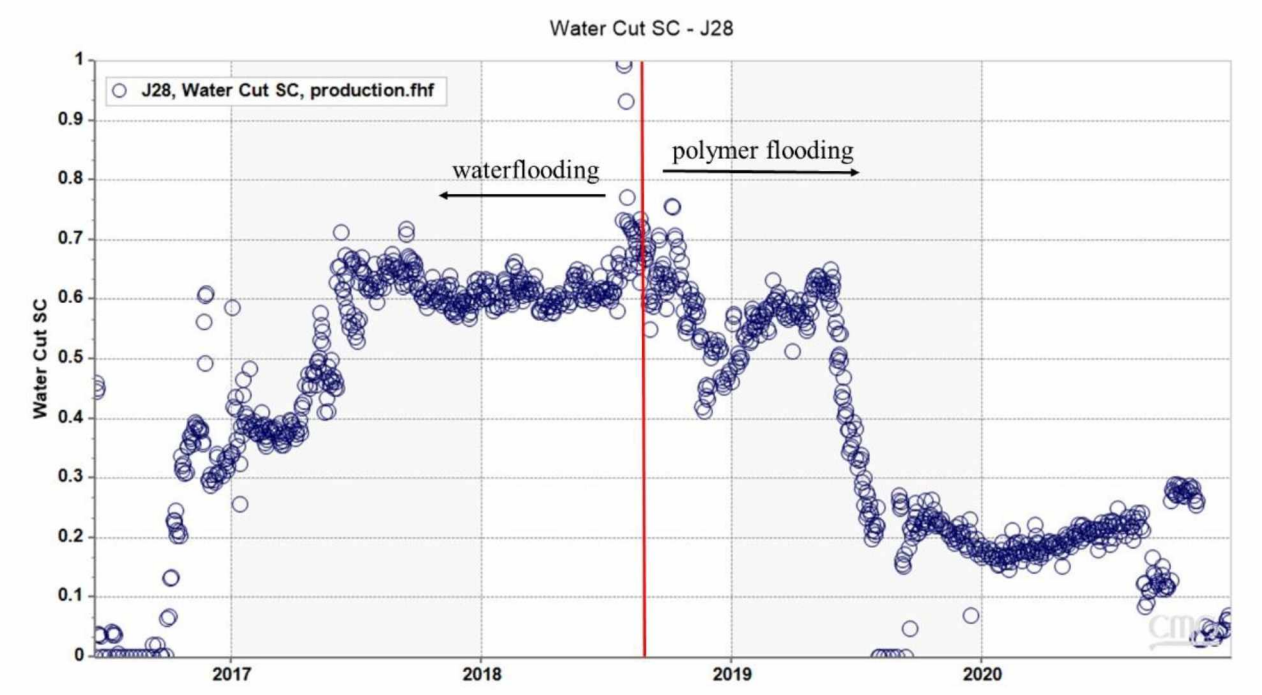

(a)

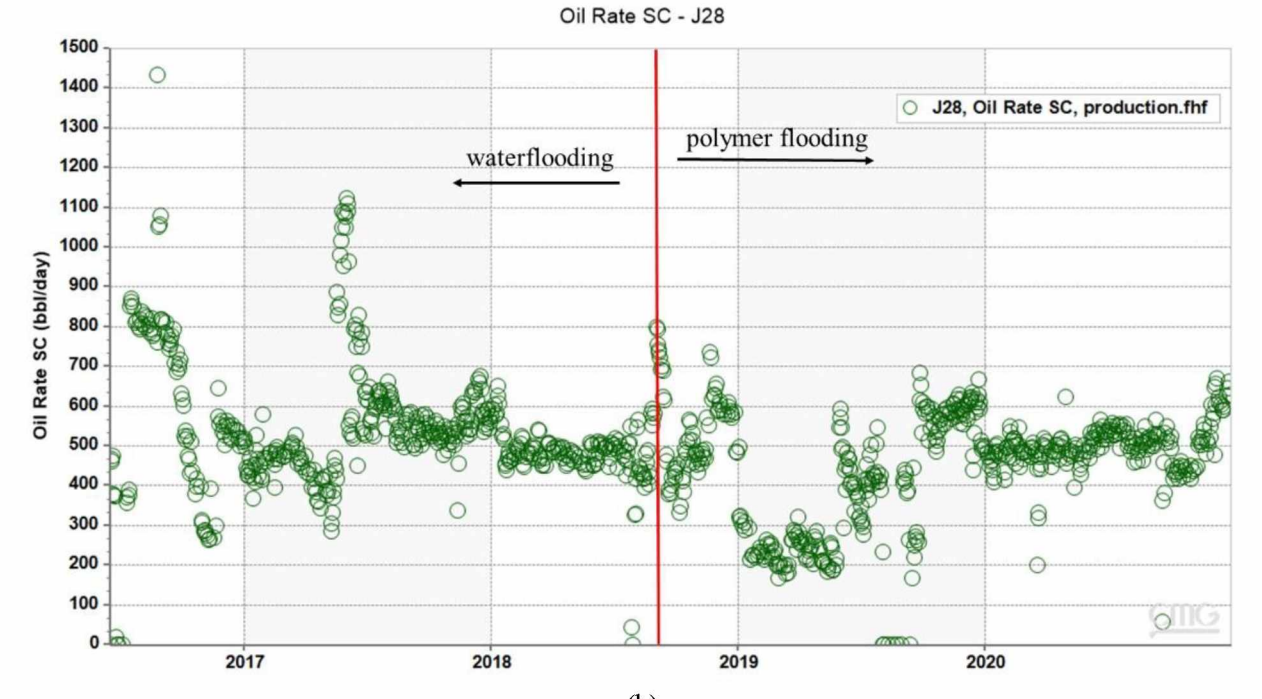

(b)

Figure 3.4-(a) water cut and (b) oil production rate for producer J-28

3.2. Reservoir modeling

3.2.1. Base reservoir model

A three-dimensional (3D) reservoir model including 193×221×8 grid blocks, as shown in Figure 3.5, has been developed for the pilot fault block, where the grey grid blocks are inactive, and the colored grid blocks are active to simulate the polymer flooding in the pattern. The selected active reservoir simulation model, including 23848 active grid blocks, covers the potential sweep area of our project wells. The 3D view of the selected active reservoir simulation model is shown in Figure 3.6. The approximate dimensions of the active reservoir simulation model are 6900 ft, 4100 ft, and 15 ft in the x, y, and z directions, respectively. The reservoir simulation model consists of eight layers in the z-direction. Each layer's basic properties are listed in Table 3.1, and other common reservoir properties are listed in Table 3.2.

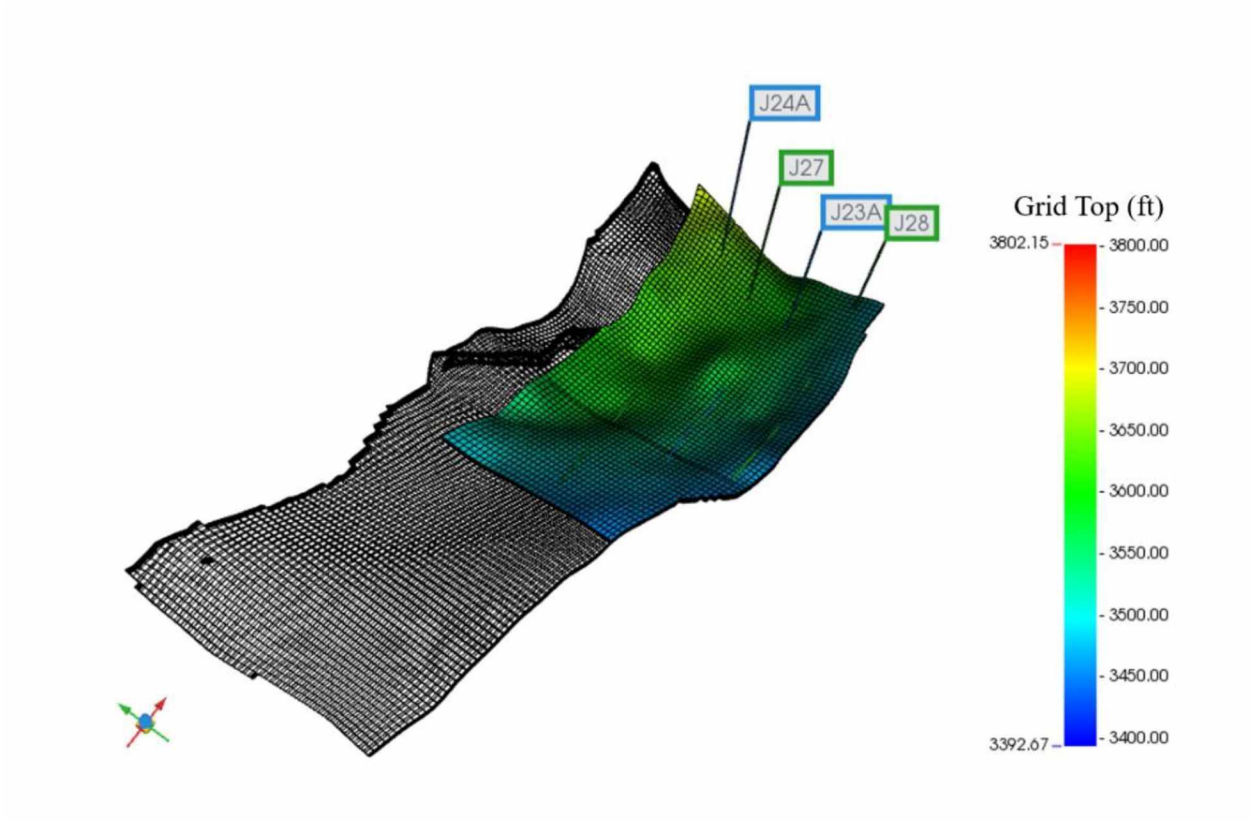

Figure 3.5-The grid top diagram of the entire J-pad reservoir model (Courtesy of Dr. Radu Girbacea with Hilcorp)

Table 3.1-Basic properties for the eight layers

Layer	Thickness (ft)	Permeability (mD)	Porosity (%)
1	2.0	1791	34.6
2	1.8	1958	34.7
3	2.0	2000	35.0
4	1.9	1826	34.9
5	1.8	1935	35.3
6	1.8	1668	34.7
7	1.9	1572	34.7
8	1.8	1510	34.2

Table 3.2-Common reservoir properties

Parameter	**value**
API °	15.4
Oil viscosity (cP)	332
Reservoir depth (ft)	3600
Reservoir thickness (ft)	15
Initial reservoir pressure (psi)	1600
Bubble point pressure (psi)	1303
Reservoir temperature (°F)	70
Rock compressibility (1/psi)	30E-6

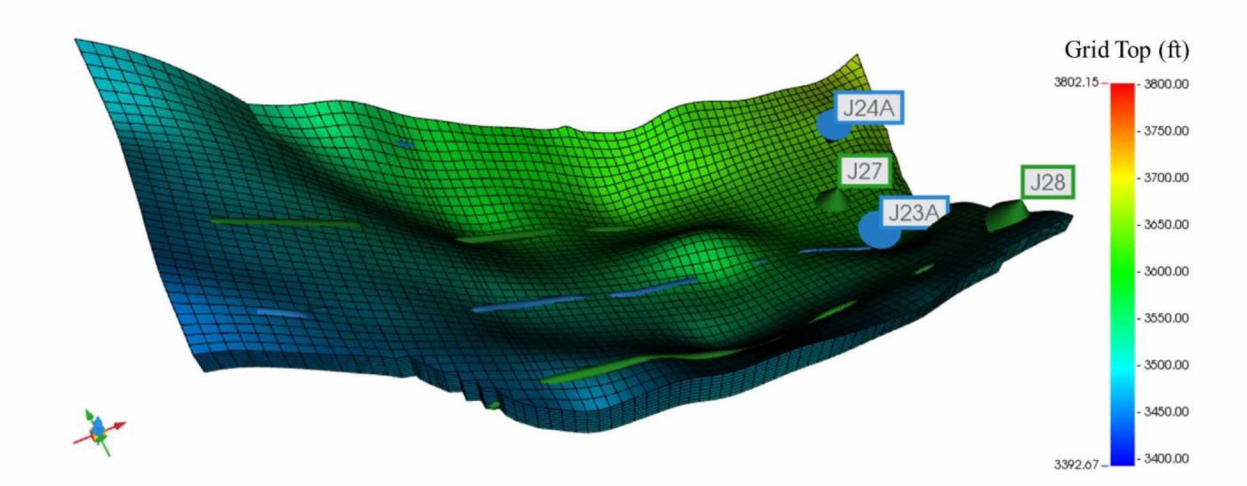

Figure 3.6-3D view of the selected active reservoir simulation model

3.2.2. High transmissibility strips

The early water breakthrough and high water cut during the pre-polymer waterflooding period indicate strong communication and short-circuiting behavior between the injecting and producing wells. Pre-polymer tracer studies confirm this. To simulate this short-circuiting effect, four high transmissibility strips at different locations and with different widths were introduced to "connect" the injectors and producers in the reservoir simulation model. Each strip is present in all eight layers of the model such that the strips in each layer are identical. As an example, the high transmissibility strips in layer 1 are illustrated in Figure 3.7. The high transmissibility strips are divided into twelve zones (a-l). In the base model, the initial transmissibility multiplier values are set to 1; these transmissibilities will be tuned respectively to conduct the history matching process.

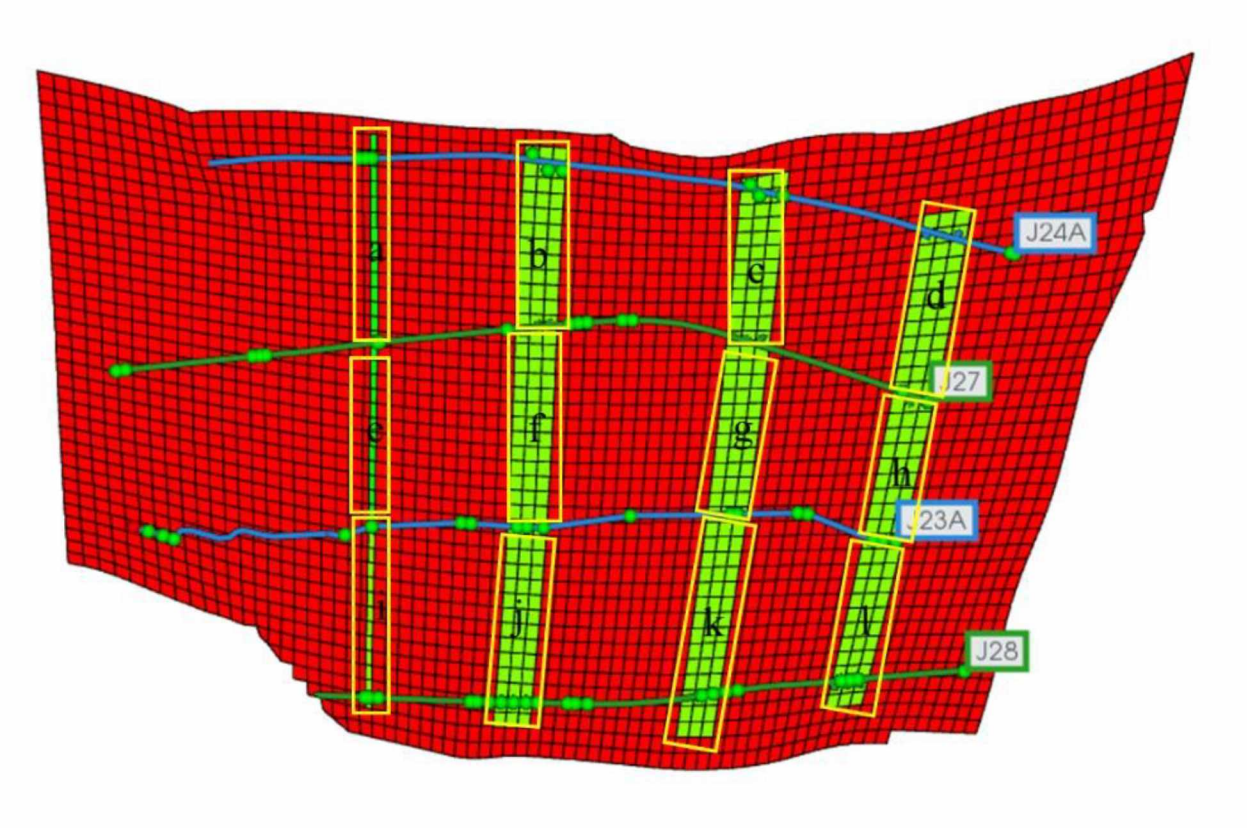

Figure 3.7-High transmissibility strips in layer 1

3.2.3. Rock-fluids data

Cores and fluid samples were collected from the Schrader Bluff formation near the project area. The cores and fluids samples were used to obtain PVT properties, relative permeability curves, and capillary pressure curves through laboratory tests. The oil/water relative permeability curves are presented in Figure 3.8. The Leverett J-function, which was converted from the measured capillary pressure curve, is shown in Figure 3.9.

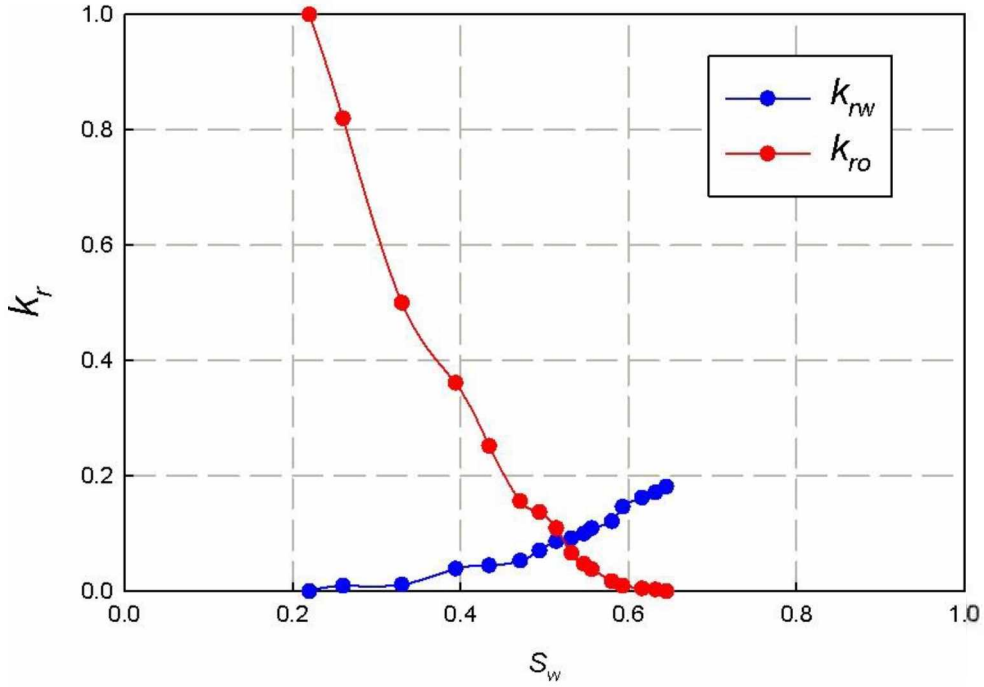

Figure 3.8-Oil/water relative permeability curve (Courtesy of Hilcorp Alaska)

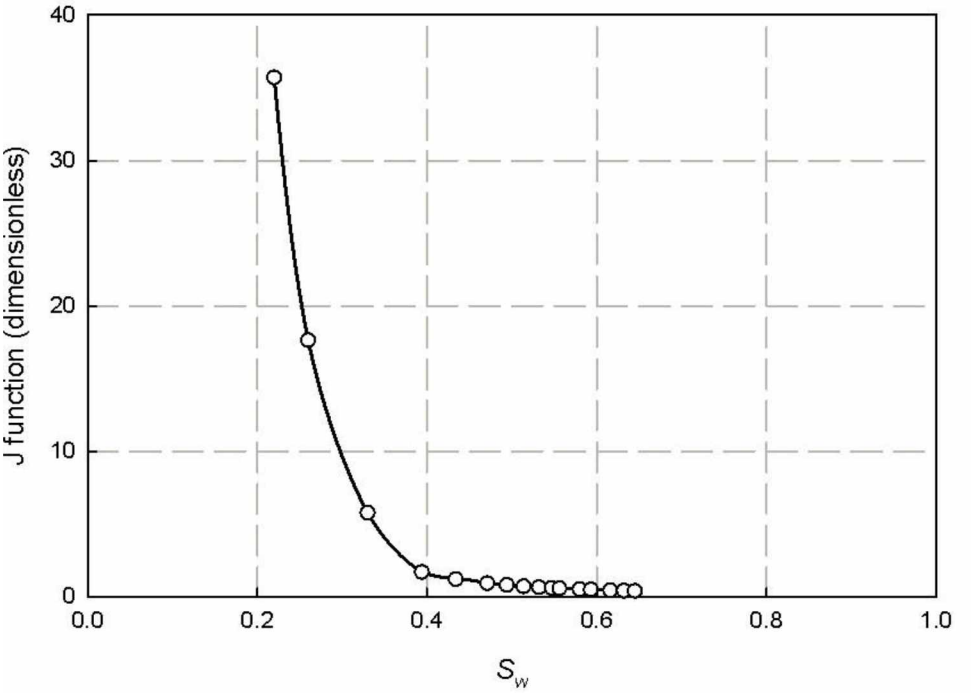

Figure 3.9-Leverett J-function (Courtesy of Hilcorp Alaska)

3.2.4. Polymer flooding data

HPAM polymer, in this case, Flopaam (FP) 3630s, was selected and used to prepare the polymer solution. The relationship of polymer viscosity with polymer concentration and shear rate, presented in Figure 3.10, was measured at 25°C in the laboratory. The injected polymer concentration was initially set to 1800 ppm with a target viscosity of 45 cP. After 600 days of polymer injection, the concentration was reduced to its current 1200 ppm target.

As can be seen from Figure 3.10(b), the viscosity of polymer solution has a high Newtonian plateau when the shear rate is very low, and then decreases under shear strain, which is modeled by the piecewise function:

$$\mu_{app} = \mu_{sw} \quad \text{for } \nu \leq \nu_{ref} \qquad \text{Equation 3.1}$$

$$\mu_{app} = \mu_{sw} \times \left(\frac{\nu}{\nu_{ref}}\right)^{n-1} \quad \text{for } \nu_{ref} < \nu < \nu_{upper} \qquad \text{Equation 3.2}$$

$$\mu_{app} = \mu_{w} \quad \text{for } \nu \geq \nu_{upper} \qquad \text{Equation 3.3}$$

where μ_{app} is the apparent viscosity of the polymer solution; μ_{sw} is the polymer-water mixture viscosity in the absence of shear thinning; μ_w is the water viscosity in the absence of polymer; ν_{ref} and ν_{upper} are the lower and upper velocity boundaries of the shear thinning regime, respectively; ν is the shear velocity; and n is the exponent.

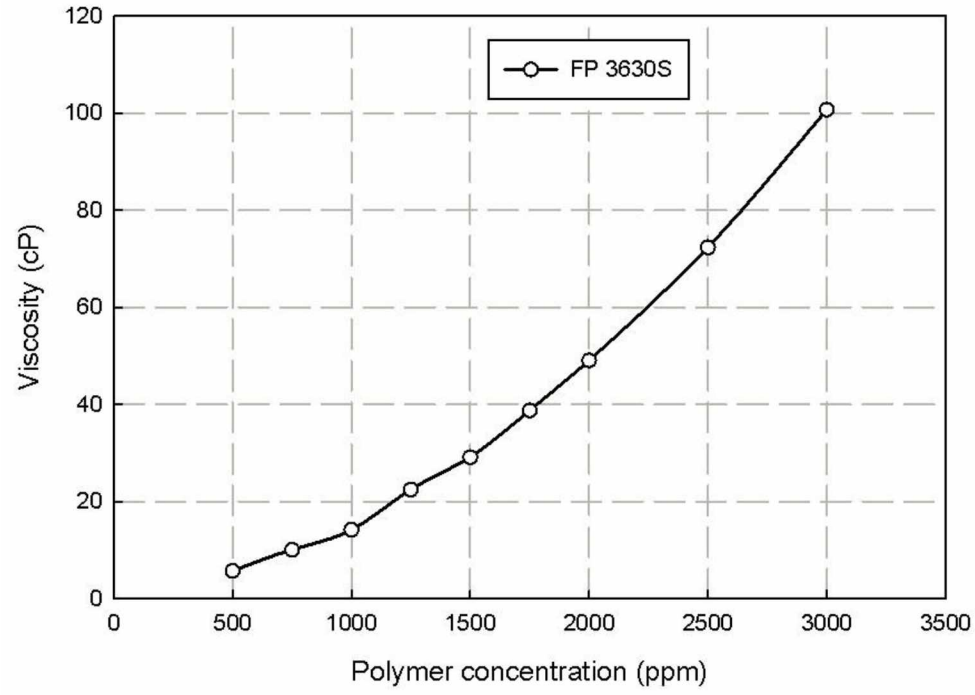

(a)

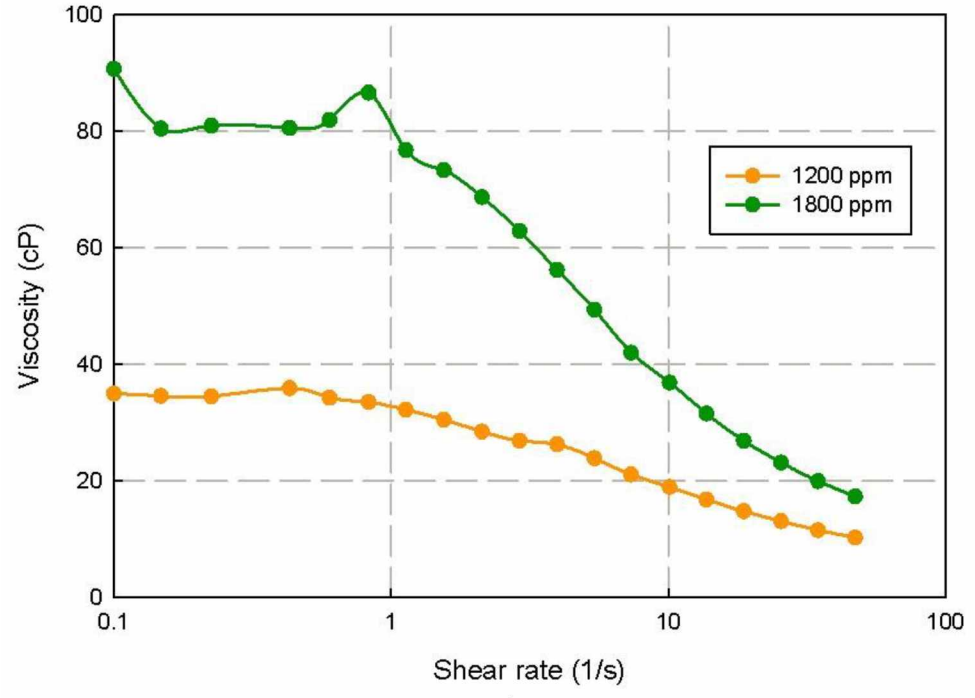

(b)

Figure 3.10-Polymer solution properties: (a) polymer loading curve (Courtesy of Hilcorp Alaska) and (b) shear viscosity curve (Courtesy of Dr. Dongmei Wang with University of North Dakota)

In the reservoir simulation model, the viscosity of the polymer solution as a function of polymer concentration and shear rate, as shown in Figure 3.11, was generated using $v_{ref} = 0.83$ and $n = 0.71$, which were obtained by fitting the polymer shear viscosity data measured in the laboratory.

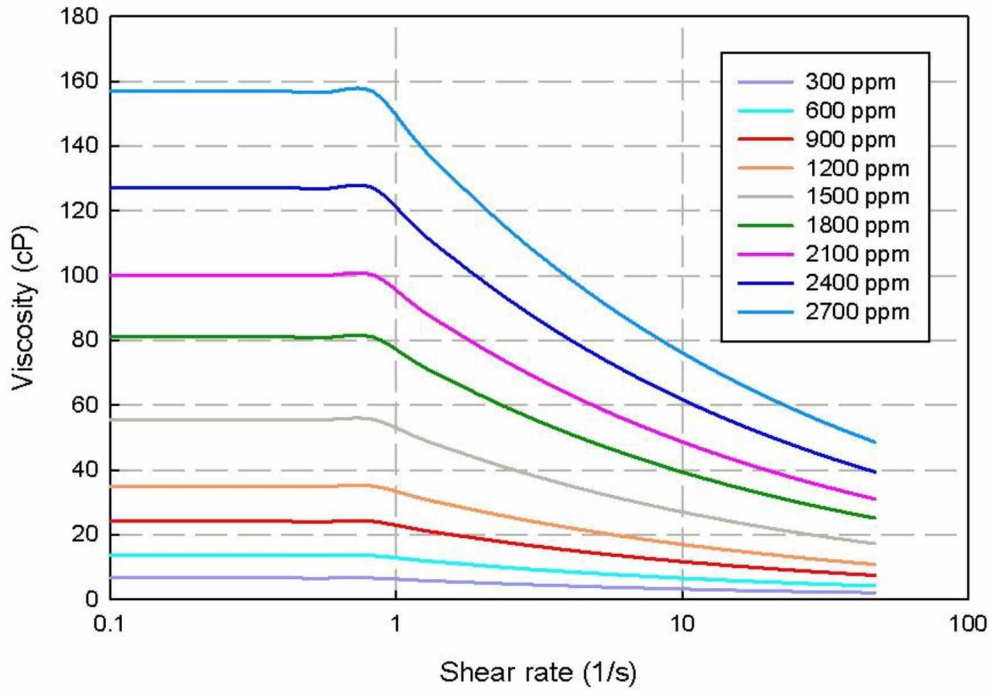

Figure 3.11-Shear effect on polymer solution viscosity at different polymer concentrations

Polymer retention experiments on the NB-sand in the Schrader Bluff formation have been carried out in the laboratory using the nitrogen chemiluminescence analysis method. The results indicate that the polymer retention values range from 28 to 533 µg/g [83]; a moderate value of 153 µg/g was used in the simulation model. The polymer retention can also decrease the mobility of the aqueous phase, reducing its effective permeability. This is described through RRF in the simulation process. Laboratory experiments indicated that this effect is negligible for the NB-sand, so a value of 1 for RRF was adopted in the simulator.

3.3. Model validation

The developed reservoir simulation model has been calibrated by history matching. During the simulation, the oil production rates for both J-27 and J-28 were constrained to honor the measured oil production rates shown in Figures 3.3(b) and 3.4(b). This is because the oil production rate is measured the most accurately by the operator and will have the greatest impact on the economics of the project. The injection rates for both J-23A and J-24A were constrained to honor the actual injection rate profiles, as shown in Figure 3.12. In addition, the maximum bottom-hole pressures (BHPs) for both injectors were set to 2700 psi, while the minimum BHPs for both producers were set to 500 psi in the waterflooding and polymer flooding periods.

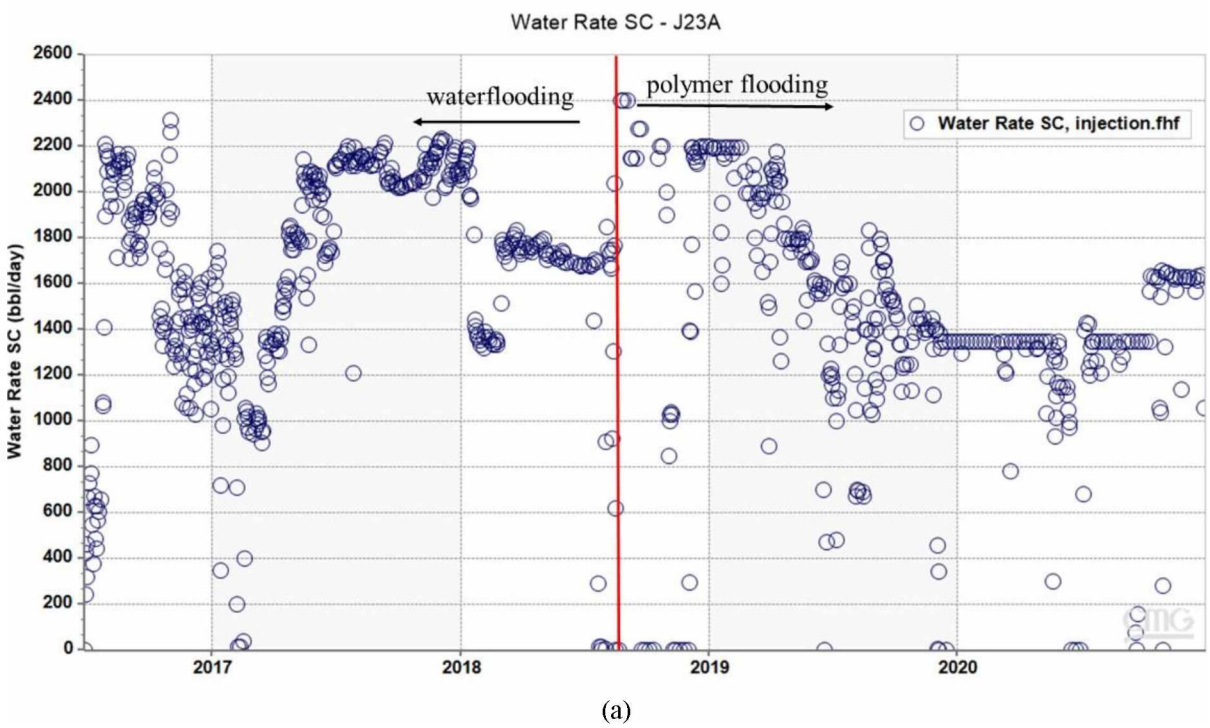

(a)

Figure 3.12-Injection rate profiles for (a) J-23A and (b) J-24A

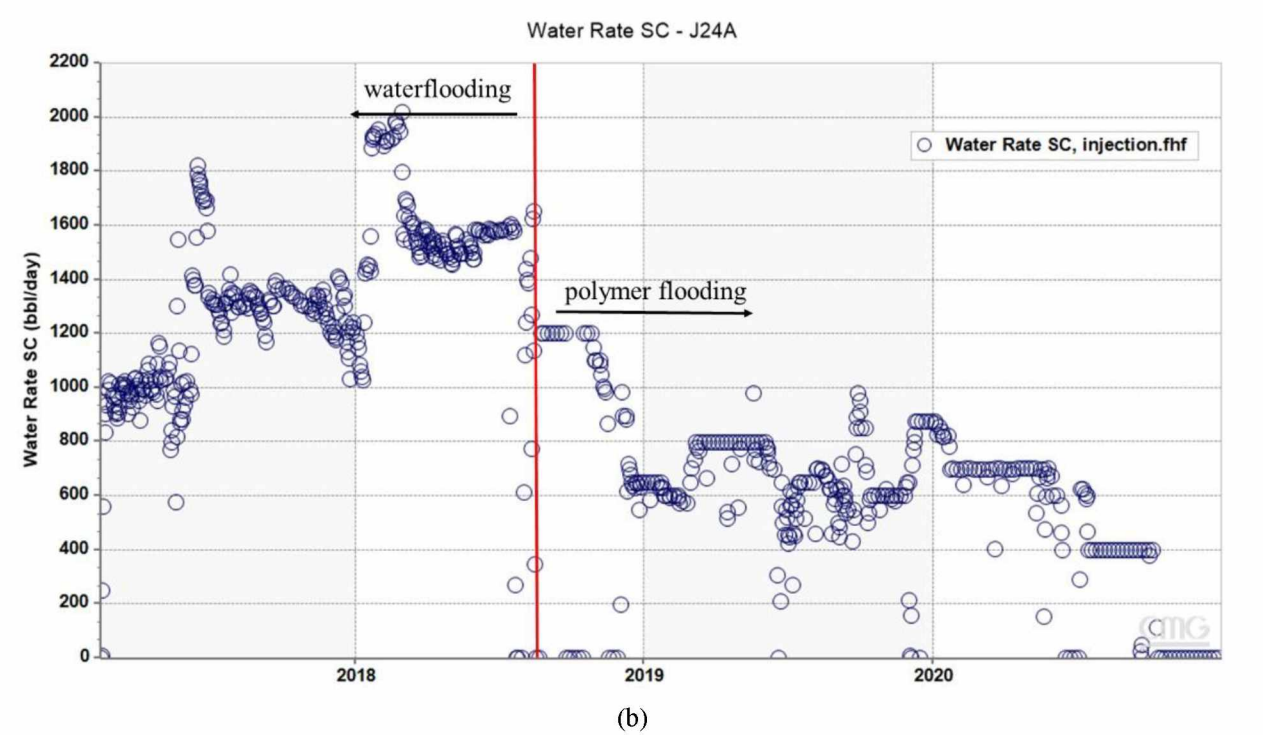

(b)

Figure 3.12 continued-Injection rate profiles for (a) J-23A and (b) J-24A

We conducted a comprehensive sensitivity analysis and found that the water cut behavior is highly sensitive to the transmissibility contrasts introduced by the high transmissibility strips. Thus, the transmissibility multipliers of the twelve high transmissibility strip zones (a-l), as shown in Figure 3.7, were manually tuned individually to match the water cut in the history matching process. The measured relative permeability curves, as shown in Figure 3.8, were also slightly tuned to adjust the mobility of the aqueous phase.

3.4. Performance prediction

After history matching, the validated reservoir simulation model was employed to forecast the oil recovery performance of the polymer flooding pilot under different development strategies, with consideration to sensitivity to polymer parameter uncertainties. The tested development strategies are listed in Table 3.3.

Table 3.3-Tested development strategies

	Test #1	Test #2	Test #3
Polymer concentration (ppm)	**300 - 2700**	1200	1200
Polymer retention (μg/g)	153	**50 - 400**	153
Injection rate (bbl/day)	1950	1950	**1450 - 2450**

3.5. Polymer EOR efficiency

Polymer EOR efficiency analysis was conducted to assess the economic feasibility of the polymer flooding pilot and identify the most beneficial development strategies (listed in Table 3.3). The incremental oil production and injected polymer amount are significant to the polymer EOR efficiency. The polymer utilization parameter is useful in evaluating these two parameters in relation to each other. Polymer utilization is defined as the ratio of cumulative polymer injection to cumulative incremental oil production, as shown in Equation 3.4. This represents how much polymer must be injected in order to produce an additional barrel of oil and thus is a measure of the efficiency of the polymer.

$$\text{polymer utilization} = \frac{\text{cumulative polymer injection (lb)}}{\text{cumulative incremental oil production (bbl)}} \qquad \text{Equation 3.4}$$

Polymer utilization has been studied to evaluate the performance of a polymer flood in different polymer pilots around the world. It is reported that polymer utilization ranges between 3.86 lbs/bbl and 5.37 lbs/bbl in the heavy oil Tambaredjo field in Suriname [84]. In the Pelican Lake field, the polymer utilization is approximately 2.93 lbs/bbl [85]. What's more, the polymer utilization of FP 3630s, the same polymer used in this project, is about 3.81 lbs/bbl for a polymer pilot in Grimbeek II field in Argentina [86, 87].

4. Reservoir simulation results and discussion

4.1. Initial simulation results

An initial run was conducted to compare the unconstrained (not history matched) simulation results with the actual production data; the water cuts of both producers obtained from the initial run are depicted in Figure 4.1. The open circles are field observations, and the solid lines represent the simulation results.

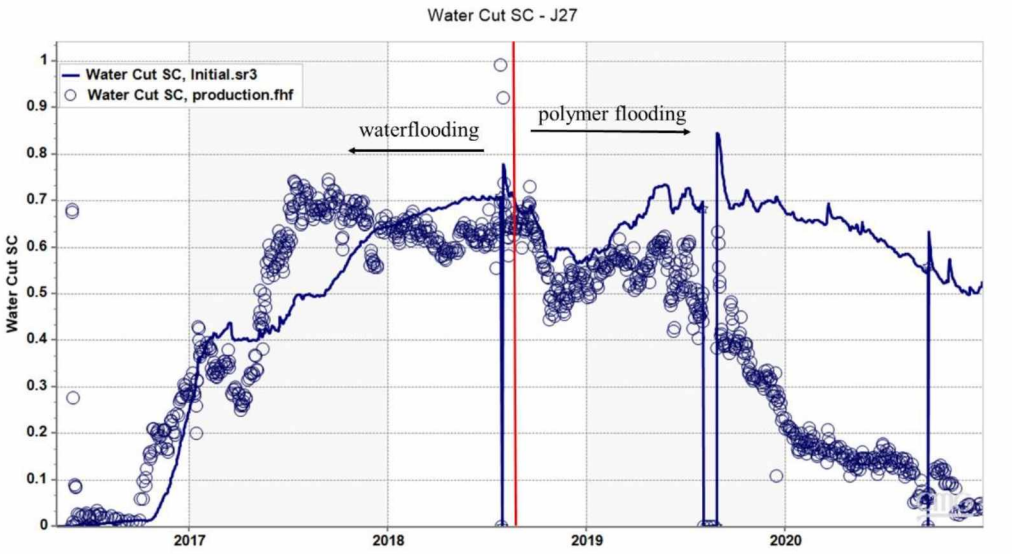

(a)

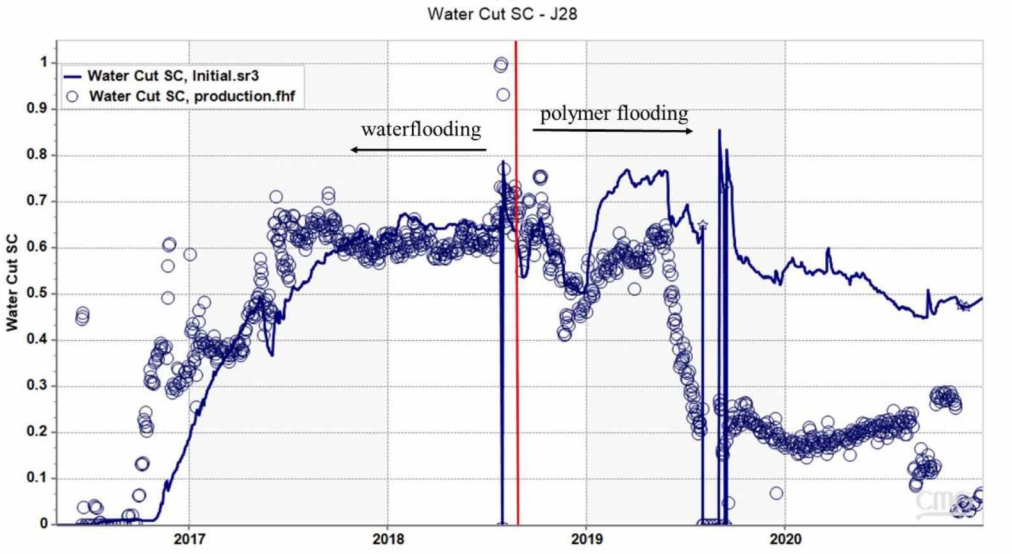

(b)

Figure 4.1-Initial simulation results of water cut for (a) producer J-27 and (b) producer J-28

As can be seen, during the water flooding period, the water cuts show sharp increases after water breakthrough in the producers, while the simulated water cuts increase more gradually. After injecting polymer, the actual water cuts reduce considerably, falling from 65% to less than 15% at both producers by June 2019. This field behavior is a result of the lower mobility polymer solution reducing the short-circuiting effects and restoring injection conformance, consistent with the concept of a reduction in viscous fingering effects. Although the simulated water cuts also decrease in the corresponding timeframe, the reduction is much less dramatic, demonstrating that the simulator is not accurately capturing the phenomenon behind the actual conformance restoration.

4.2. History matching results

4.2.1. Water cut

The HM results for the producing water cut from both J-27 and J-28 are presented in Figure 4.2. The open circles are field observations, and the solid lines represent the history matching results. It can be seen that the sharp increase in water cut after water breakthrough observed at both producers has been accurately reproduced by employing the high transmissibility strips in the reservoir simulation model. In the polymer flooding period, the transmissibility multipliers of the strips have been tuned with the polymer injection time to improve the HM results. This approach leads to the simulated results that match the field observations and achieve the extremely low water cuts in the polymer flooding period.

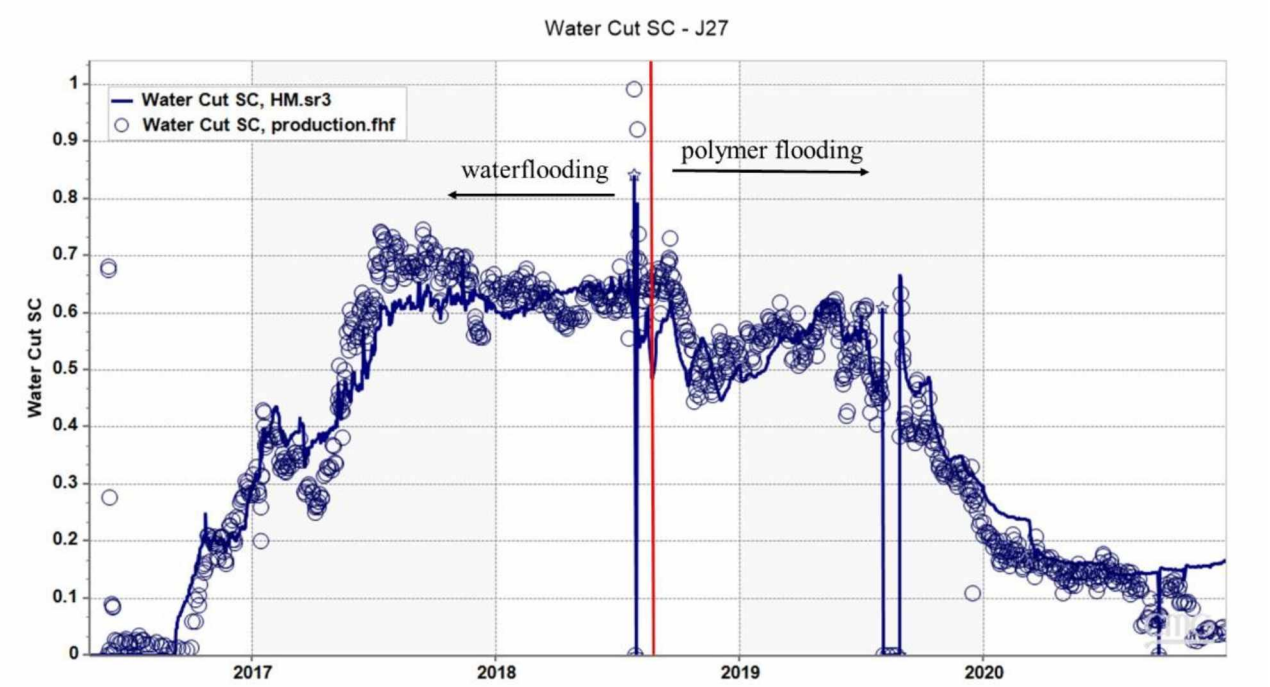

(a)

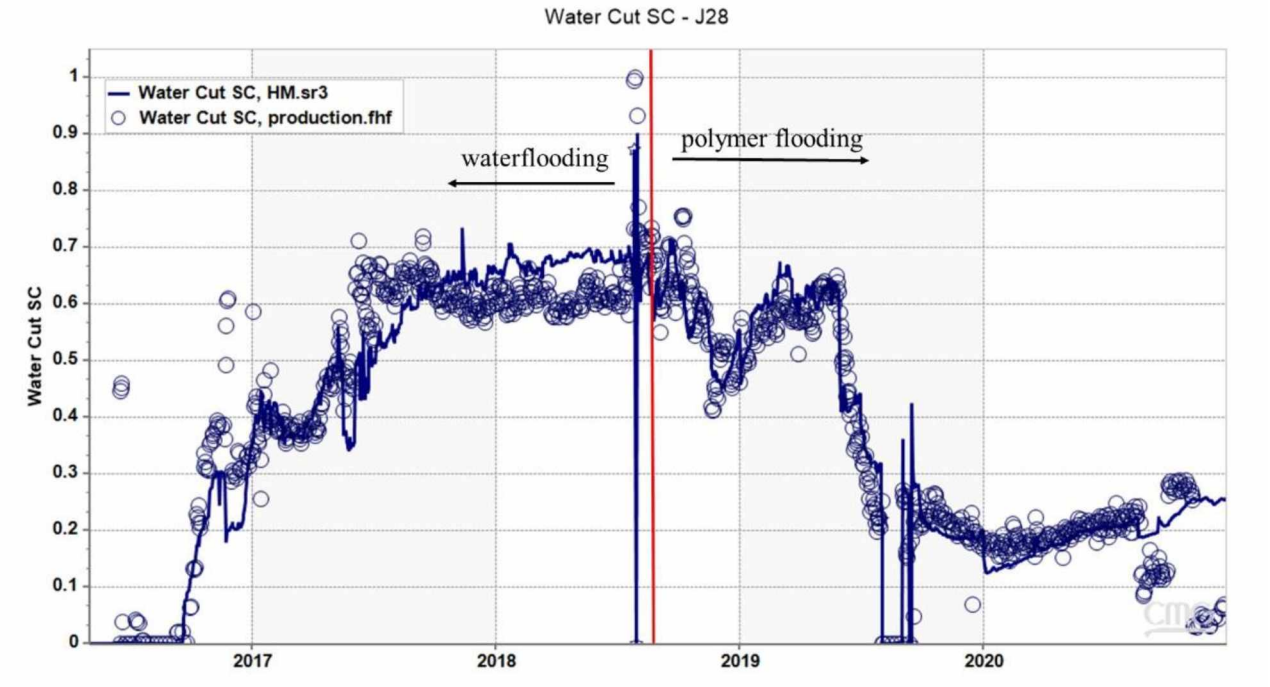

(b)

Figure 4.2-HM results of water cut for (a) producer J-27 and (b) producer J-28

4.2.2. Relative permeability modification

In the HM process, the oil/water relative permeability was modified using the power-law equations,

$$k_{rw} = k_{rw}^{*} \left(\frac{S_w - S_{wc}}{1 - S_{wc} - S_{or}} \right)^{e_w} \quad \text{Equation 4.1}$$

$$k_{ro} = k_{ro}^{*} \left(\frac{1 - S_w - S_{or}}{1 - S_{wc} - S_{or}} \right)^{e_o} \quad \text{Equation 4.2}$$

where k_{rw} and k_{ro} are water and oil relative permeability, respectively, S_w is water saturation, S_{wc} and S_{or} are critical water saturation and residual oil saturation, k_{rw}^{*} and k_{ro}^{*} are the endpoints of water and oil relative permeability curves, respectively, and e_w and e_o are exponents that determine the curvature of water and oil relative permeability curves.

The updated oil/water relative permeability curves, shown in Figure 4.3, were generated using the power-law model parameters listed in Table 4.1. As can be seen, the updated water relative permeability is slightly less than the measured data, reducing the mobility of the aqueous phase in the model. Additionally, the updated critical water saturation is increased from the lab data in order to increase the oil phase mobility.

Table 4.1-Coefficients of power law model for oil/water relative permeability

Variable	S_{wc}	S_{or}	k_{rw}^{*}	k_{ro}^{*}	e_w	e_o
Lab data	0.22	0.355	0.181	1	1.95	2.15
Updated data	0.28	0.355	0.14	1	2	2

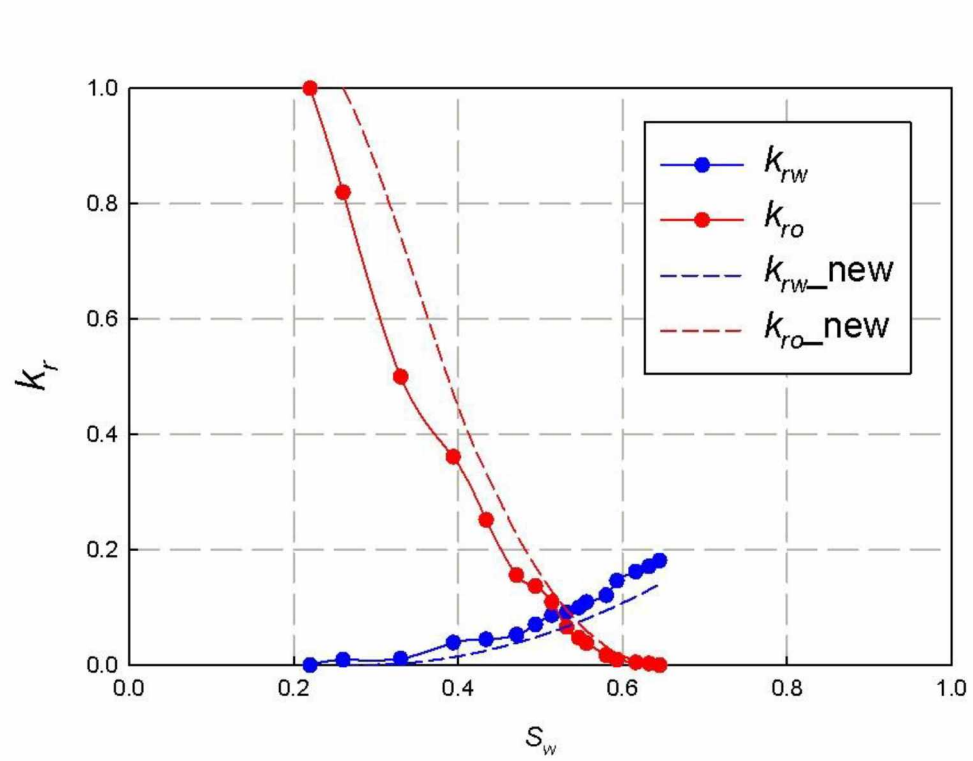

Figure 4.3-Updated oil/water relative permeability curves

4.2.3. Transmissibility contrast

Mass conservation equation, as shown in Equation 4.3, describes the flow of fluids through the porous media in the reservoir.

$$\Delta T_i^{n+1}\left(\Delta P_i^{n+1} - \gamma_i^{n+1}\Delta D\right) + Q_i^{n+1} - \frac{V}{\Delta t}\left[\left(\frac{\varphi S_i}{B_i}\right)^{n+1} - \left(\frac{\varphi S_i}{B_i}\right)^{n}\right] = 0 \qquad \text{Equation 4.3}$$

where T is fluid transmissibility; P is pressure; γ is specific gravity; D is depth; Q is well rate; V is reservoir volume; t is time; φ is porosity; S is saturation; B is formation volume factor; the subscript i represents water phase or oil phase; and superscripts n and n+1 represent old time level and new time level, respectively. Fluid transmissibility in the different directions is defined as,

$$T_{i,j} = \frac{K_j k_{ri}}{\mu_i B_i} \cdot \frac{A_j}{\Delta L_j} \cdot T_{mult} \qquad \text{Equation 4.4}$$

where K is permeability; k_r is relative permeability; μ is fluid viscosity; B is formation volume factor; A is the cross section area; L is length; T_{mult} is the transmissibility multiplier; subscript i represents water phase or oil phase; and subscript j represents the x, y, and z directions.

During the HM process, the transmissibility multipliers of the high transmissibility strips connecting adjacent injectors and producers were tuned individually; the relationships of the updated transmissibility multipliers with time are presented in Figure 4.4. As can be seen, higher transmissibilities, especially for the narrower strips (a, e, and i), have been obtained for the entire waterflooding process to achieve the exact water breakthrough and the sharp rise of water cut. The time-dependent transmissibilities of all the strips show a similar declining tendency in the polymer flooding period, slowing the polymer propagation to reduce the water production in the simulation process.

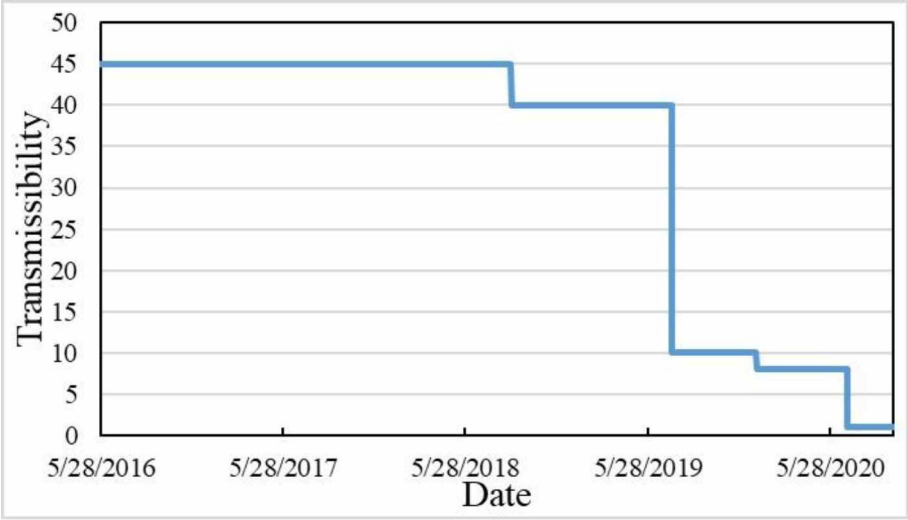

(a)

Figure 4.4-Updated transmissibility multipliers of the high transmissibility strips

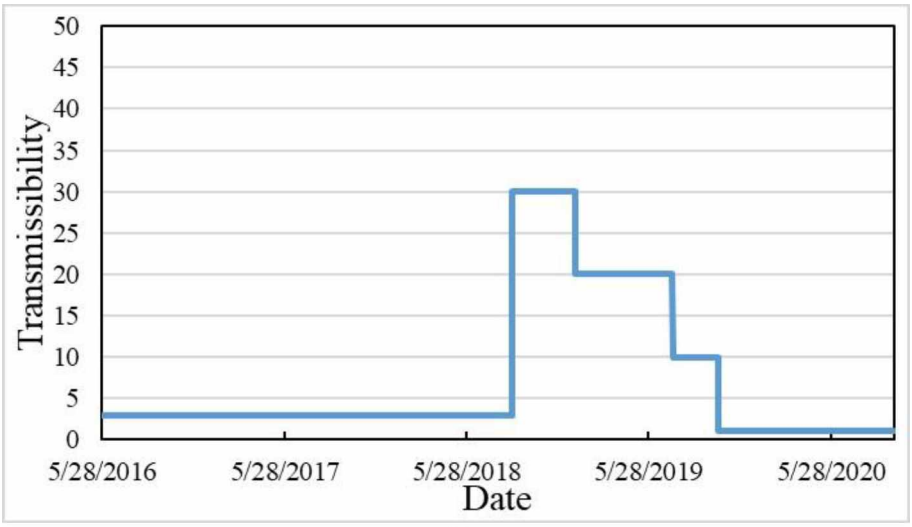

(b)

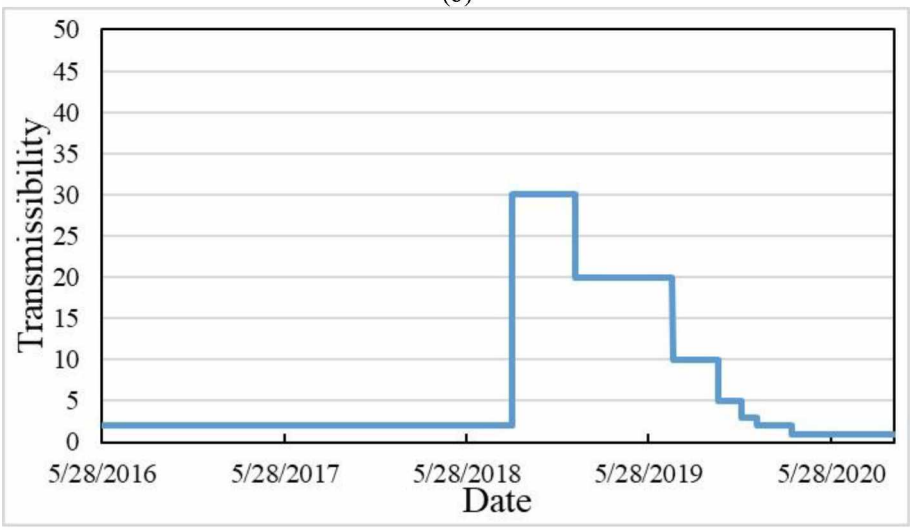

(c)

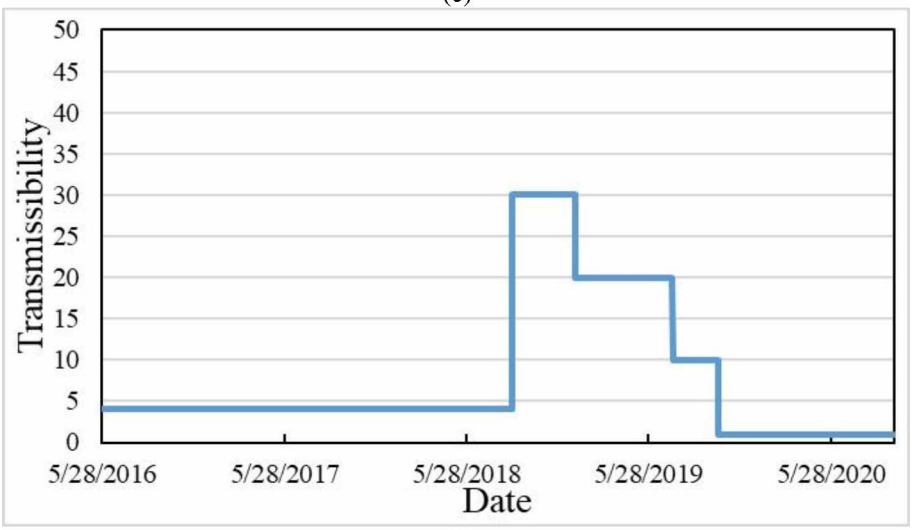

(d)

Figure 4.4 continued-Updated transmissibility multipliers of the high transmissibility strips

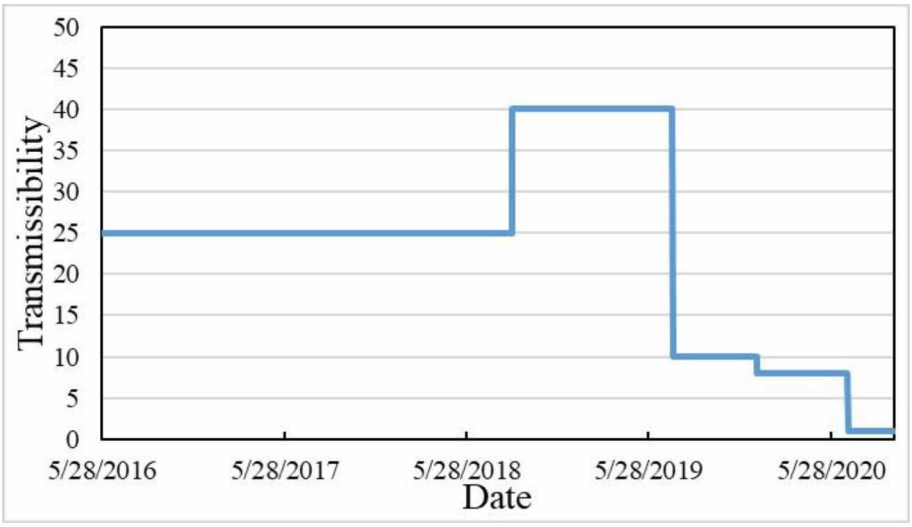

(e)

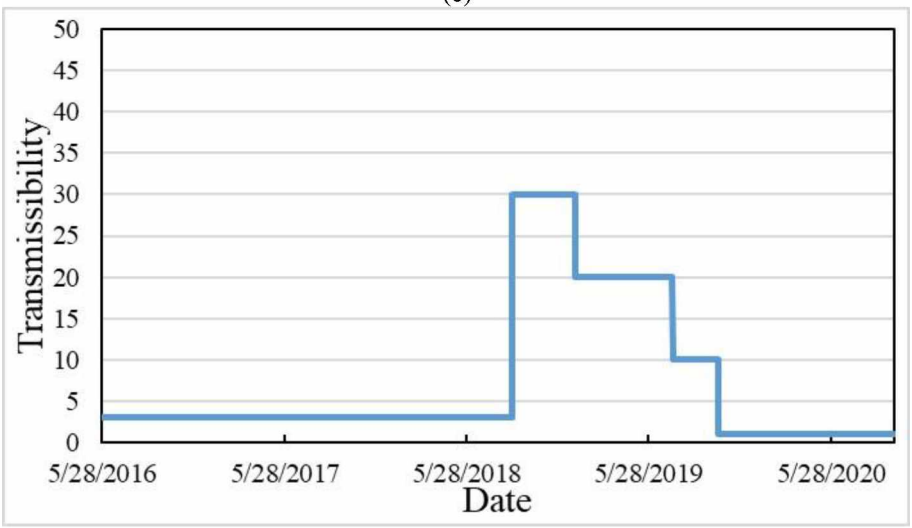

(f)

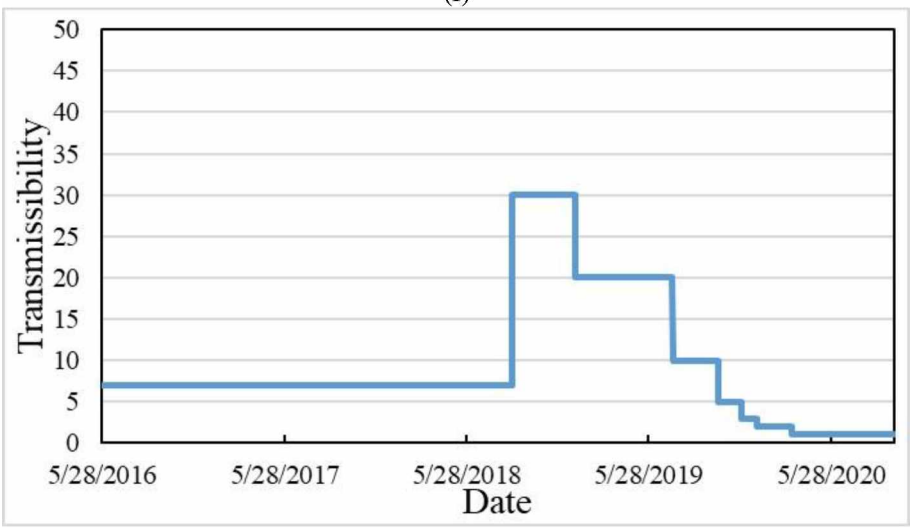

(g)

Figure 4.4 continued-Updated transmissibility multipliers of the high transmissibility strips

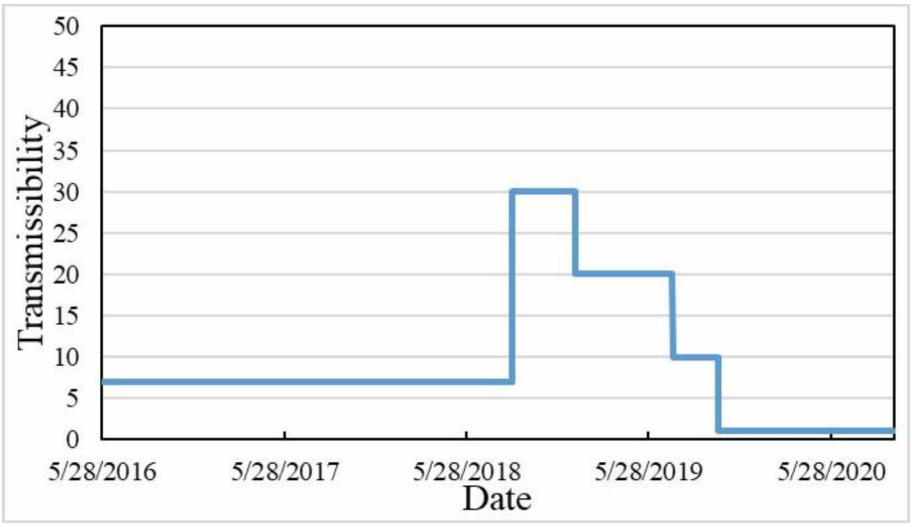

(h)

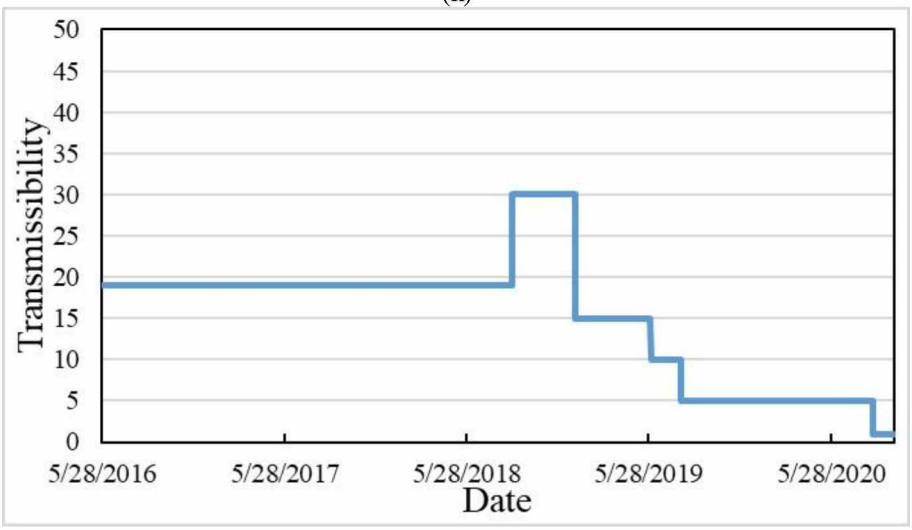

(i)

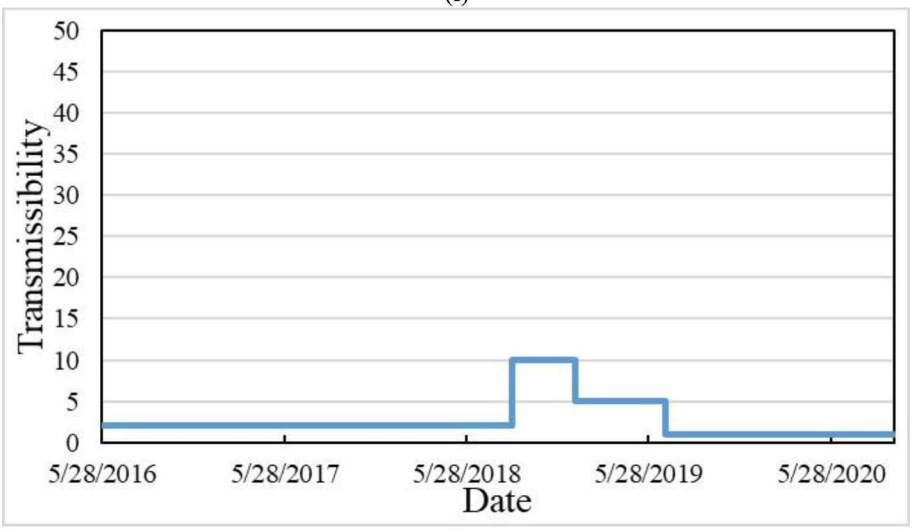

(j)

Figure 4.4 continued-Updated transmissibility multipliers of the high transmissibility strips

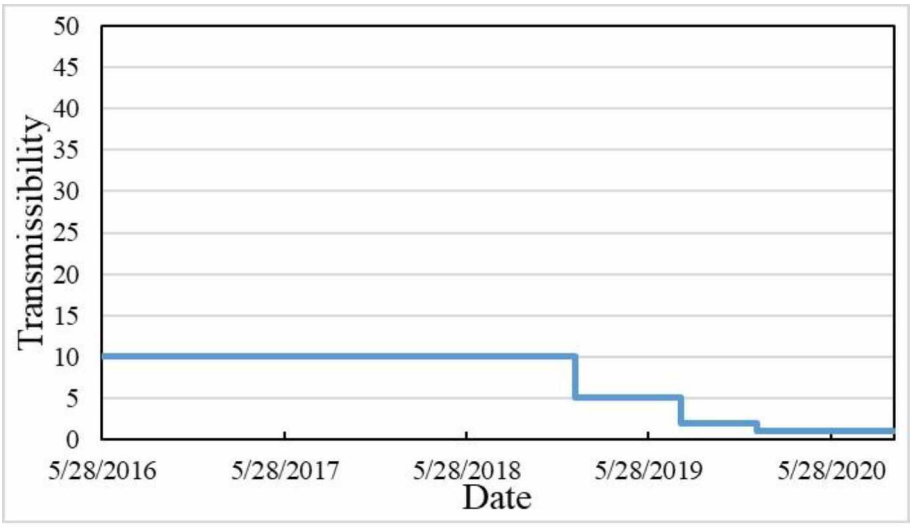

(k)

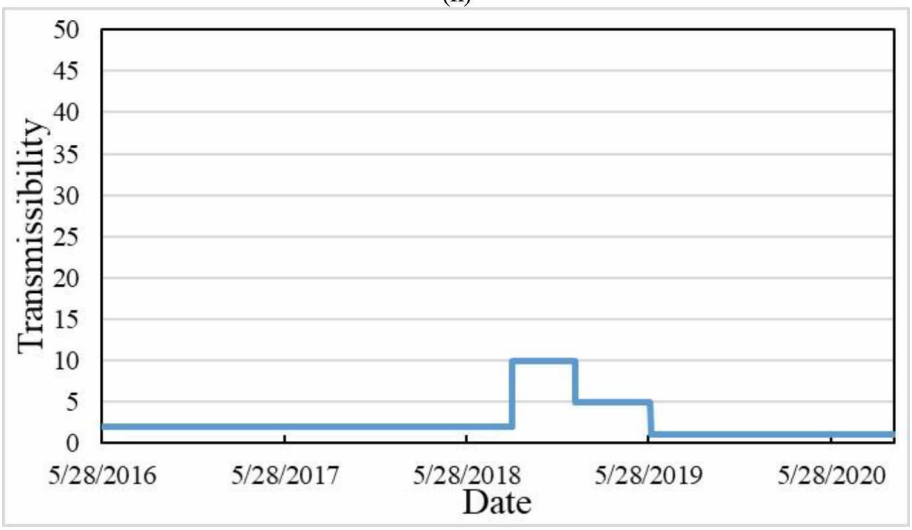

(l)

Figure 4.4 continued-Updated transmissibility multipliers of the high transmissibility strips

4.2.4. Water saturation

Representative simulated water saturation maps at the end of waterflooding and polymer injection of 0.03 and 0.08 PV are presented in Figure 4.5, and the corresponding water phase streamlines are depicted in Figure 4.6. As can be seen, water breakthrough occurs in the high transmissibility strips between injector-producer well pairs during the waterflooding period. With the polymer injection, the water saturation between adjacent high transmissibility strips keeps increasing near both injectors, and the water flow has been arrested in the high transmissibility strips, replicating

the restoration of injection conformance observed during polymer flooding. The short-circuiting behavior observed during the waterflooding period can be explained by viscous fingering effects, and the following reduction in this behavior during polymer flooding seems to corroborate this hypothesis.

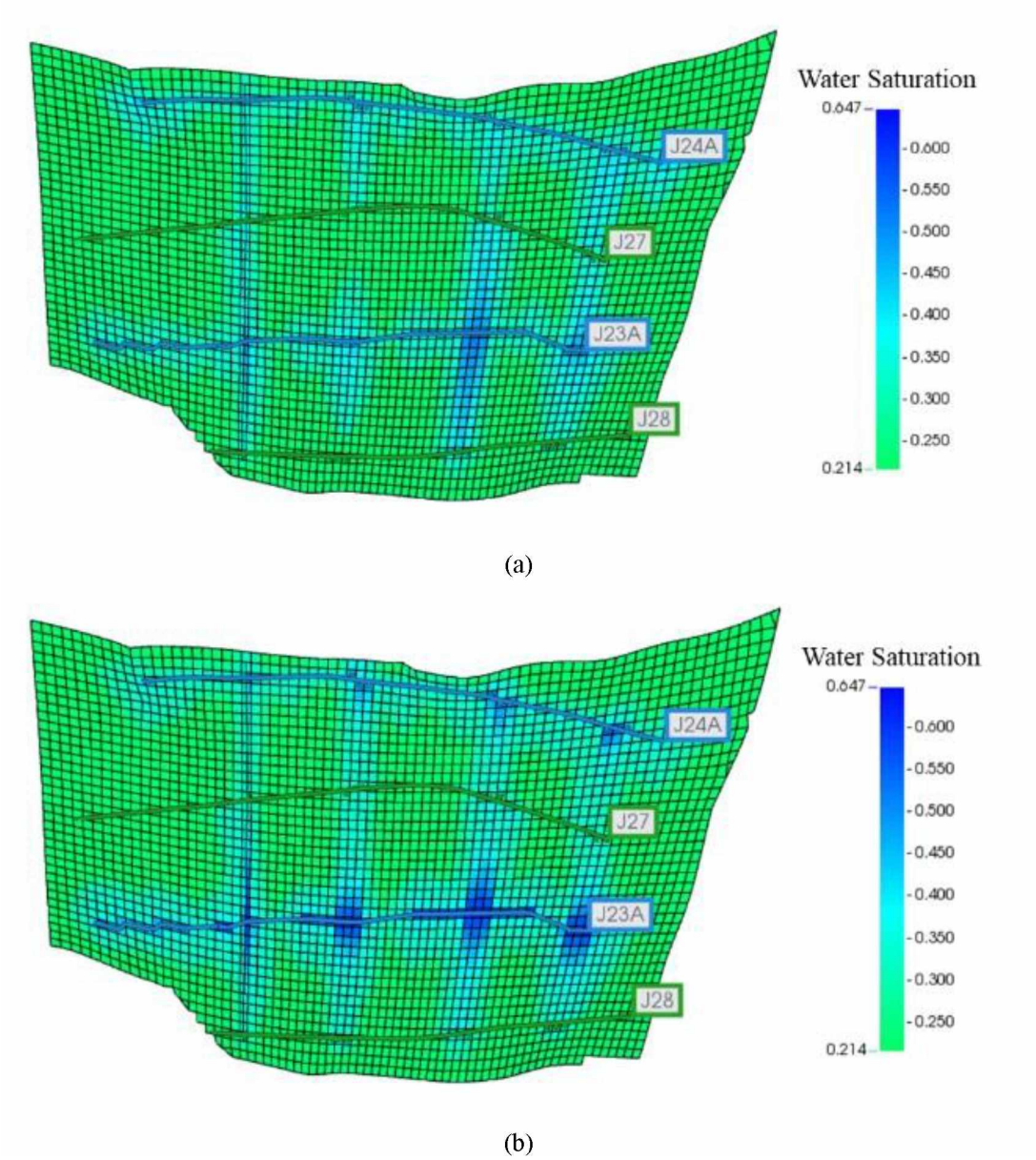

Figure 4.5-Water saturations at polymer injection of (a) 0 PV (b) 0.03 PV and (c) 0.08 PV in layer 4

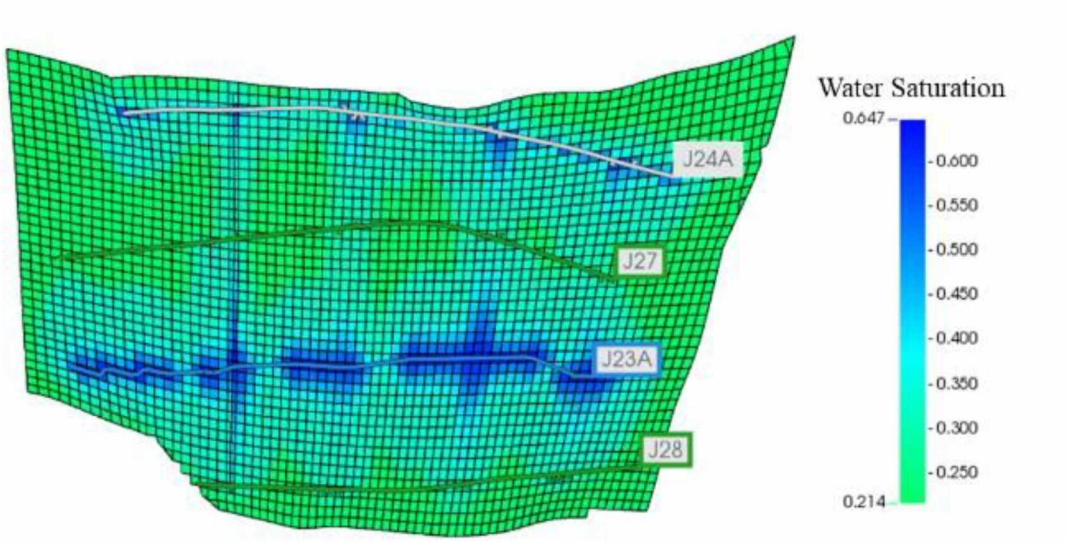

(c)

Figure 4.5 continued-Water saturations at polymer injection of (a) 0 PV (b) 0.03 PV and (c) 0.08 PV in layer 4

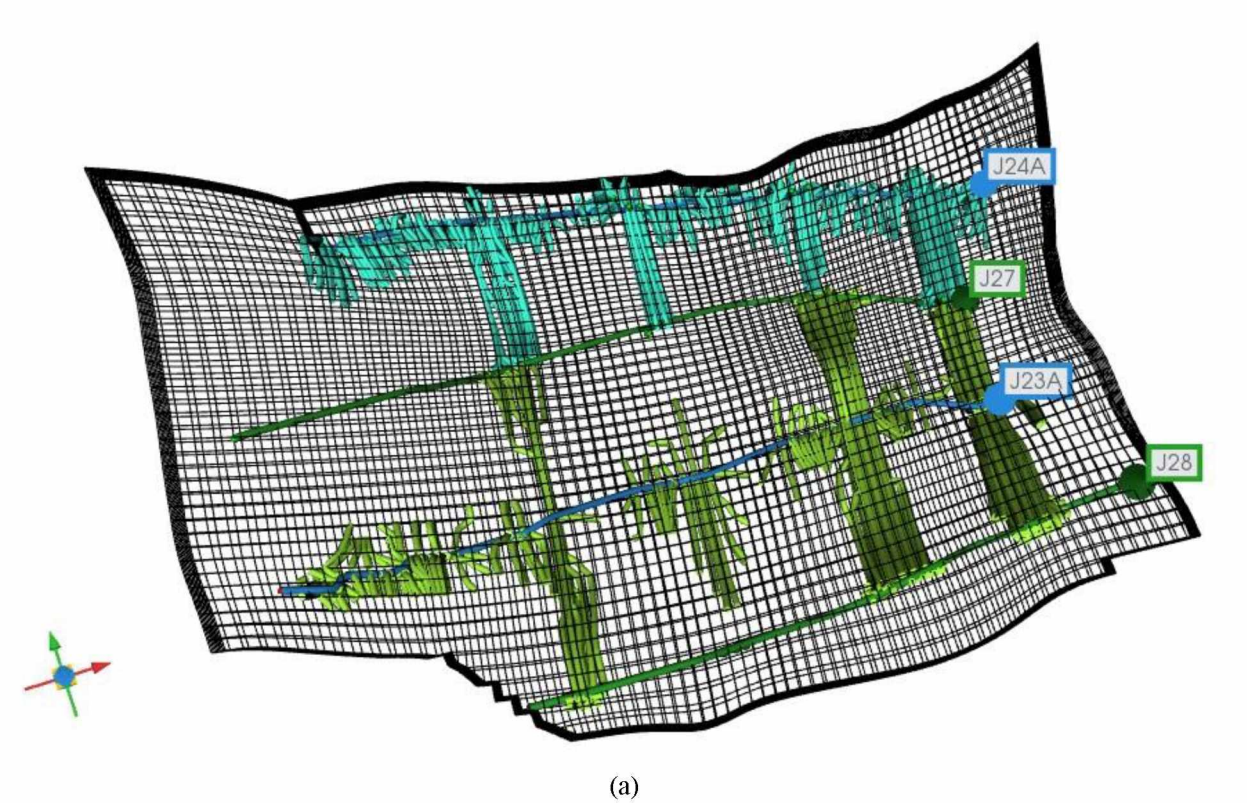

(a)

Figure 4.6-Streamlines of water phase at polymer injection of (a) 0 PV (b) 0.03 PV and (c) 0.08 PV

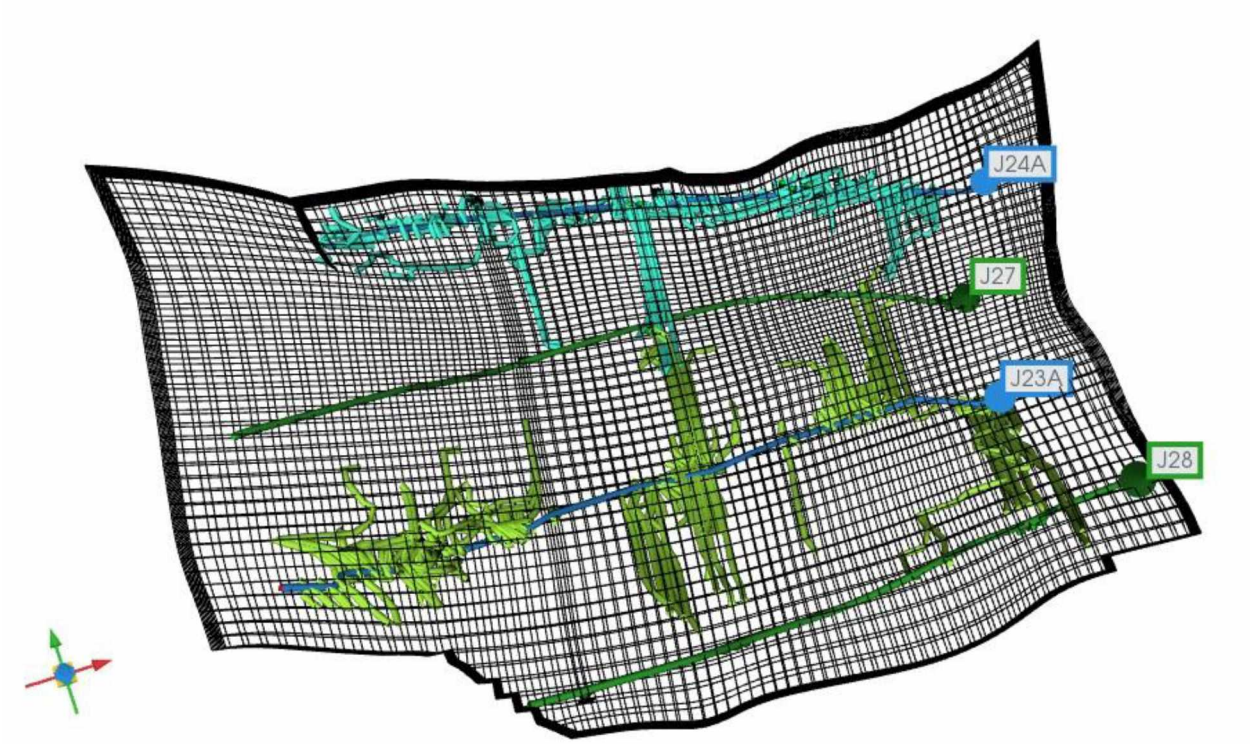

(b)

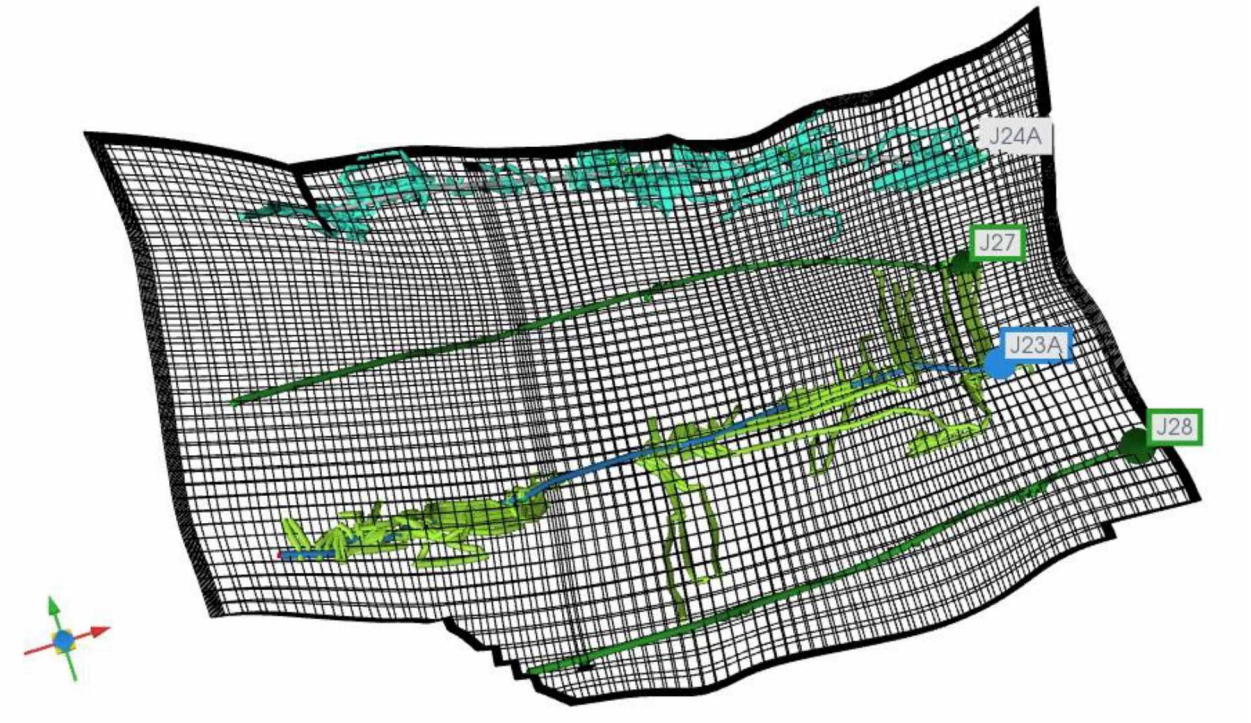

(c)

Figure 4.6 continued-Streamlines of water phase at polymer injection of (a) 0 PV (b) 0.03 PV and (c) 0.08 PV

4.3. Performance prediction results

The validated reservoir simulation model was employed to forecast the production performance of polymer flooding for an additional 30 years starting from January 2021. During the polymer flooding prediction period, the maximum BHPs for both injectors are set to 2700 psi, while the minimum BHPs for producers J-27 and J-28 are set to 700 and 500 psi, respectively. To evaluate the EOR benefit, the simulation model is also forecasted on a continued waterflooding without polymer injection, targeting a total water injection rate of 3600 bbls/day starting from August 28, 2018. For the waterflooding forecasts, maximum BHPs for the injectors are set to 2700 psi, while the minimum BHPs for the producers are set to 500 psi.

4.3.1. Polymer concentration

Simulated forecasts with injected polymer concentrations ranging from 300 to 2700 ppm have been conducted to investigate the effects of polymer concentration on the oil recovery factor (RF) and the polymer utilization. The polymer retention is fixed at 153 μg/g, and the total injection rate is fixed at 1950 bbls/day for these cases. The oil RFs for different polymer injection concentrations are listed in Table 4.2. The oil RF is plotted against time in Figure 4.7. The oil RF of continued waterflooding is 18.4% in 30 years; even a lower polymer concentration of 300 ppm markedly improves upon this. The oil RFs of polymer flooding increase with higher polymer injection concentration when the injected polymer concentration is less than 1800 ppm. If the polymer injection concentration is raised above 1800 ppm, almost no production benefit will be observed since the injectors are forced to operate under the maximum BHP constraint, resulting in a total injection rate less than 1950 bbls/day.

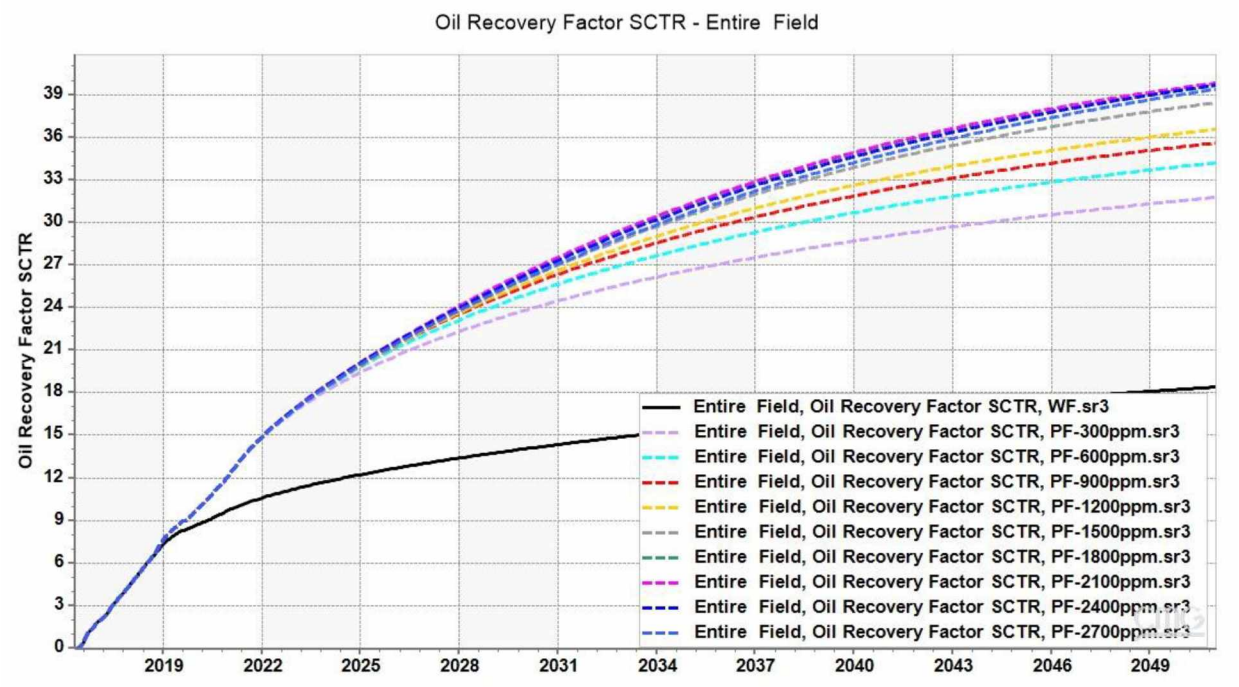

Figure 4.7-Oil RF profiles of polymer flooding with different polymer concentrations

Table 4.2-Oil RFs of simulations with different polymer concentrations

Polymer concentration (ppm)	WF	300	600	900	1200	1500	1800	2100	2400	2700
Oil RF (%)	18.4	31.8	34.2	35.6	36.5	38.4	39.6	39.8	39.7	39.4

4.3.2. Polymer retention

The effects of polymer retention on the oil RF and polymer utilization have been investigated at the current pilot polymer injection concentration of 1200 ppm. The oil RFs for different polymer retention values are given in Table 4.3, and the oil RF is plotted against time in Figure 4.8. The oil RFs decrease with higher polymer retention, suggests that this is caused by the adverse mobility ratio. More polymer is trapped in the formation if the higher retention value is used in the reservoir model, resulting in a lower polymer solution concentration propagating in the reservoir. The polymer solution can sweep more regions in the reservoir model with lower polymer retention

since the effective viscosity of the polymer solution is higher, which can displace more oil from the reservoir. For the reservoir model using higher polymer retention, the maximum polymer retention can be achieved at the swept zone after a period of time in predicting producer performance, then the sweep regions have been enlarged, reducing the difference of oil RF compared with the model using lower retention value.

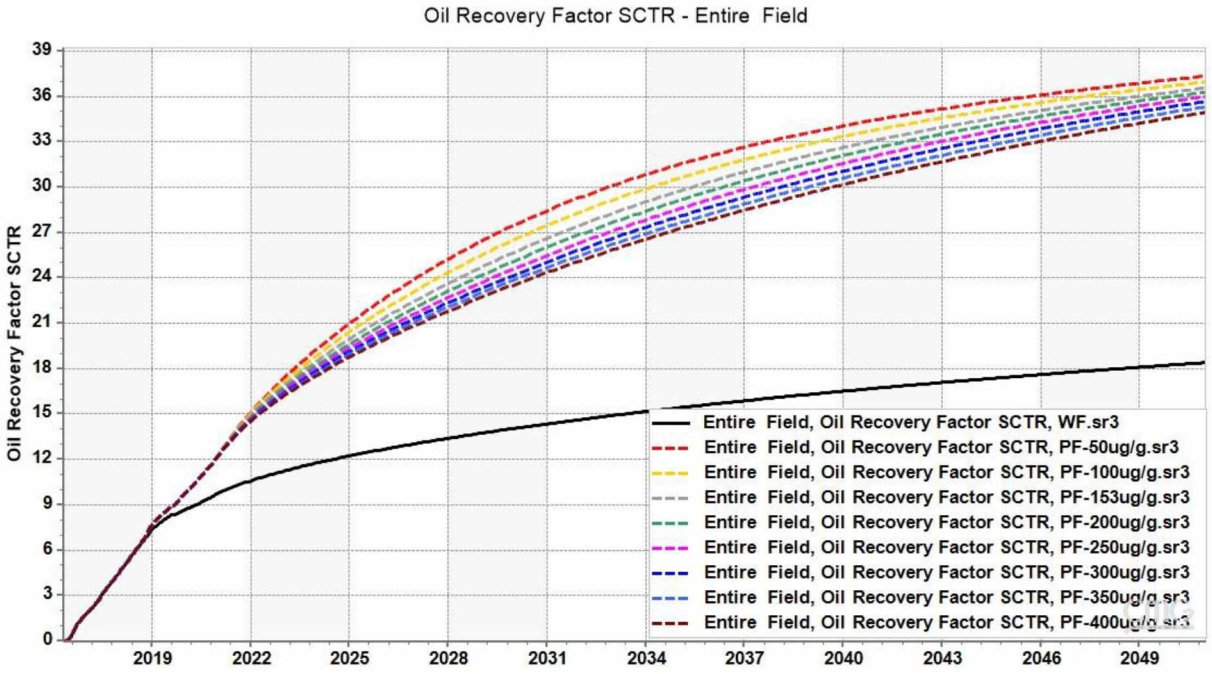

Figure 4.8-Oil RF profiles of polymer flooding with different polymer retention

Table 4.3-Oil RFs of simulations with different polymer retention

Polymer retention (μg/g)	WF	50	100	153	200	250	300	350	400
Oil RF (%)	18.4	37.3	36.9	36.5	36.3	36.0	35.6	35.3	34.9

4.3.3. Injection rate

The effects of injection rate on the oil RF and polymer utilization have been investigated through reservoir simulation. The polymer concentration is held constant at 1200 ppm and the polymer retention at 153 μg/g for these cases. The oil RFs achieved for different target injection rates are listed in Table 4.4. The relationship of oil RF with polymer injection time are depicted in Figure 4.9. The oil RFs increase with injection rate, and the increase in the rate of oil recovery is generally reduced with injection time at different injection rates.

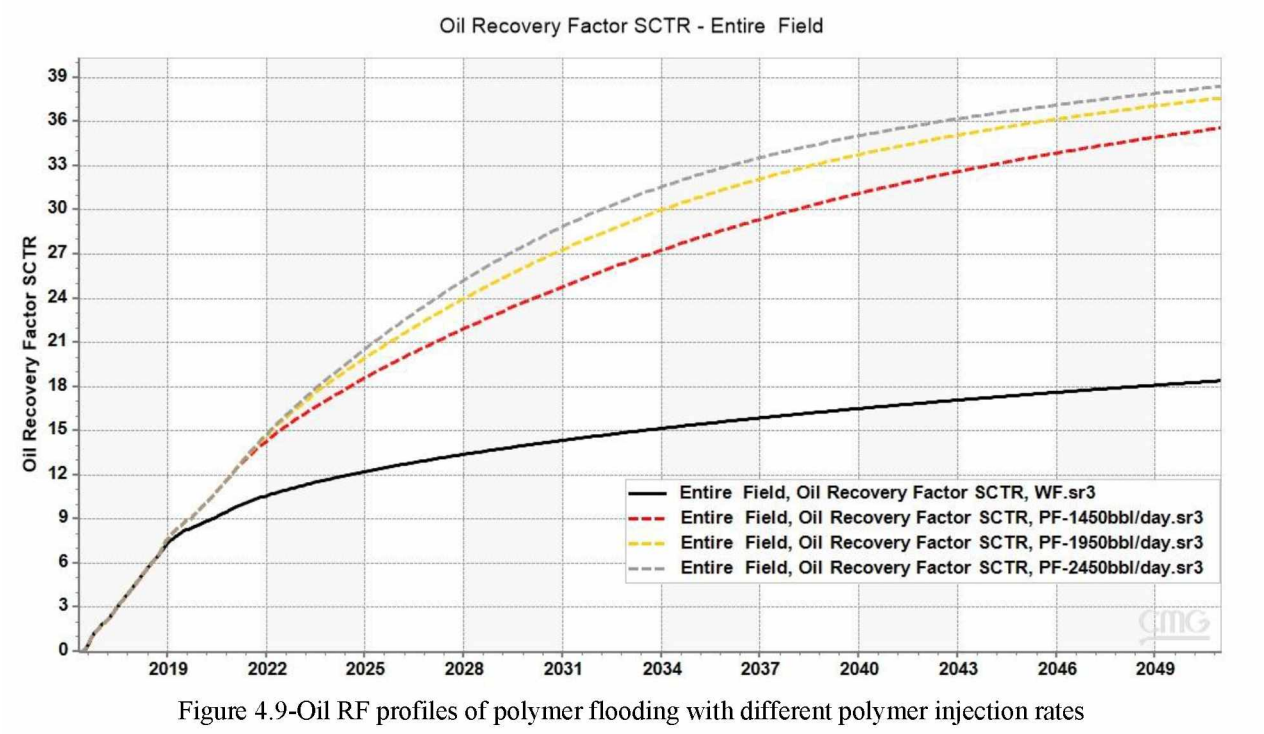

Figure 4.9-Oil RF profiles of polymer flooding with different polymer injection rates

Table 4.4-Oil RFs of simulations with different injection rates

Injection rate (bbl/day)	WF	1450	1950	2450
Oil RF (%)	18.4	35.6	37.6	38.4

4.3.4. Incremental oil recovery

The relationships of incremental oil RF after 10, 20, and 30 years at different polymer concentrations, polymer retention values, and injection rates are shown in Figure 4.10. As can be seen, the incremental oil RFs range from 10% to 13% at different polymer concentrations in 10 years. As the polymer continues to be injected, the incremental oil RFs increase with polymer concentration and reach up to 19% and 21% at the injected polymer concentration of 2100 ppm in 20 years and 30 years, respectively. However, the incremental oil RFs are almost the same for the cases using higher polymer concentrations, which is caused by the decrease in the injection rate. This was observed at the cases of the injected polymer concentration larger than 1200 ppm in the reservoir simulations. The incremental oil RFs vary from 10% to 14% at different polymer retention in 10 years. And the difference in incremental oil RFs between the lowest and highest retention values decreases to 2% in 30 years, which is due to the maximum adsorption is continuously satisfied. What's more, the differences in incremental oil RFs between adjacent time intervals decrease from 4.5% to 2% for different injection rates. Under the condition that the injection rate is satisfied, the incremental oil RF can achieve up to about 20% by injecting polymer concentration of 1200 ppm with injection rate of 2450 bbls/day for 20 years, which consumes a minimum amount of 7,500,000 lbs polymer.

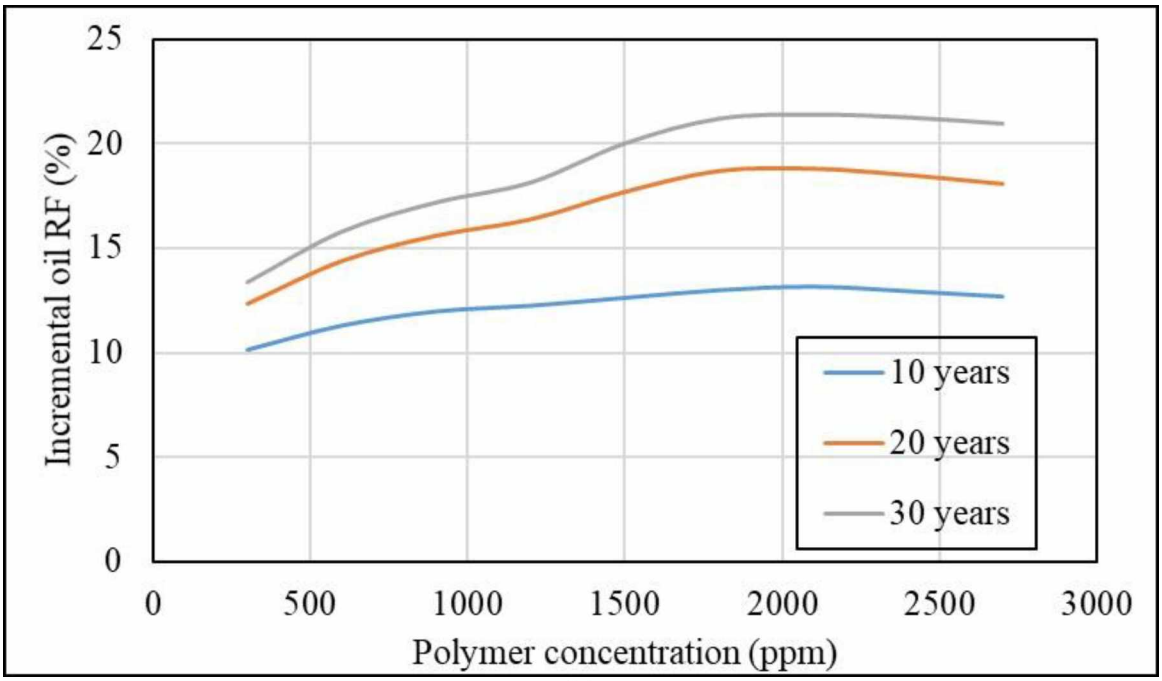

(a)

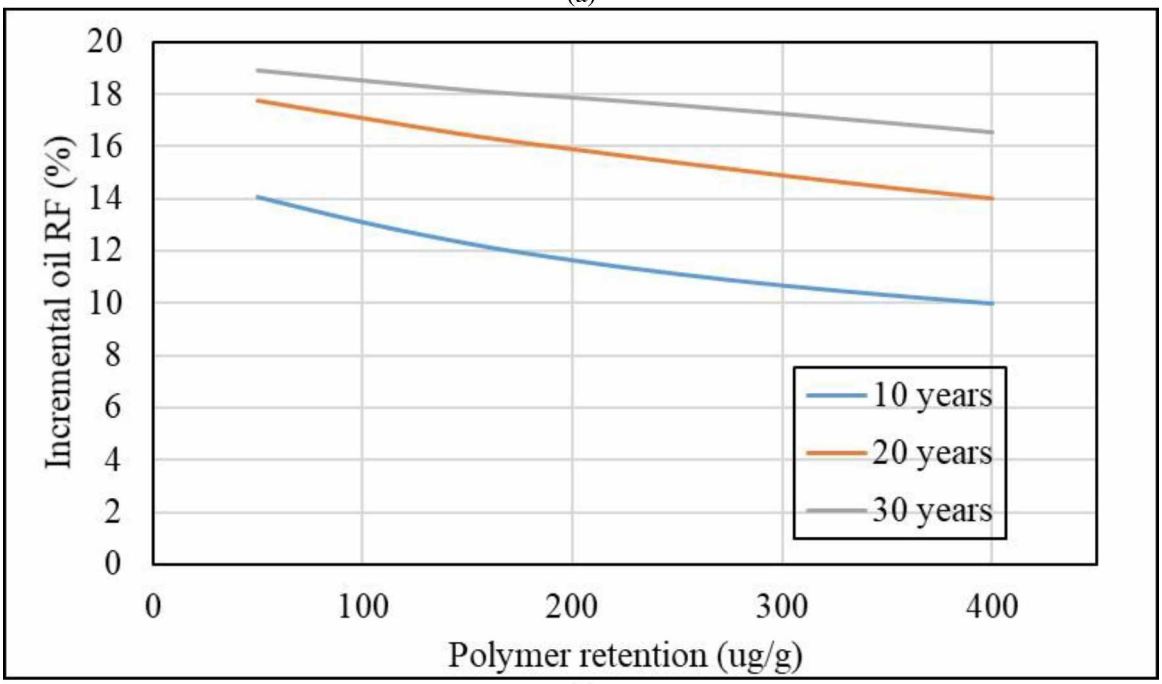

(b)

Figure 4.10-Incremental oil RF at different (a) polymer concentrations (b) polymer retention and (c) injection rates

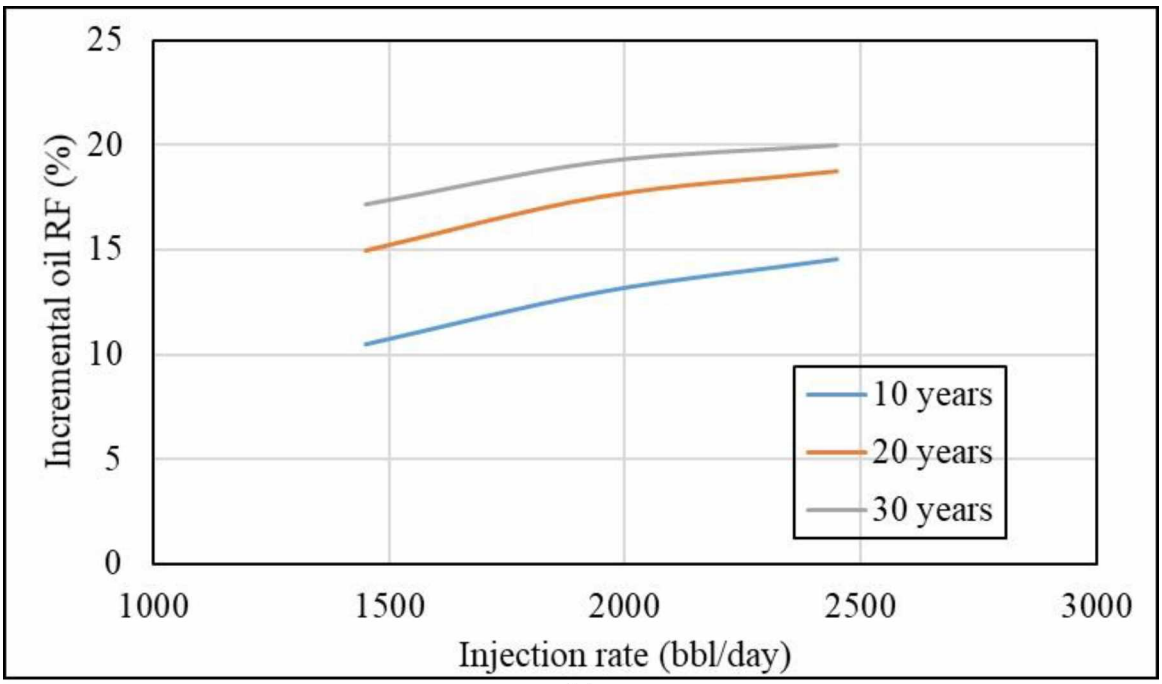

(c)

Figure 4.10 continued-Incremental oil RF at different (a) polymer concentrations (b) polymer retention and (c) injection rates

4.3.5. Polymer utilization

Time profiles of polymer utilization at different polymer concentrations, polymer retention values, and injection rates are illustrated in Figure 4.11. As can be seen, the polymer utilization increases with injection time at different polymer concentrations but remains lower than 3.5 lbs/bbl in 30 years. The increase in the polymer utilization for polymer concentration larger than 1500 ppm is slower than that for 1200 ppm from the end of 2030 which corresponds to the decrease in injected polymer amount. The polymer utilization is reduced for lower polymer retention values which indicates that the polymer is more efficient at displacing the oil if less polymer is lost to the formation rock. Similar polymer utilizations are observed at different injection rates during the early forecast times. However, the difference in polymer utilization grows with injection time, and the increase in the polymer utilization at a higher injection rate is faster than at a lower injection rate.

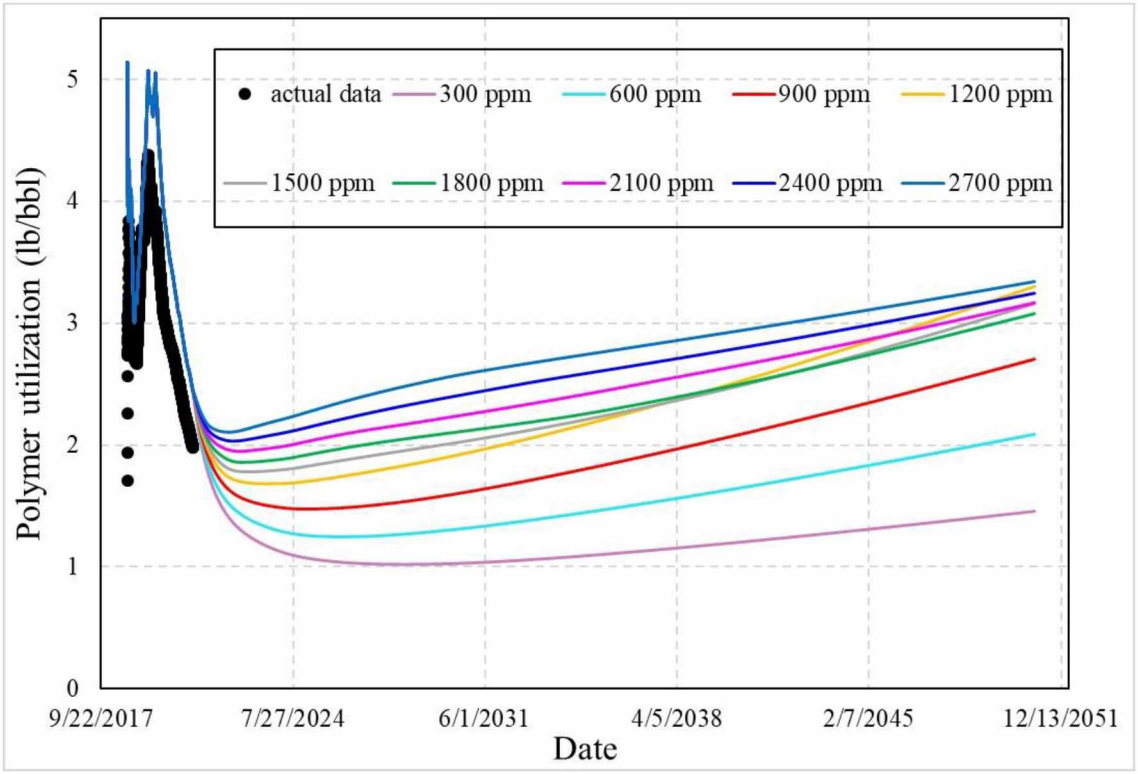

(a)

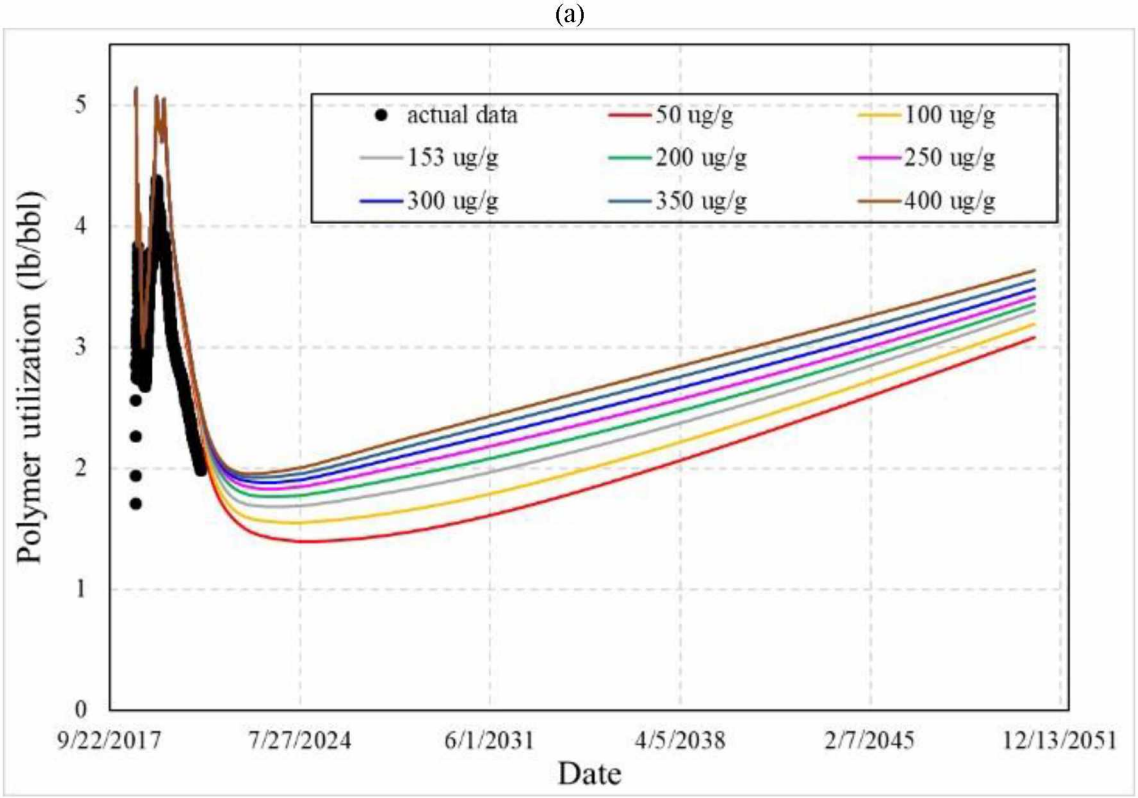

(b)

Figure 4.11-Polymer utilizations at different (a) polymer concentrations (b) polymer retention and (c) injection rates

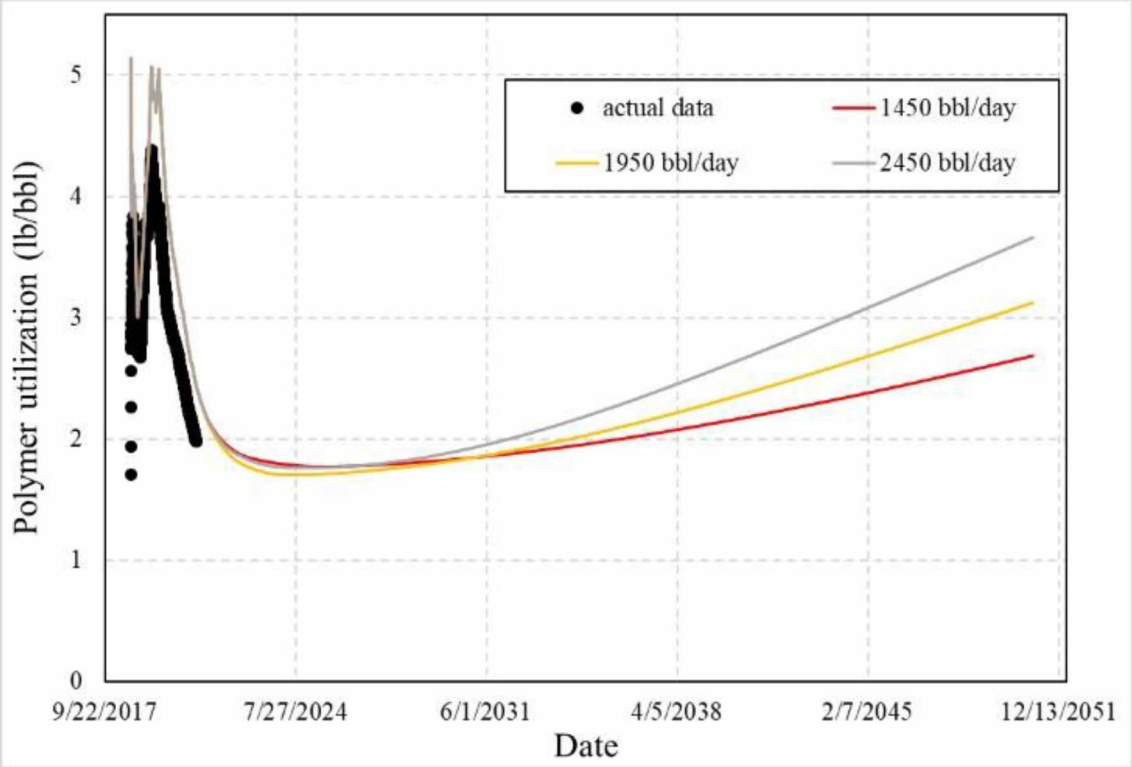

(c)

Figure 4.11 continued-Polymer utilizations at different (a) polymer concentrations (b) polymer retention and (c) injection rates

5. Conclusions and recommendations

This thesis research aimed to develop a robust history-matched reservoir simulation model, which can effectively simulate the flow pattern of fluids in the reservoir and reproduce the ongoing polymer pilot production history. The reservoir simulation model was first built based on the geological model and available rock and fluids data. Then, the developed reservoir simulation model was calibrated by constraining the production wells to honor the measured oil production rates and matching the water cut observations during the HM processes. At last, the validated reservoir simulation model was employed to forecast the well performance under different development strategies.

The HM processes were implemented by introducing high transmissibility strips to connect the injector-producer well pairs in the reservoir simulation model. The HM results reveal that higher strip transmissibilities can match the water breakthrough and sharp increase of water cut well during the waterflooding period. At the later stage of polymer flooding, the strip transmissibilities need to be reduced with time to match the significant water cut reduction. The viscous fingering effect during waterflooding and the restoration of injection conformance during polymer flooding are effectively represented by tuning the strip transmissibilities.

The performance predictions were conducted to investigate the effects of polymer concentration, polymer retention, and injection rate on oil recovery and polymer utilization. The prediction results indicate that the oil RF of continued waterflooding is 18.4% in 30 years. The oil RF of polymer flooding with polymer concentration larger than 1500 ppm can more than double compared with waterflooding. The oil RF of polymer flooding decreases with higher polymer retention and reduce

to 34.9% with polymer retention of 400 μg/g. The oil RF increases with injection rate and up to 38.4% with an injection rate of 2450 bbls/day. Moreover, polymer utilization generally increases with increasing polymer concentration, retention, and injection rate. Among the investigated scenarios, the maximum forecasted polymer utilization was 3.5 lbs/bbl in 30 years, which is still less than the polymer utilization of the same polymer used in a polymer pilot in Argentina.

The author recommends reservoir simulations to select the slug size and timing of the polymer injection, which promotes oil recovery with less polymer consumption. Further improvement on the reservoir model by history matching the production profiles after polymer breakthrough is also suggested as future work.

6. References

[1] Kamal, Medhat M. "Future Need of Petroleum Engineering." Paper presented at the SPE Western Regional Meeting, Virtual, April 2021. doi: https://doi.org/10.2118/200771-MS

[2] United States Energy Information Administration. "Annual Energy Outlook 2021 (AEO2021)", February 2021. [Online]. Available: https://www.eia.gov/outlooks/aeo

[3] Fuaadi, I.M., Pearce, J.C., and B.T. Gael. "Evaluation of Steam-Injection Designs for the Duri Steamflood Project." Paper presented at the SPE Asia-Pacific Conference, Perth. Australia, November 1991. doi: https://doi.org/10.2118/22995-MS

[4] Hanzlik, E.J., and D.S. Mims. "Forty Years of Steam Injection in California - The Evolution of Heat Management." Paper presented at the SPE International Improved Oil Recovery Conference in Asia Pacific, Kuala Lumpur, Malaysia, October 2003. doi: https://doi.org/10.2118/84848-MS

[5] Nath, D.K., Sugianto, R., and D. Finley. "Fiber-Optic Distributed Temperature Sensing Technology Used for Reservoir Monitoring in an Indonesia Steam Flood." Paper presented at the SPE International Thermal Operations and Heavy Oil Symposium, Calgary, Alberta, Canada, November 2005. doi: https://doi.org/10.2118/97912-MS

[6] Al-Bahlani, A.M. and Babadagli, T. "SAGD laboratory experimental and numerical simulation studies: A review of current status and future issues." Journal of Petroleum Science and Engineering. 68(3–4): 135-150, 2009. doi: https://doi.org/10.1016/j.petrol.2009.06.011

[7] Carpenter, Chris. "The Philosophy of Enhanced Oil Recovery." J Pet Technol 72 (2020): 43–44. doi: https://doi.org/10.2118/1220-0043-JPT

[8] Shirif, Ezeddin. "Mobility Control by Polymers Under Bottom-Water Conditions, Experimental Approach." Paper presented at the SPE Asia Pacific Oil and Gas Conference and Exhibition, Brisbane, Australia, October 2000. doi: https://doi.org/10.2118/64506-MS

[9] Morelato Assunção, Pablo , Rodrigues, Lorennzo Marrochi, and Oldrich Joel Romero. "Effect of Polymer Injection on the Mobility Ratio and Oil Recovery." Paper presented at the SPE Heavy Oil Conference and Exhibition, Kuwait City, Kuwait, December 2011. doi: https://doi.org/10.2118/148875-MS

[10] Skauge, Tormod , Vik, Bartek Florczyk, Ormehaug, Per Arne, Jatten, Berit K., Kippe, Vegard , Skjevrak, Ingun , Standnes, Dag Chun, Uleberg, Knut , and Arne Skauge. "Polymer Flood at Adverse Mobility Ratio in 2D Flow by X-ray Visualization." Paper presented at the SPE EOR Conference at Oil and Gas West Asia, Muscat, Oman, March 2014. doi: https://doi.org/10.2118/169740-MS

[11] Batychy, J.P., and F.G. McCaffery. "Low Interfacial Tension Displacement Studies." Paper presented at the Annual Technical Meeting, Calgary, Alberta, June 1978. doi: https://doi.org/10.2118/78-29-26

[12] Stukan, Mikhail , and Wael Abdallah. "Interfacial Tension (IFT) and Surface Alteration Interplay." Paper presented at the Abu Dhabi International Petroleum Conference and Exhibition, Abu Dhabi, UAE, November 2012. doi: https://doi.org/10.2118/161279-MS

[13] Bortolotti, Villiam, Macini, Paolo, and Falan Srisuriyachai. "Laboratory Evaluation of Alkali and Alkali-Surfactant-Polymer Flooding Combined with Intermittent Flow in Carbonatic Rocks." Paper presented at the Asia Pacific Oil and Gas Conference & Exhibition, Jakarta, Indonesia, August 2009. doi: https://doi.org/10.2118/122499-MS

[14] Bortolotti, V.. , Macini, P.. , and F.. Srisuriyachai. "Wettability Index of Carbonatic Reservoirs and EOR: Laboratory Study to Optimize Alkali and Surfactant Flooding." Paper presented at the International Oil and Gas Conference and Exhibition in China, Beijing, China, June 2010. doi: https://doi.org/10.2118/131043-MS

[15] Delamaide, Eric , Bazin, Brigitte , Rousseau, David , and Guillaume Degre. "Chemical EOR for Heavy Oil: The Canadian Experience." Paper presented at the SPE EOR Conference at Oil and Gas West Asia, Muscat, Oman, March 2014. doi: https://doi.org/10.2118/169715-MS

[16] Wyatt, K., Pitts, M.J., and H. Surkalo. "Field Chemical Flood Performance Comparison with Laboratory Displacement in Reservoir Core." Paper presented at the SPE/DOE Symposium on Improved Oil Recovery, Tulsa, Oklahoma, April 2004. doi: https://doi.org/10.2118/89385-MS

[17] Hatzignatiou, D.G., and Y. Lu. "Feasibility Study of CO2 Immiscible Displacement Process In Heavy Oil Reservoirs." Paper presented at the Annual Technical Meeting, Calgary, Alberta, June 1994. doi: https://doi.org/10.2118/94-90

[18] Elgaghah, Shedid, Zekri, Abdulrazag Yusef, Almehaideb, Reyadh A., and Shedid A. Shedid. "Laboratory Investigation of Influences of Initial Oil Saturation and Oil Viscosity on Oil Recovery by CO2 Miscible Flooding." Paper presented at the EUROPEC/EAGE Conference and Exhibition, London, U.K., June 2007. doi: https://doi.org/10.2118/106958-MS

[19] Mogensen, Kristian , and Siqing Xu. "Potential Applicability of Miscible N2 Flooding in High-Temperature Abu Dhabi Reservoir." Paper presented at the SPE Reservoir Characterisation and Simulation Conference and Exhibition, Abu Dhabi, UAE, September 2019. doi: https://doi.org/10.2118/196716-MS

[20] Lv, Sanbo , Liao, Xinwei , Chen, Hao , Chen, Zhiming , Lv, Xianwei , and Xiaojin Zhou. "Predicting the Effects of Acid Gas on Enhanced Oil Recovery in Hydrocarbon Gas Injection." Paper presented at the SPE Western Regional Meeting, Anchorage, Alaska, USA, May 2016. doi: https://doi.org/10.2118/180434-MS

[21] Holm, L.W.. "Miscibility and Miscible Displacement." J Pet Technol 38 (1986): 817–818. doi: https://doi.org/10.2118/15794-PA

[22] Moulds, T.P., McGuire, P.L., Jerauld, G.R., Lee, S-T., and R. Solano. "Pt. McIntyre: A Case Study of Gas Enrichment Above MME." Paper presented at the SPE Annual Technical Conference and Exhibition, Denver, Colorado, October 2003. doi: https://doi.org/10.2118/84185-MS

[23] Leung, Louis C.. "Numerical Evaluation of the Effect of Simultaneous Steam and Carbon Dioxide Injection on the Recovery of Heavy Oil." J Pet Technol 35 (1983): 1591–1599. doi: https://doi.org/10.2118/10776-PA

[24] Tran, Truynh Quoc, Neogi, P.. , and Baojun Bai. "Stability of CO2 Displacement of an Immiscible Heavy Oil in a Reservoir." SPE J. 22 (2017): 539–547. doi: https://doi.org/10.2118/184407-PA

[25] Barnhart, W., and C. Coulthard. "Weyburn CO2 Miscible Flood Conceptual Design and Risk Assessment." J Can Pet Technol 39 (2000): No Pagination Specified. doi: https://doi.org/10.2118/00-09-01

[26] Davison, R.J., Mayder, A., Hladiuk, D.W., and J. Jarrell. "Zama Acid Gas Disposal/Miscible Flood Implementation And Results." J Can Pet Technol 38 (1999): No Pagination Specified. doi: https://doi.org/10.2118/99-02-04

[27] Trivedi, J.J., Babadagli, T., Lavoie, R.G., and D. Nimchuk. "Acid Gas Sequestration During Tertiary Oil Recovery: Optimal Injection Strategies and Importance of Operational Parameters." J Can Pet Technol 46 (2007): No Pagination Specified. doi: https://doi.org/10.2118/07-03-06

[28] McGuire, P.L., and B.M. Holt. "Unconventional Miscible EOR Experience at Prudhoe Bay: A Project Summary." SPE Res Eval & Eng 6 (2003): 17–27. doi: https://doi.org/10.2118/82140-PA

[29] Zhang, Pinggang , Brodie, James , Daae, Victoria , Erbas, Demet , and Euan Duncan. "BP North Sea Miscible Gas Injection Projects Review." Paper presented at the SPE Offshore Europe Oil and Gas Conference and Exhibition, Aberdeen, UK, September 2013. doi: https://doi.org/10.2118/166597-MS

[30] Gunawan, Sugianto, and Didier Caie. "Handil Field: Three Years of Lean-Gas Injection Into Waterflooded Reservoirs." SPE Res Eval & Eng 4 (2001): 107–113. doi: https://doi.org/10.2118/71279-PA

[31] Thai, B.N., Hsu, C.F., Bergersen, B.M., Albrecht, S.L., and T.W. Richardson. "Denver Unit Infill Drilling and Pattern Reconfiguration Program." Paper presented at the SPE Permian Basin Oil and Gas Recovery Conference, Midland, Texas, March 2000. doi: https://doi.org/10.2118/59548-MS

[32] Alikhlalov, K.. , and B.. Dindoruk. "Conversion of Cyclic Steam Injection to Continous Steam Injection." Paper presented at the SPE Annual Technical Conference and Exhibition, Denver, Colorado, USA, October 2011. doi: https://doi.org/10.2118/146612-MS

[33] De Zwart, Albert Hendrik, Bakker, Peter, Glandt, Carlos Alberto, Brooks, David, and Johan Jacobus van Dorp. "A Thermal Recovery Method for Medium-Heavy Oil Reservoirs With Strong Bottom Aquifers." Paper presented at the SPE North Africa Technical Conference & Exhibition, Marrakech, Morocco, March 2008. doi: https://doi.org/10.2118/112876-MS

[34] Sasaki, K., Akibayashi, S., Yazawa, N., Doan, Q.T., and S.M. Farouq Ali. "Experimental Modeling of the SAGD Process - Enhancing SAGD Performance with Periodic Stimulation of the Horizontal Producer." SPE J. 6 (2001): 89–97. doi: https://doi.org/10.2118/69742-PA

[35] Alomair, O.. , Alarouj, M.. , Althenayyan, A.. , Alsaleh, A.. , Mohammad, H.. , Altahoo, Y.. , Alhaidar, Y.. , Alansari, S.. , and Y.. Alshammari. "Improving Heavy Oil Recovery by Unconventional Thermal Methods." Paper presented at the SPE Kuwait International Petroleum Conference and Exhibition, Kuwait City, Kuwait, December 2012. doi: https://doi.org/10.2118/163311-MS

[36] Nath, Dhirendra K., Sugianto, Riki, and Douglas B. Finley. "Fiber-Optic Distributed Temperature Sensing Technology Used for Reservoir Monitoring in an Indonesia Steam Flood." SPE Drill & Compl 22 (2007): 149–156. doi: https://doi.org/10.2118/97912-PA

[37] Stark, Shane D. "Cold Lake Commercialization of the Liquid Addition to Steam for Enhancing Recovery (LASER) Process." Paper presented at the International Petroleum Technology Conference, Beijing, China, March 2013. doi: https://doi.org/10.2523/IPTC-16795-MS

[38] Williams, Lee. L., Fong, William S., and Kumar Mridul. "Effects of Discontinuous Shales on Multizone Steamflood Performance in the Kern River Field." SPE Res Eval & Eng 4 (2001): 350–357. doi: https://doi.org/10.2118/73174-PA

[39] Anuka, Agnes , Falode, Olugbenga , Ogunshe, Adenike , and Celestine Udie. "An Overview of Microbial Enhanced Oil Recovery in Nigeria." Paper presented at the SPE Nigeria Annual International Conference and Exhibition, Virtual, August 2020. doi: https://doi.org/10.2118/203765-MS

[40] Sunmonu, Rasak Mayowa, and Mike Onyekonwu. "Enhanced Oil Recovery using Foam Injection; a Mechanistic Approach." Paper presented at the SPE Nigeria Annual International Conference and Exhibition, Lagos, Nigeria, August 2013. doi: https://doi.org/10.2118/167589-MS

[41] Dong, Pengfei , Puerto, Maura C., Ma, Kun , Mateen, Khalid , Ren, Guangwei , Bourdarot, Gilles , Morel, Danielle , Biswal, Sibani Lisa, and George J. Hirasaki. "Ultralow-Interfacial-Tension Foam-Injection Strategy in High-Temperature Ultrahigh-Salinity Fractured Oil-Wet Carbonate Reservoirs." SPE J. 24 (2019): 2822–2840. doi: https://doi.org/10.2118/190259-PA

[42] Naderi, Khosrow, and Tayfun Babadagli. "Effect of ultrasonic intensity and frequency on heavy-oil recovery from different wettability rocks." Paper presented at the International Thermal Operations and Heavy Oil Symposium, Calgary, Alberta, Canada, October 2008. doi: https://doi.org/10.2118/117324-MS

[43] McGuire, P.L., Spence, A.P., and R.S. Redman. "Performance Evaluation of a Mature Miscible Gas Flood at Prudhoe Bay." Paper presented at the SPE/DOE Improved Oil Recovery Symposium, Tulsa, Oklahoma, April 2000. doi: https://doi.org/10.2118/59326-MS

[44] Young, J. P., Mathews, W. L., and E. J. Hulm. "Alaskan Heavy Oil: First CHOPS at a Vast, Untapped Arctic Resource." Paper presented at the SPE Western Regional Meeting, Anaheim, California, USA, May 2010. doi: https://doi.org/10.2118/133592-MS

[45] Targac, G.W., Redman, R.S., Davis, E.R., Rennie, S.B., McKeever, S.O., and B.C. Chambers. "Unlocking the Value in West Sak Heavy Oil" Paper presented at the SPE International Thermal Operations and Heavy Oil Symposium, Calgary, Alberta, Canada, November 2005. doi: https://doi.org/10.2118/97856-MS

[46] Burton, Robert C., Chin, Lee, Davis, Eric Robert, Enderlin, Milton Bock, Fuh, Giin-Fa, Hodge, Richard M., Ramos, Rico, VanDeVerg, Phil, Werner, Michael, Mathews, William Lloyd, and Sean David Petersen. "North Slope Heavy-Oil Sand-Control Strategy: Detailed Case Study of Sand-Production Predictions and Field Measurements for Alaskan Heavy-Oil-Multi-Lateral Field Developments." Paper presented at the SPE Annual Technical Conference and Exhibition, Dallas, Texas, October 2005. doi: https://doi.org/10.2118/97279-MS

[47] Paskvan, Frank , Turak, Joe , Jerauld, Gary , Gould, Tom , Skinner, Robert , and Amitabh Garg. "Alaskan Viscous Oil: EOR Opportunity, or Waterflood Sand Control First?." Paper presented at the SPE Western Regional Meeting, Anchorage, Alaska, USA, May 2016. doi: https://doi.org/10.2118/180463-MS

[48] McGuire, P.L., Redman, R.S., Jhaveri, B.S., Yancey, K.E., and S.X. Ning. "Viscosity Reduction WAG: An Effective EOR Process for North Slope Viscous Oils." Paper presented at the SPE Western Regional Meeting, Irvine, California, March 2005. doi: https://doi.org/10.2118/93914-MS

[49] Seright, R.S.. S.. "Potential for Polymer Flooding Reservoirs with Viscous Oils." SPE Res Eval & Eng 13 (2010): 730–740. doi: https://doi.org/10.2118/129899-PA

[50] Dandekar, Abhijit , Bai, Baojun , Barnes, John , Cercone, Dave , Ciferno, Jared , Ning, Samson , Seright, Randy , Sheets, Brent , Wang, Dongmei , and Yin Zhang. "First Ever Polymer Flood Field Pilot - A Game Changer to Enhance the Recovery of Heavy Oils on Alaska's North Slope." Paper presented at the SPE Western Regional Meeting, San Jose, California, USA, April 2019. doi: https://doi.org/10.2118/195257-MS

[51] Ning, Samson, Barnes, John, Edwards, Reid, Dunford, Kyler, Eastham, Kevin, Dandekar, Abhijit, Zhang, Yin, Cercone, Dave, and Jared Ciferno. "First Ever Polymer Flood Field Pilot to Enhance the Recovery of Heavy Oils on Alaska's North Slope - Polymer Injection Performance." Paper presented at the SPE/AAPG/SEG Unconventional Resources Technology Conference, Denver, Colorado, USA, July 2019. doi: https://doi.org/10.15530/urtec-2019-643

[52] Dandekar, Abhijit , Bai, Baojun , Barnes, John , Cercone, Dave , Ciferno, Jared , Edwards, Reid , Ning, Samson , Schulpen, Walbert , Seright, Randy , Sheets, Brent , Wang, Dongmei , and Yin Zhang. "First Ever Polymer Flood Field Pilot to Enhance the Recovery of Heavy Oils on Alaska's North Slope Pushing Ahead One Year Later." Paper presented at the SPE Western Regional Meeting, Virtual, April 2021. doi: https://doi.org/10.2118/200814-MS

[53] Ning, Samson , Barnes, John , Edwards, Reid , Schulpen, Walbert , Dandekar, Abhijit , Zhang, Yin , Cercone, Dave , and Jared Ciferno. "First Ever Polymer Flood Field Pilot to Enhance the Recovery of Heavy Oils on Alaska North Slope – Producer Responses and Operational Lessons Learned." Paper presented at the SPE Annual Technical Conference and Exhibition, Virtual, October 2020. doi: https://doi.org/10.2118/201279-MS

[54] Dandekar, A., Bai, B., Barnes, J. , Cercone, D., Ciferno, J. , Edwards, R., Ning, S. , Schulpen, W., Seright, R., Sheets, B., Wang, D., and Y. Zhang. "Heavy Oil Polymer EOR in the Challenging Alaskan Arctic - It Works!." Paper presented at the SPE/AAPG/SEG Unconventional Resources Technology Conference, Houston, Texas, USA, July 2021. doi: https://doi.org/10.15530/urtec-2021-5077

[55] Mostaghimi, Peyman , Kamali, Fatemeh , Jackson, Matthew D., Muggeridge, Ann H., and Christopher C. Pain. "A Dynamic Mesh Approach for Simulation of Immiscible Viscous Fingering." Paper presented at the SPE Reservoir Simulation Symposium, Houston, Texas, USA, February 2015. doi: https://doi.org/SPE-173281-MS

[56] Luo, Haishan , Delshad, Mojdeh , Pope, Gary A., and Kishore K. Mohanty. "Interactions Between Viscous Fingering and Channeling for Unstable Water/Polymer Floods in Heavy Oil Reservoirs." Paper presented at the SPE Reservoir Simulation Conference, Montgomery, Texas, USA, February 2017. doi: https://doi.org/10.2118/182649-MS

[57] Fabbri, C.. , Romero, C.. , Aubertin, F.. , Nguyen, M.. , Hourcq, S.. , and G.. Hamon. "Secondary Polymer Flooding in Extra-Heavy Oil: Gaining Information on Polymer-Oil Relative Permeabilities." Paper presented at the SPE Enhanced Oil Recovery Conference, Kuala Lumpur, Malaysia, July 2013. doi: https://doi.org/10.2118/165237-MS

[58] Delaplace, P.. , Delamaide, E.. , Roggero, F.. , and G.. Renard. "History Matching of a Successful Polymer Flood Pilot in the Pelican Lake Heavy Oil Field, Canada." Paper presented at the SPE Annual Technical Conference and Exhibition, New Orleans, Louisiana, USA, September 2013. doi: https://doi.org/10.2118/166256-MS

[59] Sabirov, Denis Galievich, Demenev, Roman Aleksandrovich, Isakov, Kirill Dmitrievich, Ilyasov, Ilnur Rustamovich, Orlov, Alexander Gennadievich, and Nikolay Aleksandrovich Glushchenko. "Reservoir Simulation of Polymer Flooding: Challenges and Current Results." Paper presented at the SPE Russian Petroleum Technology Conference, Virtual, October 2020. doi: https://doi.org/10.2118/201948-MS

[60] Jennings Jr., H. 1957. Surface Properties of Natural and Synthetic Porous Media. Production Monthly 21: 20-24.

[61] Behrenbruch, Peter , Kennaird, Tony , Duy Bui, Khang , and Minh Triet Do Huu. "Capillary Pressure Drainage Curves: Modelling and Prediction of Capillary Entry Pressure." Paper presented at the SPE/IATMI Asia Pacific Oil & Gas Conference and Exhibition, Jakarta, Indonesia, October 2017. doi: https://doi.org/10.2118/186949-MS

[62] Leverett, M.C.. "Capillary Behavior in Porous Solids." Trans. 142 (1941): 152–169. doi: https://doi.org/10.2118/941152-G

[63] Goda, Hussam (Sam), and Peter Behrenbruch. "A Universal Formulation for the Prediction of Capillary Pressure." Paper presented at the SPE Annual Technical Conference and Exhibition, Denver, Colorado, USA, October 2011. doi: https://doi.org/10.2118/147078-MS

[64] Skauge, Tormod , Vik, Bartek Florczyk, Ormehaug, Per Arne, Jatten, Berit K., Kippe, Vegard , Skjevrak, Ingun , Standnes, Dag Chun, Uleberg, Knut , and Arne Skauge. "Polymer Flood at Adverse Mobility Ratio in 2D Flow by X-ray Visualization." Paper presented at the SPE EOR Conference at Oil and Gas West Asia, Muscat, Oman, March 2014. doi: https://doi.org/10.2118/169740-MS

[65] Kumar, Mridul, Hoang, Viet Thai, and Cengiz Satik. "High Mobility Ratio Water Flood Performance Prediction: Challenges and New Insights." Paper presented at the SPE International Improved Oil Recovery Conference in Asia Pacific, Kuala Lumpur, Malaysia, December 2005. doi: https://doi.org/10.2118/97671-MS

[66] Cannella, W.J., Huh, C., and R.S. Seright. "Prediction of Xanthan Rheology in Porous Media." Paper presented at the SPE Annual Technical Conference and Exhibition, Houston, Texas, October 1988. doi: https://doi.org/10.2118/18089-MS

[67] Seright, Randall S., Seheult, J. Mac, and Todd Talashek. "Injectivity Characteristics of EOR Polymers." SPE Res Eval & Eng 12 (2009): 783–792. doi: https://doi.org/10.2118/115142-PA

[68] Masuda, Yoshihiro, Tang, Ke-Chin, Miyazawa, Masashi, and Shoichi Tanaka. "1D Simulation of Polymer Flooding Including the Viscoelastic Effect of Polymer Solution." SPE Res Eng 7 (1992): 247–252. doi: https://doi.org/10.2118/19499-PA

[69] Meter, Donald M. and R. Byron Bird. "Tube flow of non-Newtonian polymer solutions: PART I. Laminar flow and rheological models." Aiche Journal 10 (1964): 878-881.

[70] Sorbie, K. S. (1991). Polymer-Improved Oil Recovery. Boca Raton, Fl: CRC Press

[71] Flory, P.J. 1953. Principles of Polymer Chemistry. Ithaca, New York: Cornell University Press

[72] Delshad, Mojdeh, Kim, Do Hoon, Magbagbeola, Oluwaseun Adedeji, Huh, Chun, Pope, Gary Arnold, and Farhad Tarahhom. "Mechanistic Interpretation and Utilization of Viscoelastic Behavior of Polymer Solutions for Improved Polymer-Flood Efficiency." Paper presented at the SPE Symposium on Improved Oil Recovery, Tulsa, Oklahoma, USA, April 2008. doi: https://doi.org/10.2118/113620-MS

[73] Ma, Yiwei , and Mark W. McClure. "The Effect of Polymer Rheology and Induced Fracturing on Injectivity and Pressure-Transient Behavior." SPE Res Eval & Eng 20 (2017): 394–402. doi: https://doi.org/10.2118/184389-PA

[74] Sorbie, K. S. (1991). Polymer-improved oil recovery. Springer Science & Business Media.

[75] Cohen, Yoram, and F.R. Christ. "Polymer Retention and Adsorption in the Flow of Polymer Solutions Through Porous Media." SPE Res Eng 1 (1986): 113–118. doi: https://doi.org/10.2118/12942-PA

[76] Huang, Yaduo, and K.S. Sorbie. "The Adsorption and In-Situ Rheological Behavior of Xanthan Solution Flowing Through Porous Media." Paper presented at the SPE/DOE Enhanced Oil Recovery Symposium, Tulsa, Oklahoma, April 1992. doi: https://doi.org/10.2118/24153-MS

[77] Goudarzi, Ali , Delshad, Mojdeh , and Kamy Sepehrnoori. "A Critical Assessment of Several Reservoir Simulators for Modeling Chemical Enhanced Oil Recovery Processes." Paper presented at the SPE Reservoir Simulation Symposium, The Woodlands, Texas, USA, February 2013. doi: https://doi.org/10.2118/163578-MS

[78] Al-Shalabi, Emad W. "A New Insight into Modeling of Polymer Flooding in Carbonate Reservoirs." Paper presented at the SPE Latin American and Caribbean Petroleum Engineering Conference, Virtual, July 2020. doi: https://doi.org/10.2118/198958-MS

[79] Hoteit, Hussein , Alexis, Dennis , Adepoju, Olaoluwa O., Chawathe, Adwait , and Taimur Malik. "Numerical and Experimental Investigation of Polymer-Induced Resistance to Flow in Reservoirs Undergoing a Chemical Flood." Paper presented at the SPE Annual Technical Conference and Exhibition, Dubai, UAE, September 2016. doi: https://doi.org/10.2118/181720-MS

[80] Dawson, Rapier, and Ronald B. Lantz. "Inaccessible Pore Volume in Polymer Flooding." SPE J. 12 (1972): 448–452. doi: https://doi.org/10.2118/3522-PA

[81] Sorbie, K.S., Parker, A., and P.J. Clifford. "Experimental and Theoretical Study of Polymer Flow in Porous Media." SPE Res Eng 2 (1987): 281–304. doi: https://doi.org/10.2118/14231-PA

[82] Manichand, R.N.. N., and R.S.. S. Seright. "Field vs. Laboratory Polymer-Retention Values for a Polymer Flood in the Tambaredjo Field." SPE Res Eval & Eng 17 (2014): 314–325. doi: https://doi.org/10.2118/169027-PA

[83] Wang, Dongmei , Li, Chunxiao , and Randall S. Seright. "Laboratory Evaluation of Polymer Retention in a Heavy Oil Sand for a Polymer Flooding Application on Alaska's North Slope." SPE J. 25 (2020): 1842–1856. doi: https://doi.org/10.2118/200428-PA

[84] Delamaide, E.. , Let, K. Moe, Bhoendie, K.. , Paidin, W. R., and S.. Jong-A-Pin. "Interpretation of the Performance Results of a Polymer Flood Pilot in the Tambaredjo Oil Field, Suriname." Paper presented at the SPE Annual Technical Conference and Exhibition, Dubai, UAE, September 2016. doi: https://doi.org/10.2118/181499-MS

[85] Delamaide, Eric "Comparison of Primary, Secondary and Tertiary Polymer Flood in Heavy Oil - Field Results." Paper presented at the SPE Trinidad and Tobago Section Energy Resources Conference, Port of Spain, Trinidad and Tobago, June 2016. doi: https://doi.org/10.2118/180852-MS

[86] Juri, J. E., Ruiz, A. M., Pedersen, G.. , Pagliero, P.. , Blanco, H.. , Eguia, V.. , Vazquez, P.. , Bernhardt, C.. , Schein, F.. , Villarroel, G.. , Tosi, A.. , and V.. Serrano. "Grimbeek2: First Successful Application Polymer Flooding in Multilayer Reservoir at YPF. Interpretation of Polymer Flooding Response." Paper presented at the SPE Latin America and Caribbean Petroleum Engineering Conference, Buenos Aires, Argentina, May 2017. doi: https://doi.org/10.2118/185487-MS

[87] Juri, Juan-E, Ruiz, Ana, Serrano, Viviana, Guillen, Paula, Thill, Mercedes, Kichick, Lucas, Alonso, Pablo, Lucero, Ariel, De Miranda, Victor, Mac Donald, Walter, Figueroa, Emilio, Robina, Nestor, Vera, Maximiliano, Figueroa, Emilio, Di Pauly, Fernando, Rojas, Walter, and Natalia Ojeda. "A Successful 18%STOOIP 4-Injector Polymer Pilot Expands To 80 New Injectors In 6 Years Adopting A Modular Concept In Grimbeek Fluvial Reservoirs." Paper presented at the International Petroleum Technology Conference, Dhahran, Kingdom of Saudi Arabia, January 2020. doi: https://doi.org/10.2523/IPTC-20285-MS